Study on Growth and Characteristics of Thermally Evaporated Organic Semiconductor Layers

(加熱蒸着した有機半導体層の成長と特性に関する研究)

July 2018

Doctor of Engineering

Aye Myint Moh

Toyohashi University of Technology

別紙４－１（課程博士（英文））

Date of Submission（month, day, year）： 7.9.2018

Department Mechanical Engineering	Student ID Number	D 159105
Applicant's name	Aye Myint Moh	

Supervisors	Izaki Masanobu Seiji Yokoyama

Abstract（Doctor）

Title of Thesis	Study on Growth and Characteristics of Thermally Evaporated Organic Semiconductor Layers (加熱蒸着した有機半導体層の成長と特性に関する研究)

Approx. 800 words

The organic semiconductors have been employed in electronics and optoelectronic devices because of their wide range of properties. A great number of organic materials have been used as the active layer for applications in organic electronics such as organic light emitting diodes (OLEDs), organic field effect transistors (OFETs), and organic photovoltaic devices (OPVs). Organic layers have been prepared by using several methods of solution process such as spin-coating, and vacuum process such as vacuum thermal evaporation. The structure and quality of the resultant organic layers affects the performance of the electronic devices, and the amorphous and bulk-heterojunction structure that was a nano-scale mixture of the n-type and p-type organic semiconductor have been employed for organic PV devices.

Organic semiconductors of π-conjugated small molecules are promising and versatile organic semiconductors for the electronics and optoelectronic devices including organic PV devices because of the high mobility relating to the diffusion length of the carrier. The transporting phenomena of the mobility is affected by the molecular arrangement in the organic semiconductor layers, and the arrangement of the thin layers installed into the devices has been controlled by adjusting the growth including the preparation technique, substrate and under-layer material, and the deposition rate. The heteroepitaxial growth has been generally employed for the fabrication of electronics and optoelectronics devices constructed of inorganic semiconductors, and the lattice relationship at the hetero-interface between the layer and substrate material affects the atomic arrangement of the resultant inorganic layer. The information and knowledge on the growth of organic semiconductors is still insufficient compared with that for inorganic semiconductors.

In this thesis, the structure of single layers and bi-layers of π-conjugated small molecules of 2,7-dioctyl[1]benzothieno[3,2-b][1]benzothiophene (C8-BTBT) and N,N'-dioctyl-3,4,9,10- perylenedicarboximide (PTCDI-C8) prepared on single crystal substrates by a vacuum thermal evaporation was investigated with X-ray diffraction (XRD) and atomic force microscopy (AFM). The purpose of this work is to characterize the growth of organic semiconductors including the effects of the under-layer material and orientation and to propose the tentative growth model applicable for the development of next generation π-conjugated small molecular based devices.

In Chapter 1, the background and purpose of this study was mentioned.

In Chapter 2, the preferred orientation and growth behavior of C8-BTBT deposited on quartz glass, (11$\underline{2}$0)A-, (0001)C-, (1$\underline{1}$02)R-single-crystal Al_2O_3 (sapphire), (100)-, and (111)-single-crystal MgO substrates were investigated by XRD and AFM. The (001) out-of-plane orientation with a similar in-plane orientation was developed irrespective of the substrate material and orientation, and the degree of the development was reflected by the grain structure of the substrates.

In chapter 3, effects of the layer thickness and preparation temperature of the C8-BTBT layer on C-sapphire substrate on the growth and characteristics have been investigated with XRD, AFM, optical absorption measurement, and resistivity measurement with and without light irradiation. The C8-BTBT layers with the optical bandgap energy around 3.3 eV possessed the (001) out-of-plane

orientation irrespective of the layer thickness and preparation temperature. The C8-BTBT layers were growing up in direction parallel to the substrate surface keeping almost constant height, and the continuous layer was formed by the coalescence of the C8-BTBT grains. The electrical resistivity decreased with increase in the preparation temperature due to the increase in the grain size, and the light irradiation induce the drastic decrease to 42-28 Ωcm. The tentative growth mechanism governed by π-π-stacking-induced molecular ordering and diffusion of molecules on the substrates was proposed based on the experimental results.

In chapter 4, the preferred orientation and structure of PTCDI-C8 layers on the Al_2O_3 and MgO substrates were investigated by XRD and AFM observation. The (001) out-of-plane orientation was developed irrespective of the substrate material and orientation, and the continuous layer composed of needle-like grains was formed at the thickness of 15 nm followed by the grain growth with the thickness. The growth of the PTCDI-C8 layer was similar to that for C8-BTBT layer, and the proposed growth mechanism is adequate to the PTCDI-C8 growth.

In Chapter 5, the surface state of C8-BTBT/PTCDI-C8 bi-layers prepared on C-sapphire substrate were investigated by XRD, AFM, and Kelvin Force Microscopy (KFM). The lattice relationship of (001)-C8-BTBT//(001)-PTCDI-C8 was developed irrespective of the stacking order, but the C8-BTBT/PTCDI-C8 bi-layer showed an excellent performance in the surface morphology and potential homogeneity compared with the PTCDI-C8/C8-BTBT bi-layer, suggesting the importance of the stacking order in the fabrication of the bi-layer and the π-π-stacking-induced molecular ordering of each layer on the growth.

In Chapter 6, the results obtained in this study was summarized. The tentative growth mechanism proposed based on the experimental results was adequate to the growth of the single layers and bi-layers of C8-BTBT and PTCDI-C8, and the growth model and experimental results obtained here will support to the improvement of the performance of future π-conjugated based organic semiconductor layers and device fabrication for organic-based applications.

CONTENTS

CHAPTER 1: Introduction

CHAPTER 2: Growth of C8-BTBT molecules on inorganic single crystal substrates with various orientations

CHAPTER 3: Growth and characteristics of C8-BTBT layers on C-sapphire substrate by thermal evaporation

CHAPTER 4: Growth and characteristics of PTCDI-C8 layers on single crystal substrates with various orientations

CHAPTER 5: Fabrication and structure of PTCDI-C8/C8-BTBT bi-layer

CHAPTER 6: Summary

CHAPTER 1

Introduction

1.1 Organic semiconductors

The organic semiconductors have a wide range of properties as thermal, physical, optical, electrical, and magnetic characteristics which make them possible to be employed in large area, and lightweight electronics and optoelectronic applications.**[1–5]** Since impressive development in organic semiconductor materials as conductive halogen-doped polyacetylene with

conductivity up to 10^5 S/m have been discovered by Shirakawa, Heeger, and MacDiarmid, the research interest has been focused on the use of molecular based materials in electronics applications.**[6]** The semiconducting properties of organic materials exhibit the π-conjugation system. This π-conjugated bonds in organic materials allow for electron delocalization along molecule which give rise the semiconducting properties including conductivity and electronic behaviors. By applying these concepts, it have been demonstrated that the suitability of organic semiconductor materials in a wide range of commercial devices including displays, smart tags, diodes, transistors, solar cells and sensors.**[7–11]** All of these electronic devices mainly based on organic layers which serve as the active layer. Since the quality of the active organic layers is directly linking to the performance of the devices, fabricating the organic layers with promising organic materials and characterization of its formations are highly required for development of efficient devices.

The π-conjugated organic semiconductors are promising and versatile materials for electronics and optoelectronic devices.**[12–15]** Many research have been progressed and focused on the development of high performance organic devices built from conjugated organic molecules because high efficient organic light-emitting diodes (OLEDs) was demonstrated by C.W. Tang and S. A. VanSlyke in 1987.**[16]** A great number of π-conjugated organic materials have been used for application in organic electronics; organic light emitting diodes (OLEDs), organic field effect transistors (OFETs), and organic photovoltaic devices (OPVs), etc.**[5][17–20]** In general, charge transport property of charge carrier mobility is very important factor for these devices. It have been reported the comprehensive review of the progress in carrier mobility of organic semiconductors with the year from 1984 to 2014 in **Figure 1.1 and Table 1.1.[21][22]**

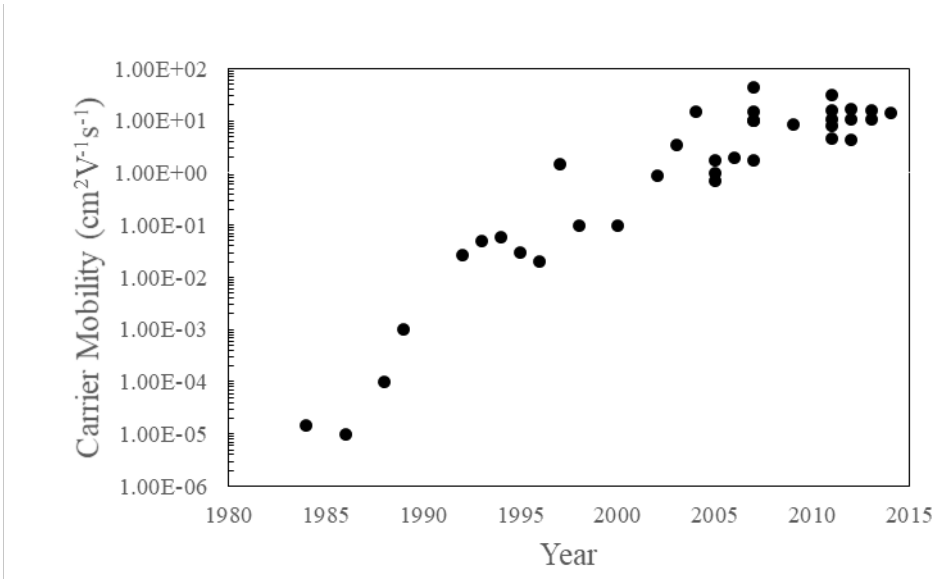

Figure 1.1 Evolution of field-effect mobility value of organic semiconductor based TFTs.

Table 1.1 The reported results for highest field effect mobility values of organic semiconductor based TFTs 1984 to 2014.

Year	**Organic Semiconductors**	**Deposition Method**	**Mobility** ($cm^2V^{-1}s^{-1}$)	**Refer-ence**
1964	Cu-pthalocyanine	Vacuum deposition	Not Reported	**[23]**
1983	Polyacetylene	Solution process	Not Reported	**[24]**
1984	Merocyanine		1.5×10^{-5}	**[25]**
1986	Polythiophene	Solution process	10^{-5}	**[26]**
1988	Polyacetylene Poly(3-hexylthiophene) Phthalocyanine	Solution process Solution process Vacuum deposition	10^{-4} 10^{-4}	**[27]** **[28]** **[29]**
1989	Poly(3-alkylthiophene) α-sexithiophene	Solution process Vacuum deposition	10^{-3} 10^{-3}	**[30]** **[31]**

1992	α-sexithiophene Pentacene	Vacuum deposition Vacuum deposition	0.027 2×10^{-3}	**[32]**
1993	α- ω-dihexyl-sexithiophene Polythienylenevinylene	Vacuum deposition Solution process	0.05 0.22	**[33]** **[34]**
1994	α- ω-dihexyl-sexithiophene	Vacuum deposition	0.06	**[35]**
1995	α-sexithiophene Pentacene	Vacuum deposition Vacuum deposition	0.03 0.038	**[36]** **[37]**
1996 1996	Phthalocyanine Poly(3-hexylthiophene) Pentacene	Vacuum deposition Solution process Vacuum deposition	0.02 0.045 0.62	**[38]** **[39]** **[40]**
1997	Pentacene Bis(dithienothiophene) trans-trans-2,5-Bis-[2-5-(2,2-bithienyl)ethenyl]thio-phene(BTET)	Vacuum deposition Vacuum deposition Vacuum deposition	1.5 0.05 0.01	**[41]** **[42]** **[43]**
1998	Poly(3-hexylthiophene) α- ω-dihexyl-quaterthiophene Dihexyl-anthradithiophene	Solution process Vacuum deposition	0.1 0.23 0.15	**[44]** **[45]** **[46]**
2000	α- ω-dihexyl-quinquethiophene	Solution process	0.1	**[47]**
2002	Pentacene **N,N'-dioctyl-3,4,9,10-perylene tetracarboxylic diimide (PTCDI-C8)**	Solution process **Vacuum deposition**	0.89 **0.6**	**[48]** **[49]**
2003	Pentacene	Vacuum deposition	3.4	**[50]**

2004	Rubrene	Single crystal	15	**[51],[52]**
2005	Rubrene	Solution process	0.7	**[53]**
2006	2,7-Diphenyl[1]ben-zothieno[3,2-b]benzothiophene (DPh-BTBT)	Vacuum deposition	2	**[54]**
2007	TIPS-pentacene Pentacene Rubrene Hexamethlenetetrathiafulvalene (HMTTF) titanyl phthalocyanine (TiOPc)	Solution process Single crystal Single crystal Single crystal Vacuum deposition	1.8 15-40 43 10 10	**[55]** **[56]** **[57]** **[58]** **[59]**
2009	Dinaphtho[2,3-b:2',3'-f]thieno[3,2-b]-thio-phene(DNTT)	Single crystal	8.3	**[60]**
2011	**2,7-dioctyl[1]benzothieno[3,2-b][1]benzothiophene (C8-BTBT)** TIPS-pentacene C10-DNTT C10-DNTT Dianthracen-[2,3-b:2',3'f] thieno[3,2-b]thiophene (DATT)	**Single crystal, Solution process** Solution process Vacuum deposition Solution process Single crystal	**31.3** 4.6 8 11 16	**[61]** **[62]** **[63]** **[64]** **[65]**

2012	Hexacene C13-BTBT Dithienylthieno(3,2-b)thiophene (DTT) and N-alkyl diketo-pyrrolo-pyrrole (DPP)	Single crystal Vacuum deposition Solution process	4.3 17.2 10.5	**[66]** **[67]** **[68]**
2013	TIPS-pentacene Bis(benzothieno) naphthalenes (BBTN)	Solution process Vacuum deposition	11 15.6	**[69]** **[70]**
2014	Poly (thineoisoindigo-alt-naph-thalene)(PT IIG-Np)	Solution process	14.4	**[71]**

According to those charge carrier mobility values, progression is the development of designing and synthesis of new materials, deposition techniques and controlling the growth during deposition which make improving the interface between substrate-molecules and/or molecules-molecules.**[42][72]** The performance and efficiency analysis of the π-conjugated small organic molecular based devices have been emphasized since some devices including OFET based displays, radio frequency identification tag, OLED display and lighting were commercially available. However, some challenges still remain for good performance molecular based devices as the stability of the devices with high mobility. To fulfill these statements, the organic thin films with high crystallinity and less defect concentration are highly demanded.

1.2 Structure of organic semiconductor devices

The organic semiconductors are promising materials to be used in organic electronics and optoelectronics devices. **[73–75]** The different properties and structure of the organic molecular layers determine the performance of the organic electronics devices. Different kinds of organic electronics and optoelectronics devices demand different properties of the layer structure. For instance, highly order monocrystalline structure is particularly required for high performance organic field effect transistors (OFETs) and organic photovoltaic devices (OPVs). **[76–78]** In contrast, amorphous structure with high uniformity and smooth surface formation is desirable for organic light emitting devices (OLEDs) because of the hopping-type charge transfer and highest quantum yield in amorphous structure layers.**[79]**

Different electronics and optoelectronics structure or configuration of devices required the different properties of semiconductor layers as molecular packing structure including molecular orientation and grain structure within the organic active layers. Among the development of various molecular based electronic devices, two typical devices OPVs and OTFTs are described here.

1.2.1 Organic Photovoltaics (OPVs)

The organic semiconductor layers serve as active layers in organic photovoltaics OPVs devices and it convert light energy to electricity. OPVs could be fabricated by using different device structures including single layer cells, and layers stacking of organic active layers as heterojunction cells, tandem cells and so on. The single layer structure of OPVs showed poor performance with power conversion efficiency less than 0.1% before the mid1980s.**[80]** In 1986, efficiency improvement become 1% have been achieved by stacking the bi-layer of electron donor (D) and electron acceptor (A) as heterojunction type solar cells.**[16]** The molecular blend

type co-deposited bulk heterojunction solar cell was developed by Hiramoto et al.**[81,82]** The different configurations of heterojunction OPVs are shown in **Figure 1.2**.

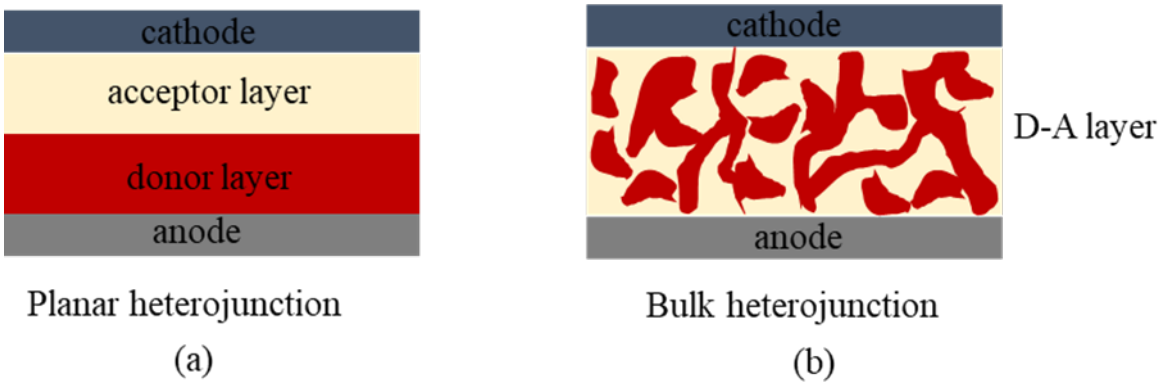

Figure 1.2 Schematic diagrams of structure of OPVs (a) bi-layer planar heterojunction (b) bulk-heterojunction.

In heterojunction cells, donor layer and acceptor layer of photoactive layers were sandwiched between two electrodes; cathode and anode. There are four basic principles **(in Figure 1.3)** for the operation of heterojunction OPVs. They are (1) light absorption and formation of excitons, (2) exciton diffusion to the donor-acceptor interface, (3) exciton dissociation, and (4) charge carrier transport and charge collection at the electrodes. **[83]**

When the solar spectrum is directed onto the organic semiconductor layer and absorption of photons which lead to the electron-hole pairs of excitons formation in the first step of the operations. After absorption of light, photo generated excitons diffuse inside the layer within a few nanometer range 5-20 nm.**[84]** Since the exciton diffusion length in organic semiconductor have a limitation, it is required for exciton to reach a donor-acceptor interface. Exciton dissociation occurs at the donor-acceptor interface when the difference in energy level of LUMO

of donor and acceptor is higher than exciton binding energy. Exciton recombination may happen when excitons do not reach the donor-acceptor interface, and in this case, photocurrent could not be generated. Exciton dissociation is one of the crucial steps for performance of the OPVs which is affected by the interface structure as the planar heterojunction or bulk heterojunction. The excitons require to dissociate at the donor-acceptor interface in order to collect the charge at the electrodes. It is clearly seen that these process of the OPVs are affected by the structure including orientation, morphology, and grain structure of the donor-acceptor layers.**[17][85]**

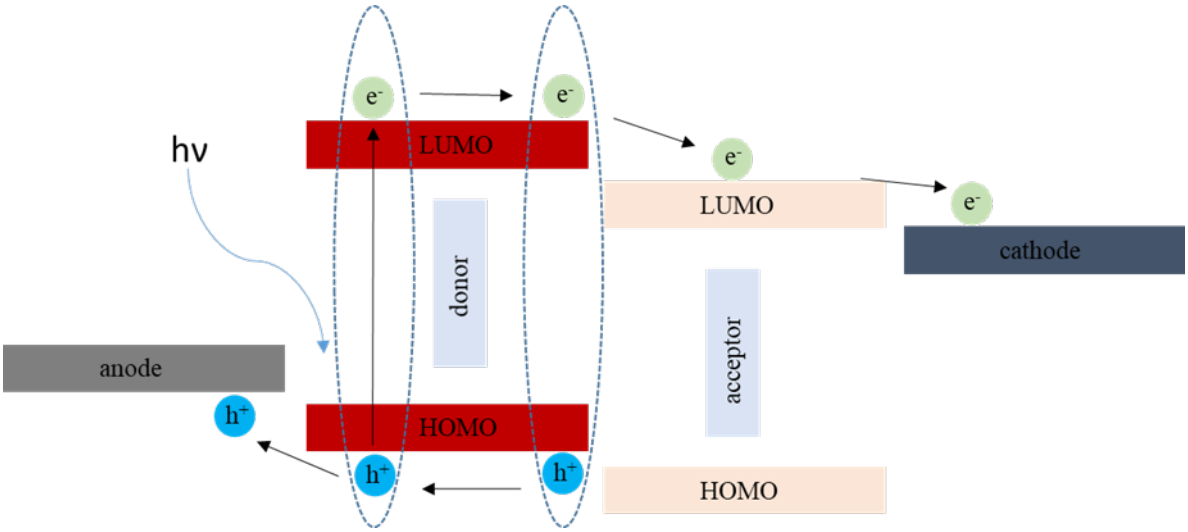

Figure 1.3 Schematic diagram of basic principles for the operation of heterojunction OPVs (1) light absorption and formation of excitons, (2) exciton diffusion to the donor-acceptor interface, (3) exciton dissociation, and (4) charge carrier transport and charge collection at the electrodes.

1.2.2 Organic Field Effect Transistors (OFETs)

Organic Field Effect Transistors are fundamental building block for electronic devices as displays, sensors, radio frequency identification tags and so on.**[9,10][86,87]** Generally, OFETs can be fabricated by three basic layers (1) Organic semiconductor layer (2) three-electrodes (gate, source and drain), and (3) an insulating layer. Four basic types of conventional OFETs device structures are shown in **Figure1.4**.

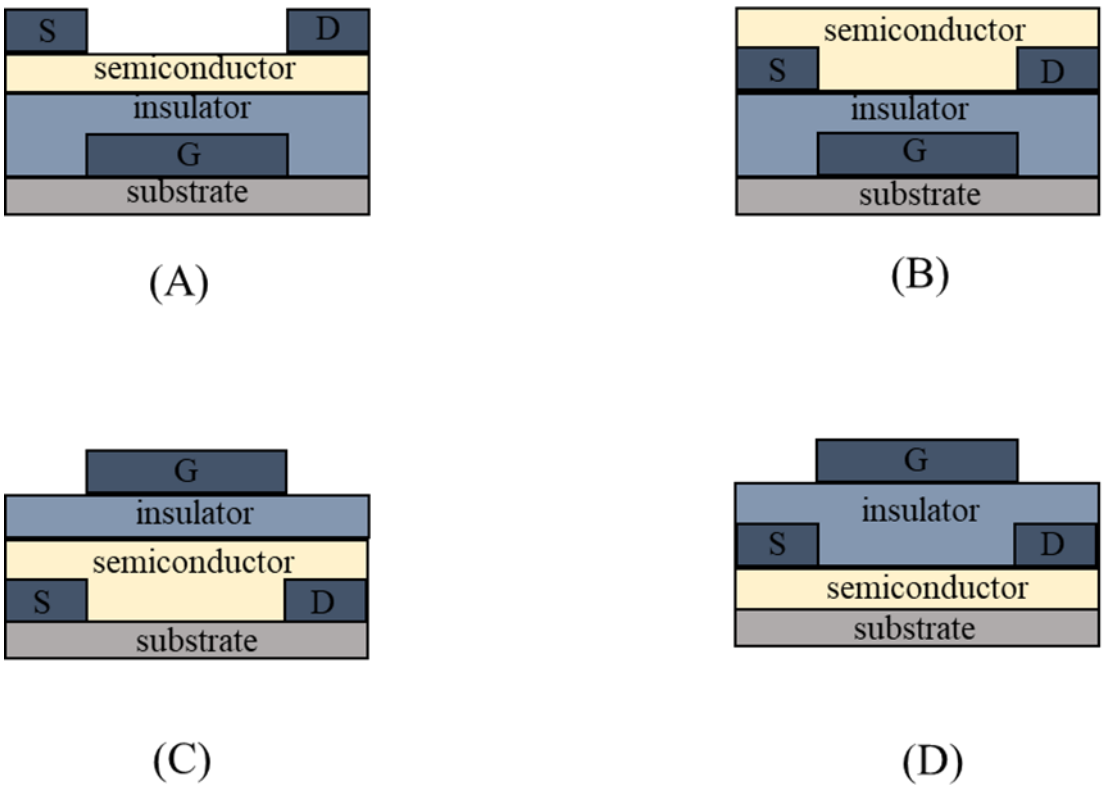

Figure 1.4 Schematic diagrams of typical structure of FETs (A), (B) Bottom-gate, and (C), (D) Top-gate.

Basically, two ohmic contacts of the source and drain electrodes are stacking together with organic semiconductor layer and gate electrode is in contact with an insulating layer. The density of charge carrier are formed at the insulator-organic semiconductor interface when the

voltage is applied to the gate electrode. It provides the conducting channel between the source and drain.**[75][88,89]**

High crystalline structure of organic thin films are required for OFETs in order to obtain high charge carrier mobility. It is possible to achieve the high carrier mobility device since the charge transport direction is directly linking to the molecular orientation; for example, the standing up molecular orientation and lying down molecular orientation in the system of the active layer. In the molecular layers with standing up molecular orientation; that is, π-π stacking direction is parallel to the substrate, in this case, device structure in **Figure 1.5** could be considered as suitable device structure because charge transportation direction meets the π-π stacking direction. The lying down molecular orientation, i.e, π-π stacking direction is nearly normal or perpendicular to the substrate, in this case, different configurations as in **Figure 1.6** is required to meet high carrier mobility in charge transportation process.**[90]**

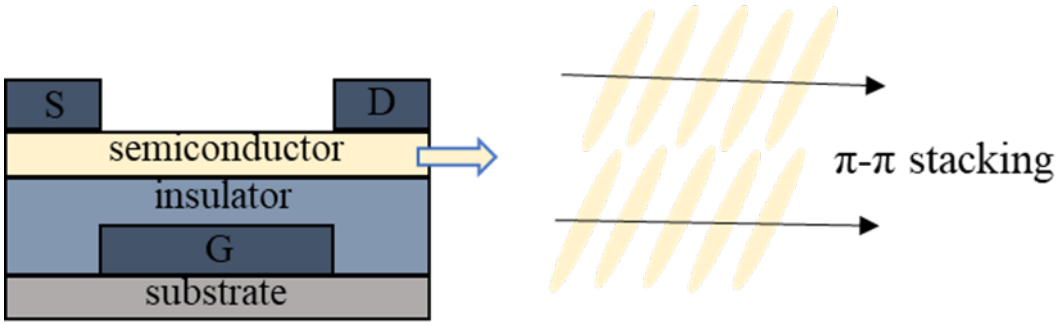

Figure 1.5 Structure of conventional OFET with lateral π-π stacking direction of molecules in organic semiconductor layer.

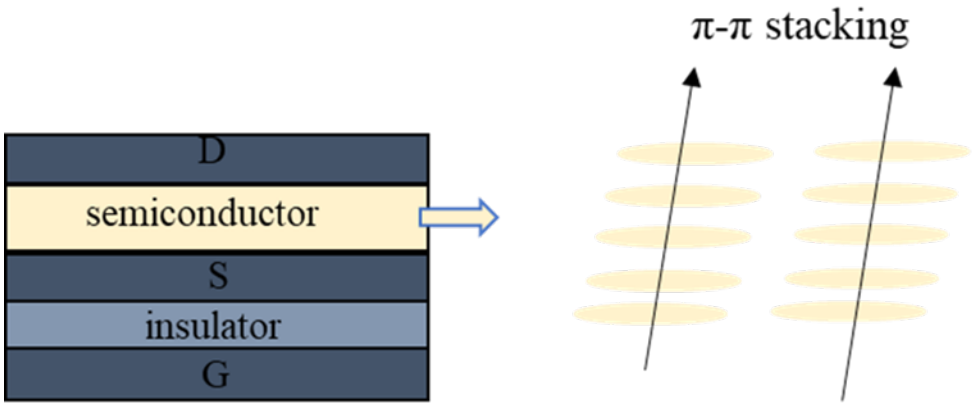

Figure 1.6 Structure of vertical-structure OFET (VOFET) with vertical π-π stacking direction of molecules in organic semiconductor layer.

1.3 Importance of the growth control to enhance the performance

The growth of organic semiconductors; single crystal growth to molecular thin film growth have been widely studied because of their application in organic electronics.**[91]** The performance of the organic devices mainly depend on charge carrier transport in molecular layers. The charge carrier transport from one molecule to another along π-molecular orbital and related to the electron cloud splitting with its nearest molecules. The overlapping degree of neighboring molecular orbital within packing structure determine the charge carrier transport in organic semiconductor which turn linking to the electrical properties.**[92]** In semiconductor, the electrical conductivity is the transport of the electric current density. The drift current density J^{drift} is proportional to the carrier drift velocity, carrier concentration and charge carrier. It can be written as follows;

$$J_n^{drift} = -q\, n\, v_{dn} = q\, n\, \mu_n E \qquad (1.1)$$

$$J_p^{drift} = q\, p\, v_{dp} = q\, p\, \mu_p E, \qquad (1.2)$$

where, drift velocity for electrons $v_{dn} = -\mu_n E$, **[93]** and drift velocity for holes $v_{dp} = \mu_p E$

n = carrier concentration of electrons, p = carrier concentration of holes, q = electric charge carrier.

The total drift current density can be expressed as

$$J^{drift} = J_n^{drift} + J_p^{drift} = q\,(n\,\mu_n + p\,\mu_p)\,E \quad (1.3)$$

According to Ohm's Law, $J = \sigma E = E/\rho$, where, σ = conductivity and ρ = resistivity

For n-type semiconductor, $$\rho_n \approx \frac{1}{q\,n\,\mu_n} \quad (1.4)$$

For p-type semiconductor, $$\rho_p \approx \frac{1}{q\,p\,\mu_p} \quad (1.5)$$

The diffusion length of the carrier can be expressed as,

$$L_D = \mu_n \tau_n E, \quad (1.6)$$

$$L_D = \mu_p \tau_p E \quad (1.7)$$

Where, μ_n and μ_p are the hole and electron drift mobility, τ_n and τ_p are trapping lifetime of the electrons and holes, and E is the electric field.

The charge transport properties of a deposited semiconductor layer can be determined by the charge carrier mobility so that the charge carrier mobility is the key of the determining factor for the performance of the organic based electronic devices. The charge carrier diffusion and mobility of organic semiconductor strongly depends on the prepared layer structure and orientation including grain structure of the deposited layer.**[90]** And randomly orientated and oriented molecular structure **(Figure 1.7)** are also determining the charge transfer processes in layers. The randomly orientated layer with disordered layer could reduce the carrier diffusion length. The higher crystalline order with oriented layer favored to improve the exciton diffusion length which is leading to the high performance film. **[94]**

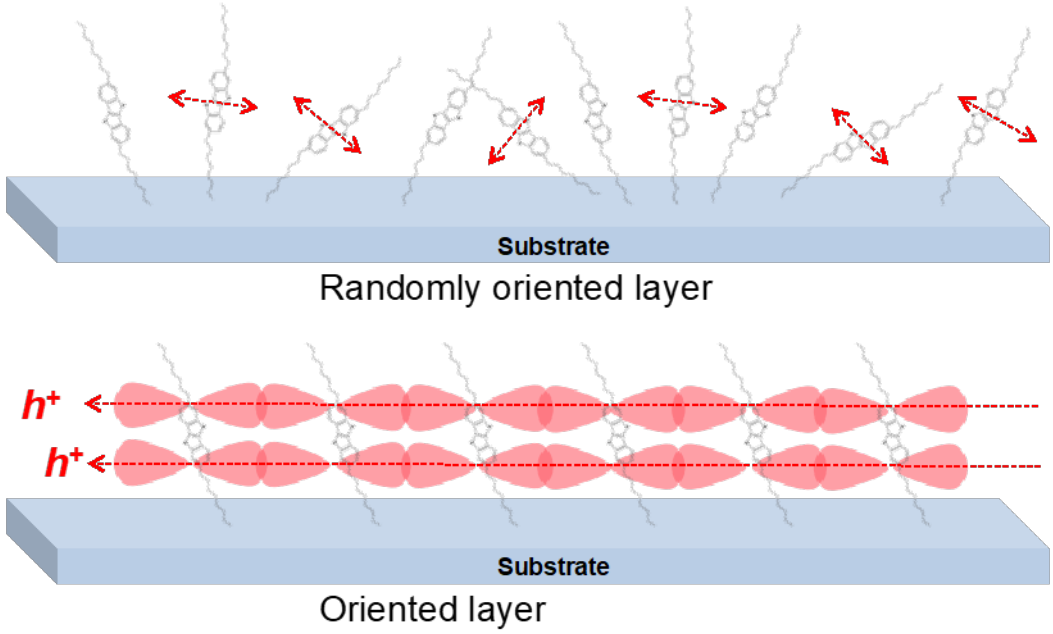

Figure 1.7 Schematic illustration of organic layer structure (a) randomly oriented (b) oriented layer on substrate.

A large charge carrier mobility is demanded for all electronic applications. It is speculated that the mobility of the organic semiconductor mainly relies on the transfer integral and reorganization energy and both of these are very important parameters in molecular packing structure.**[95,96]** The transfer integral is the splitting of the highest occupied molecular orbital (HOMO) and the lowest unoccupied molecular orbital (LUMO) which define the distance between π-overlapping distances with neighboring molecules. The reorganization energy is the energy loss when a charge carrier passes through a molecule and is dependent on the conjugation length, degree, and packing of the organic molecules. It is believed that the large transfer integral and low reorganization energy turn out to be high carrier mobility.**[97–100]** Hence, these two parameters which in turn depend on the molecular packing structure of the organic semiconductors.

In general, it is well known that four different kinds of molecular packing structure; Herringbone stacking without π-π overlapping between adjacent molecules, Herringbone stacking with π-π overlapping between adjacent molecules, Lamellar 1D-π-stacking and Lamellar 2D-π-stacking which are shown in **Figure 1.8.[5][101]** Most of studies in molecular based device performance have proven that the molecular packing structure is a key role in charge transport process. In addition to packing structure, crystallinity, orientation, grain structure and morphology are also the factors influencing the performance.**[102–104]**

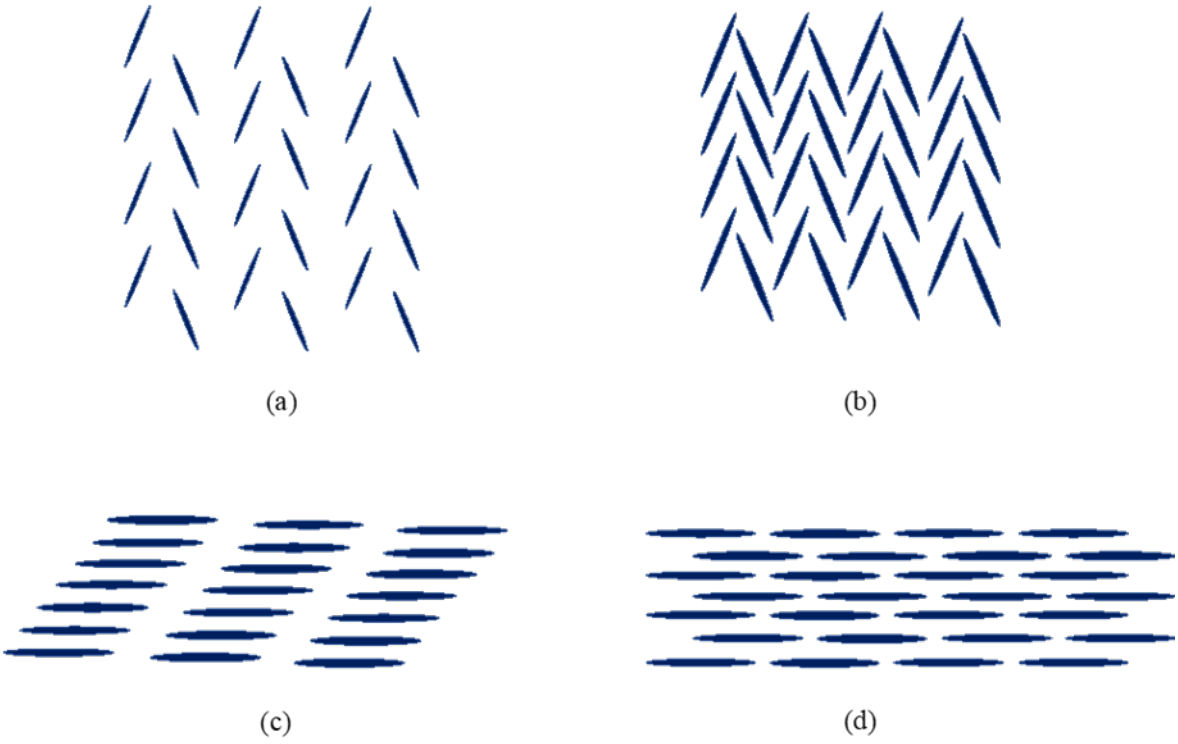

Figure 1.8 Four typical packing structure of conjugated molecules (a) Herringbone stacking without π-π overlapping between adjacent molecules (b) Herringbone stacking with π-π overlapping between adjacent molecules (c) Lamellar 1D-π-stacking (d) Lamellar 2D-π-stacking.

It has been speculated that internal ordering of the organic layers structure could enhance the charge carrier mobility. The performance of the device efficiency could be improved by controlling the structure of semiconducting layers. In order to deposit the ordered semiconducting molecular layers, many techniques have been used including solution deposition, organic molecular beam epitaxy (OMBE) and vacuum deposition and so on.**[104–107]** It has been proved that the quality of the films depends not only on the preparation techniques but also affected by the parameters like choice of substrate materials, deposition rate, layer thickness, substrate temperature during deposition process. Moreover, surface tuning method as self-assembled monolayer (SAM) which is the first prior to deposition of organic semiconductor layers have been able to improve the order of the molecular structure and morphology.**[108]**

The charge carrier transport as electrical properties and light absorption as optical properties of films depend mainly on the molecular packing and orientation. It has been reported that the orientation of the α,ω-dihexyl-sexithiophene (DH6T) and α-sexithiophene (6T) could be controlled by using Ag(111) substrate, in such case, long axis of molecules are almost normal to the substrate (upright standing) or lying down on the substrate.**[109]** One of the structure controlling could be done by substrate materials and the manipulating the interface between molecule and substrate materials. The π-conjugated based organic thin films exhibit anisotropic properties so that the molecular orientation could be tuned.

Therefore, controlling the growth of the prepared layers and characterization of the deposited layers together with understanding of the structure including preferred orientation, grain structure and morphology of the deposited organic layers support the information of how to design and fabricate for quality controlled high-performance electronic devices.

1.4 Growth of inorganic and organic thin films and preparation techniques for organic layers

1.4.1 General concepts of thin film growth

Thin film growth are very important for many applications including coating and semi-conductor devices. The physical mechanism of adsorption, surface diffusion, chemical binding and atomic processes at surface and interface were in the process of the thin film growth. And, deposition parameters as deposition rate, and substrate temperature effect the growth of thin films. Generally, thin films were deposited on substrate material, and there are two modes of growth which depend on how the relation occur between the substrate and films, homoepitaxial growth in which crystallographic relation between the substrate and film are under epitaxial, heteroepitaxial growth in which the relation between the substrate material and films are not identical. Thin film growth is controlled by thermodynamics and kinetics. Three scenarios have been described based on the growth modes depending on the interaction between surface and interface energies. There are three different growth modes Frank-van der Merwe (layer-by-layer), Volmer-Weber (islands), Stranski-Krastanov (layer plus islands) according to the surface energies such as the substrate surface (γ_s), the film surface (γ_f), and the surface-film interface (γ_i). The growth modes are shown in **Figure 1.9**. **[110,111]**

The layer-by-layer growth is the 2D growth which is the one monolayer tends to be completely covered before the next layer formed. The continuous layers with less number of defects formed in 2D growth mode. The 2D layer-by-layer growth could be achieved for epitaxial growth,i.e, lattice-matched materials. The Volmer-Weber growth or islands growth is the formation of three dimensional islands. In this mode, atoms or molecules are strongly bound to each other than to the substrate which leads to the 3D islands. In the Stranski-Krastanov growth mode, islands are formed after forming the first few layers. In this growth mode, a transition of growth modes 2D layer-by-layer growth to 3D islands growth happens.

The Volmer-Weber and Stranski-Krastanov growth modes tend to form the formation of amorphous or polycrystalline structrue.

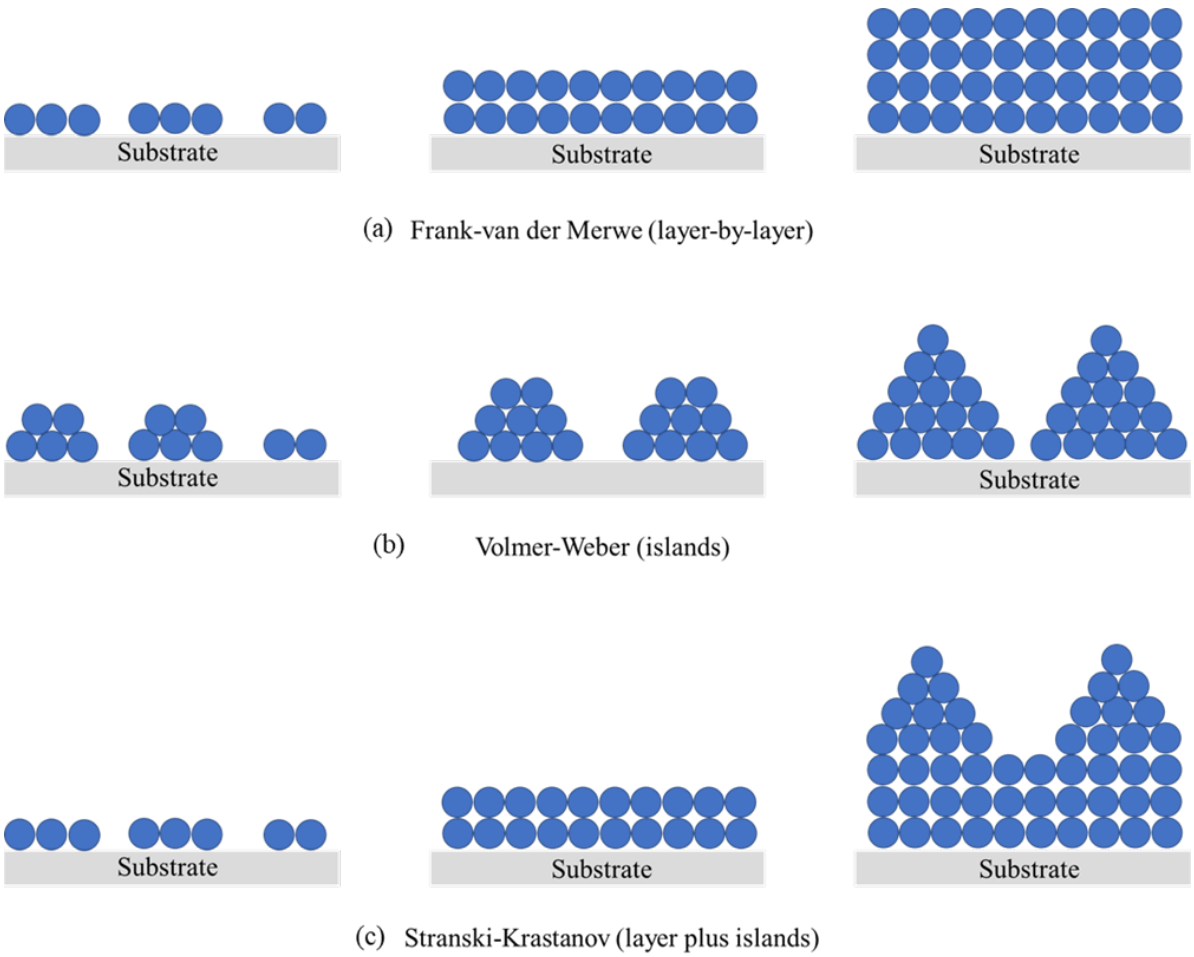

Figure 1.9 Schematic illustration of the growth modes: (a) Frank-van der Merwe (layer-by-layer), (b) Volmer-Weber (islands), (c) Stranski-Krastanov (layer plus islands).

Heteroepitaxial growth is crucial for fabricating semiconductor devices. The lattice relation between the deposited film and substrate determine the quality of the films. For example, inorganic thin film of ZnO were prepared on Au(111) and the lattice mismatch between film and substrate is (1x1)ZnO(0001)[11$\underline{2}$0]//(1x1)Au(111)[110] 12.7%. This film showed randomly oriented ZnO layer with poor performance. The quality of the thin film could

be improved by controlling the substrate with lattice matching. The ZnO film prepared on Ga:ZnO film with the lattice relation of (1x1)ZnO(0001)[11$\underline{2}$0]//Ga:ZnO(0001)[11$\underline{2}$0] in mismatch 0.8%. That improved ZnO films showed the (0001) oriented ZnO with good performance.**[112]** Hence, the interface between the film and substrate material in order to get the good quality film could be controlled by substate materials.

1.4.2 Preparation techniques for organic semiconductors and organic thin film growth

Organic semiconductors have different kind of properties and it has been used in wide range of applications; conductive coatings, flexible light sources and displays, low-cost printed integrated circuits, and plastic solar cells. Generally, organic semiconductors can be divided into two major classes: conjugated polymers and conjugated low-molecular weight materials (small-organic molecules). Since chemical properties of these materials are different, two major processing methods were performed in order to form organic thin films; solution-processed deposition and dry-processed deposition.

Polymeric macro-molecules are composed of repetition of monomer, and they are soluble in organic solvents so that they can be deposited by solution process. For example, the alkyl-substituted polythiophenes, poly(3-hexylthiophene) (P3HT) is a type of highly soluble polymer in a various kind of organic solvents **[28]** and those kinds of soluble polymers have been prepared by solution process (also called wet processing) such as spin-coating, dip-coating, drop coating, screen printing, inkjet-printing and so on.

There are two sub-group of small-organic molecular materials; pigments which are insoluble in organic solvents, and dyes which are soluble. In the case of deposition of small organic molecules, since most of small-organic molecules are insoluble in organic solvent, they are deposited by dry processes as thermal vacuum evaporation or thermal sublimation in vacuum. The promising materials and widely studied of small-organic molecules are pentacene,

sexithiophene and copper phthalocyanine. Whatever, it is still challenging the controlled growth of organic semiconductor layers by using solution process or vacuum process.

Organic Thin Film Growth

Organic thin film growth exhibit different growth behaviors as compared to the inorganic thin film growth. Inorganic semiconductors are composed of covalent bonding between neighboring atoms while organic semiconductors are established by weak van der Waals forces between molecules. Hlawacek et.al demonstrated that the additional effects of organic thin film growths which are not observed in atomic inorganic growth. **[113]**

Organic molecules are anisotropic objects and which have internal degrees of freedom including the orientational degree of freedom and the vibrational degree of freedom. The orientational degree of freedom **(Figure 1.10)** which is a new phenomenon because the orientation of molecule may change during the growth, for instance, the long axis of molecules almost upright position on the substrate, and the long axis of molecules almost lying down position. One of the difference between inorganic and organic thin film growth is that this qualitative phenomenon of orientational degree of freedom are not included in metal or inorganic thin film growth. The vibrational degree of freedom effect to the diffusion behavior of molecules on the substrate surface, and the interaction between substrate and deposited layer.**[114]**

Another point of difference between organic thin film growth and inorganic film growth is that interaction potential. The interaction between molecules, in such case, van der waal interaction in molecule-molecule, and atomic absorption between substrate-molecule interaction which are different. A close lattice matching is required for conventional inorganic semiconductor thin films growth due to avoid the high density of misfit dislocations. Contradictory

to inorganic growth system, it has been found that the crystalline order can be achieved in organic growth system even though the molecule and substrate materials mismatch are highly different.

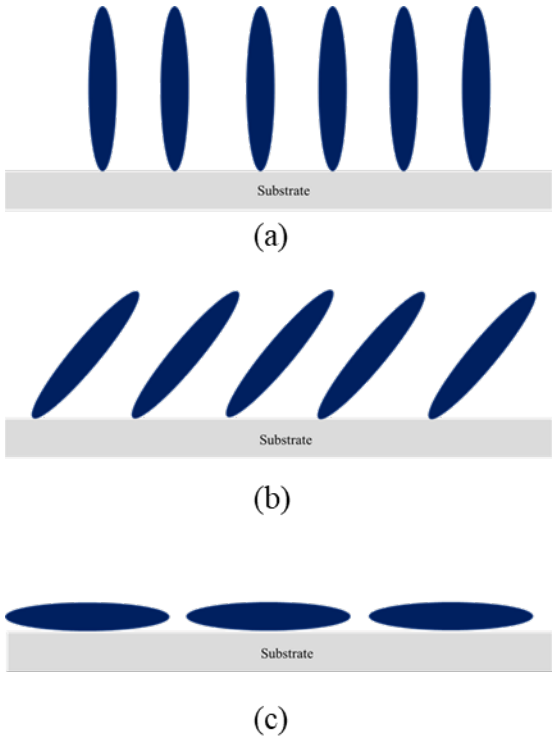

Figure 1.10 Schematic illustration of organic thin film growth (a) upright position (b) almost standing position with the orientational degrees of freedom (b) lying down position on the substrate.

The size differences between unit cells of the molecules and substrates which can cause the low-symmetry structure with multiple domains.**[111]** The surface of the substrate with dangling bonds limited the diffusion and this may lead to disorder film formations because the molecules may dissociate.

1.5 Organic Semiconductor Materials investigated in this work

In this thesis, we examined the growth and characteristics of the vacuum-evaporated donor and acceptor type organic molecules of 2,7-dioctyl[1]benzothieno[3,2-b][1] benzothiophene (C8-BTBT) and N,N'-dioctyl-3,4,9,10-perylenedicarboximide (PTCDI-C8) on single crystal substrates. Both of these molecules compose of conjugated core and alkyl side chains.

Donor type: 2,7-dioctyl[1]benzothieno[3,2-b][1] benzothiophene (C8-BTBT)

Acceptor type: N,N'-dioctyl-3,4,9,10-perylenedicarboximide (PTCDI-C8)

The choice of C8-BTBT and PTCDI-C8 molecules is motivated by the reason of they are promising materials to be used in optoelectronics devices and high carrier mobility values have been obtained. The chemical structure of C8-BTBT and PTCDI-C8 are shown in **Figure 1.11**.

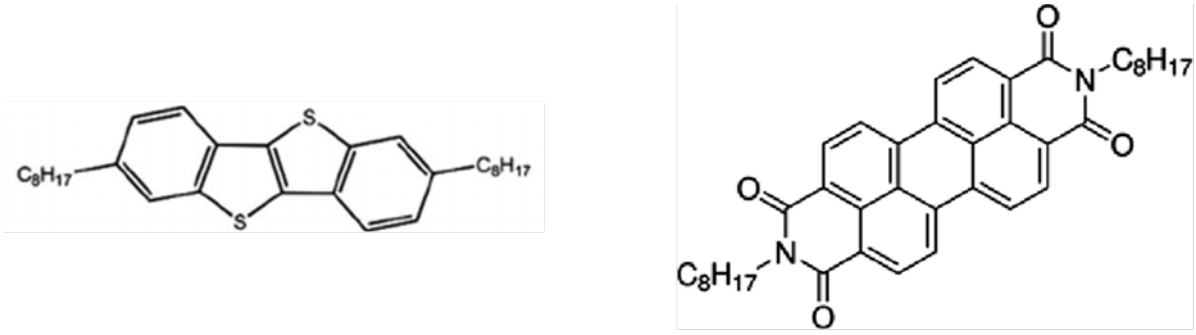

(a) (b)

Figure 1.11 The chemical structures of small conjugated molecules (a) 2,7-dioctyl[1]benzothieno[3,2-b][1]benzothiophene (C8-BTBT), and (b) N,N'-dioctyl-3,4,9,10-perylenedicarboximide (PTCDI-C8).

2,7-dioctyl[1]benzothieno[3,2-b][1] benzothiophene (C8-BTBT)

2,7-dioctyl[1]benzothieno[3,2-b][1] benzothiophene is a member of BTBT derivatives and it is one of the promising materials to be used in electronic devices. The empirical formula C_{30} H_{40} S_2 with a formula weight 464.77 g/mol and the melting point is at 108-112 °C. This molecule consists of a one BTBT core and two alkyl chains with a lamella-like alternating structure which is shown in **Figure 1.12**. It is monoclinic lattice structure with a space group of $P2_1/a$.**[115]** The crystallographic unit cells of C8-BTBT are shown in **Table 1.2**.

Table 1.2 Crystallographic unit cells of C8-BTBT

	a (nm)	b (nm)	c (nm)	α (deg)	β (deg)	γ (deg)
C8-BTBT	0.5927	0.788	2.918	90	92.443	90

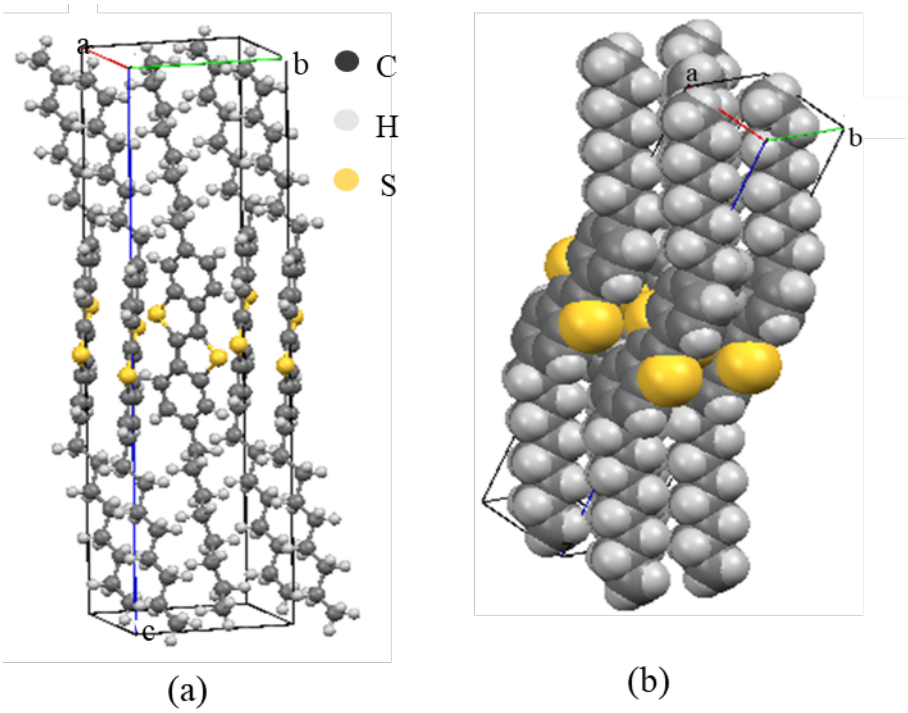

Figure 1.12 Molecular packing structure of 2,7-dioctyl[1]benzothieno[3,2-b][1]benzothiophene (C8-BTBT), (a) ball and stick structure, (b) space filling structure.

N, N'-dioctyl-3,4,9,10-perylenedicarboximide (PTCDI-C8)

N,N'-dioctyl-3,4,9,10-perylenedicarboximide (PTCDI-C8) is one of the perylene derivatives and has been used in active layer of electronic and optoelectronic applications. The chemical formula is C_{40} H_{42} N_2 O_4 with a molecular weight of 614.77 g/mol and the melting point is above 300 °C. This molecule is composed of a perylene core and two alkyl side chains with herringbone crystal structure. A schematic diagram of PTCDI-C8 is shown in Figure **1.13.** It belongs to triclinic lattice structure with space group $P\bar{1}$. The crystallographic structure of PTCDI-C8 has been characterized by A. L. Briseno et.al.**[116,117]** The structure of PTCDI-C8 parameter slightly altered according to the phase of thin film or bulk. The crystallographic data of both types are given in Table 1.3.

Table 1.3 Crystallographic unit cells of PTCDI-C8 thin film and bulk structure

	a (nm)	b (nm)	c (nm)	α (deg)	β (deg)	γ (deg)
PTCDI-C8 (Thin film)	0.900	0.489	2.165	95	100.7	112.8
PTCDI-C8 (Bulk)	0.850	0.468	1.972	88.43	94.01	97.21

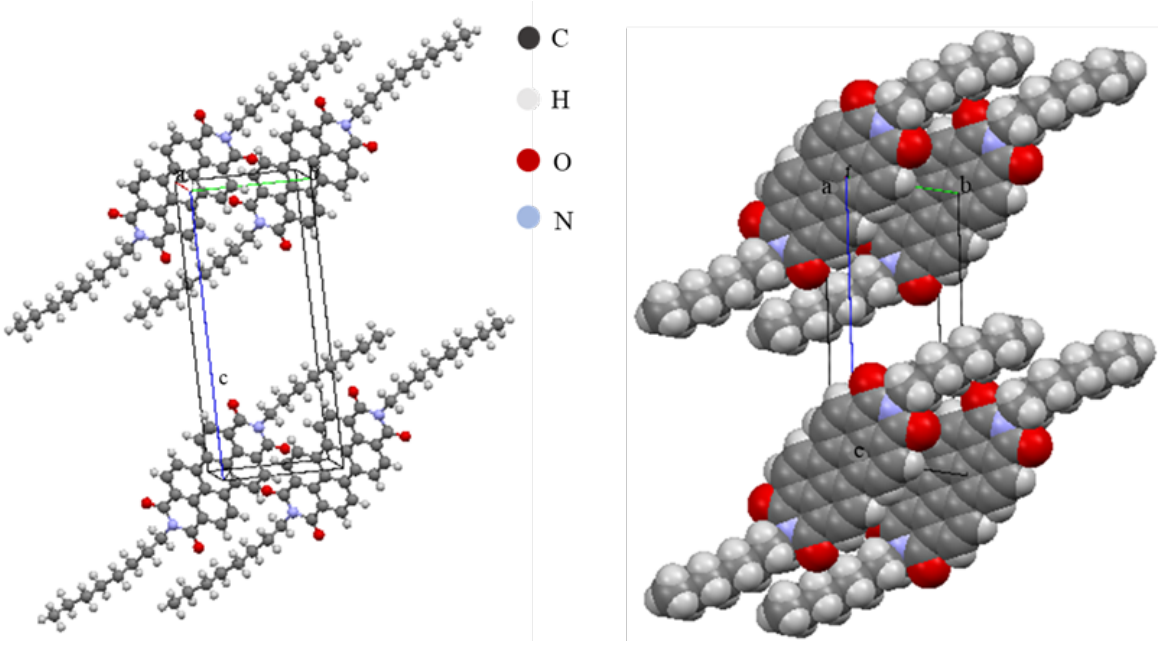

Figure 1.13 Molecular packing structure of N,N'-dioctyl-3,4,9,10-perylenedicarboximide (PTCDI-C8), (a) ball and stick structure, (b) space filling structure.

1.6 Growth of organic molecules C8-BTBT and PTCDI-C8

This work mainly focuses on the fabrication and growth of conjugated small-organic molecular based materials by vacuum thermal evaporation technique. Vacuum thermal evaporation can be used to deposit the small-organic semiconductor materials which are insoluble in organic solvents. **Figure 1.14** shows the vacuum evaporation system used in this work.

Figure 1.14 Vacuum Thermal Evaporation System

Vacuum evaporation take place inside the bell jar and are equipped with a turbo-molecular pump and oil free scroll pump for evacuation process. The filament which acts as heating up for the source materials, and crucible, sensor head and substrate holder are installed inside the vacuum chamber. Water cooling pipes are equipped to the chamber externally. For controlling the evaporation process of thickness and deposition rate during deposition, the quartz

crystal microbalance sensor is equipped between the crucible and shutter and connect with controller. When the current applied to source materials through filament under vacuum, the evaporated materials is deposited on the substrate which is placing upside down position on the substrate holder. Vacuum thermal evaporation technique offers to control the formation of thin film by the deposition parameters; such as deposition rate, substrate temperature, and layer thickness. The vacuum evaporation technique is capable of precise control of the film thickness and producing the multilayer thin films.

The surface state of the deposited layers is strongly influenced by the thin-film growth, including the choice of the substrate materials and substrate temperature, flux density and the rate of the deposited materials and so on. The growth of organic thin film directly influences the properties of organic semiconductors such as absorption, charge carrier mobility and energy levels, etc. High charge carrier mobility have been obtained by controlling the organic thin film growth, and minimize the defect concentration and grain boundaries. Since film structure including molecular ordering, orientation, morphology, roughness and defect densities are consequence of the growth, manipulation and engineering of the film growth become indispensable. And, it is also needed to understand the mechanisms for the growth of organic films to optimize the film structure. The kinetic and thermal properties of molecules during deposition process, the driving forces, interaction between surface and interfaces, etc., and these factors impact the growth and nucleation of deposited molecules.

1.7 Design of the growth of the C8-BTBT and PTCDI-C8

In this thesis, C8-BTBT and PTCDI-C8 have been used as an organic semiconducting materials and it is required to understand the growth and structure of these organic molecules by vacuum thermal evaporation on single crystal substrates. In the growth of molecular thin films, the orientation of the molecules in single layer, bi-layer and multilayers with respect to substrate depends mainly on the molecule-substrate interaction or molecule-molecule intermolecular interaction. The role of substrate type strongly influence on the interface between substrate-molecule, and on the growth of organic layers. Therefore, characterization of the layer structure of the organic semiconductor with respect to substrate material and understanding of the molecular packing structure in prepared layers are important role to determine the optical properties as light absorption, and electrical properties as charge carrier transport. It is also evidence that deposition parameters effect the growth of organic semiconductors.

In this study, we designed the heteroepitaxial growth of π-conjugated organic semiconductors on quartz glass, (11$\underline{2}$0) A-, (0001) C-, and (1$\underline{1}$02) R-single crystal Al_2O_3 (sapphire), and (100)-, and (111)-single crystal MgO substrates by vacuum thermal evaporation. These layers were deposited with different layer thickness and different substrate temperature. The influence of substrate materials, layer thickness and substrate temperature has been investigated for structural properties, optical properties of light absorption and electrical properties of the deposited organic layers. Understanding the structure and controlling the grain structure of deposited molecules on substrates could be an effective way to progress in organic electronic devices.

1.8 Research objectives

Our research work is focusing on heteroepitaxial growth of organic layers on single crystal substrates which are of interest as this structures and configurations are applied in organic based electronic devices. The development of organic electronics mainly depends on the optical and electrical properties of the prepared organic layers. Low crystallinity and random orientation of the prepared layer limit the carrier mobility. On the other hand, organic based devices require highly ordered structure of crystalline properties with preferred orientation. The choice of substrate type has made possible to control the structure and morphology of the organic layers. And also, deposition parameters as layer thickness and substrate temperature were also possible to control the structure of layers including morphology, grain structure and surface roughness. Therefore, characterization of the growth and structure of the organic layers is crucial for performance of devices. Several information including the following points are required for the field of organic based applications.

- To investigate the structure and morphology of heteroepitaxial growth of organic semiconductor molecule C8-BTBT on inorganic single crystal aluminum oxide and magnesium oxide substrates with various orientations.

- To investigate the structural, morphological, optical and electrical properties of C8-BTBT organic layer on single crystal C-sapphire substrate with the effect of layer thickness and substrate temperature.

- To investigate the growth, structure and optical characteristics of vacuum evaporated PTCDI-C8 layer on single crystal substrates of A-, C-, R- sapphire, and (111)-MgO, and (100) MgO substrates.

- To investigate the surface state and morphology of the bi-layer structure of C8-BTBT and PTCDI-C8 by different stacking sequences.

The overall objective of this thesis is to investigate and control of interfaces between organic–organic and organic-single crystal substrate in order to improve the performance of organic devices.

1.9 Outline of this study

In this thesis, we study the growth of π-conjugated organic molecules 2,7- dioctyl[1] benzothieno[3,2-b]benzothiophene (C8-BTBT) and N,N'-dioctyl-3,4,9,10-perylenedicarboximide (PTCDI-C8) deposited on single crystal sapphire and MgO substrates. The designing of the molecular layers with preferred orientation has been prepared by using vacuum thermal evaporation technique. The dependence of optical and electrical properties on the structure and morphology of organic molecular layers were demonstrated. Moreover, the effect of layer thickness and substrate temperature variation on the structure and morphology of deposited molecular layers were described. The structure of the organic layer strongly impacts on the optical and electrical properties of the devices. Since the molecular based electronic devices performance is mainly rely on the deposited organic layers, understanding the formation of layer, i.e structure, which optimize the future progress of the technology of electronic and optoelectronic molecular based devices.

Chapter two gives the growth of p-type organic semiconductor 2,7-dioctyl[1]benzothieno[3,2-b]benzothiophene (C8-BTBT) on quartz glass, (11$\underline{2}$0) A-, (0001) C-, and (1$\underline{1}$02) R-single crystal Al_2O_3 (sapphire), and (100)-, and (111)-single crystal MgO substrates by vacuum thermal evaporation. The morphology and structure of C8-BTBT layers on single crystal substrates with various orientations were investigated by atomic force microscopy (AFM) observations and X-ray diffraction (XRD) analysis. The growth of C8-BTBT on single crystal substrates shows that molecule-molecule interaction is stronger than the molecule-substrate interaction according to π-π-stacking-induced molecular ordering with (001) out-of-plane orientation development regardless of substrate material and orientation.

In **chapter three**, organic semiconductor 2,7-dioctyl[1]benzothieno[3,2-b] benzothiophene (C8-BTBT) were deposited only on a single crystal (0001)Al_2O_3 (C-sapphire) by vacuum thermal evaporation. The effects of layer thickness and preparation temperature on structural,

morphological, optical and electrical characteristics were investigated by X-ray diffraction analysis, atomic force microscopy observation, optical absorption measurement, and resistivity measurement with and without light irradiation. C8-BTBT layers on C-sapphire substrate show (001) out-of-plane orientation irrespective of the preparation conditions; layer thickness and substrate temperature. The C8-BTBT layer was formed by the growth of (001)-C8-BTBT islands in direction parallel to the substrate surface and then the growth in direction normal to the substrate surface after the formation of the continuous layer.

In **chapter four**, the growth of vacuum evaporated N,N'-dioctyl-3,4,9,10-perylenedicarboximide (PTCDI-C8) layers on single crystal Al_2O_3 and MgO substrates with various orientations were investigated by X-ray diffraction analysis and atomic force microscopic observation. The optical band gap energy was estimated from optical absorption spectra. The growth of the PTCDI-C8 was governed by the π-π stacking like the C8-BTBT growth.

Chapter five presents the fabrication of bi-layer structure with different stacking sequence of 2,7-dioctyl[1]benzothieno[3,2-b][1]benzothiophene (C8-BTBT) and (001)-N,N' dioctyl-3,4,9,10-perylenedicarboximide (PTCDI-C8) on (0001) Al_2O_3 (C-sapphire) substrate by vacuum thermal evaporation. The orientation, morphology and surface state of vacuum evaporated bi-layers of C8-BTBT and PTCDI-C8 on C-sapphire substrate were investigated by X-ray diffraction and scanning probe microscopy (SPM). The stacking sequence strongly affected to the morphology and surface potential of the bi-layer C8-BTBT and PTCDI-C8 layers.

Finally, **chapter six** gives a short summary of the results observed from our experiments.

REFERENCES

[1] F.M. Li, A. Nathan, Y. Wu, and B. S. Ong, Organic Thin film Transistor Integration: A Hybrid Approach, First Edition, Wiley-VCH Verlag GmbH and Co.KGa A. 1-12 (2011).

[2] M.O. Neill, S.M. Kelly, Ordered Materials for Organic Electronics and Photonics, Adv. Mater., **23**, 566 (2011).

[3] K. Asadi, M. Li, P.W.M. Blom, M. Kemerink, D.M. De Leeuw, Organic ferroelectric opto-electronic memories, Mater. Today., **14**, 592 (2011).

[4] Y. Lin, X. Zhan, Small molecule semiconductors for high-efficiency organic photovoltaics, Chem. Soc. Rev., **41**, 4245 (2012).

[5] C. Wang, H. Dong, W. Hu, Y. Liu, D. Zhu, Semiconducting π-Conjugated Systems in Field-Effect Transistors:a material odyssey of organic electronics, Chem. Rev., **112,** 2208 (2012).

[6] H. Derivatives, J. Louis, A.G. Macdiarmid, Synthesis of Electrically Conducting Organic Polymers : Halogen Derivatives of Polyacetylene, $(CH)_x$, J Chem Soc Chem Comm, **474**, 578 (1977).

[7] Y.M. Yang, W. Chen, L. Dou, W. Chang, H. Duan, B. Bob, G. Li, Y. Yang, High-performance multiple-donor bulk heterojunction solar cells, Nat. Photonics, **9**, 190 (2015).

[8] H. Nothofer, U. Scherf, M. Gross, D.C. Mu, K. Meerholz, D. Neher, C. Bra, È.P. Chemie, Improving the performance of doped p -conjugated polymers for use in organic light-emitting diodes, Nature, **405**, 661 (2000).

[9] P.F. Baude, D.A. Ender, M.A. Haase, T.W. Kelley, D. V Muyres, S.D. Theiss, P.F. Baude, D.A. Ender, M.A. Haase, T.W. Kelley, D. V Muyres, S.D. Theiss, Pentacene-based radio-frequency identification circuitry Pentacene-based radio-frequency identification circuitry, Appl. Phys. Lett., **3964**, 10 (2006).

[10] S.J. Bardeen, W. Shockley, Organic thin film transistors, Mater. Today., **7**, 20 (2004).

[11] A.N. Sokolov, M.E. Roberts, Z. Bao, Fabrication of low-cost electronic biosensors sensors capable of operating in biologically relevant media, Mater. Today., **12**, 12 (2009).

[12] L. Zang, Y. Che, and J.S. Moore, One-Dimensional Self-Assembly of Planar π-Conjugated Molecules : Adaptable Building Blocks for Organic Nanodevices, Acc. Chem. Res., **41**, 1596 (2008).

[13] B. Mukherjee, K. Sim, T.J. Shin, J. Lee, M. Mukherjee, M. Ree, S. Pyo, Organic phototransistors based on solution grown, ordered single crystalline arrays of a π-conjugated molecule, J. Mater. Chem., **22**, 3192 (2012).

[14] S. Gunes, H. Neugebauer, and N.S. Sariciftci, Conjugated Polymer-Based Organic Solar Cells, Chem. Rev., **107**, 1324 (2007).

[15] B. Mukherjee, Large photoresponse from a small molecule: Application in photodetector and pseudo-transistor, Optik (Stuttg)., **126**, 1258 (2015).

[16] C.W.Tang, and S. A. VanSlyke, Organic electrolumescent diodes, Appl. Phys. Lett. **51**, 913 (1987).

[17] H. Hoppe, and N.S. Sariciftci, Organic solar cells: An overview, J. Mater. Res. **19**, 1924 (2004).

[18] A. Mishra, and P. Bäuerle, Small Molecule Organic Semiconductors on the Move : Promises for Future Solar Energy Technology, Angew. Chem. Int. Ed. **51**, 2020 (2012).

[19] C.D. Dimitrakopoulos, and D.J. Mascaro, Organic thin-film transistors: A review of recent advances, IBM J. Reasearch Dev. **45**, 11 (2001).

[20] W. Kowalsky, E. Becker, T. Benstem, H.H. Johannes, D. Metzdorf, H. Neuner, and J. Schöbel, Organic semiconductors: fundamentals and applications, Adv. Solid State Phys. **40**, 795 (2000).

[21] O. Abanoz, C. Dimitrakopoulos, Recent advances in organic field effect transistors, Turk J Phys. **38**, 497 (2014).

[22] C.D. Dimitrakopoulos, P.R.L. Malenfant, Organic thin film transistors for large area electronics, Adv. Mater. **14**, 99 (2002).

[23] G.H. Heilmeier, and L.A. Zanoni, Surface studies of α-copper phthalocyanine films, J. Phys. Chem. Solids, **25**, 603 (1964).

[24] F. Ebisawa, J. Kurokawa, S. Nara, J. Appl. Phys. **54**, 3255 (1983).

[25] K. Kudo, Field Effect Measurement of Organic Dye Films, Jpn. J. Appl. Phys. **23**, 230 (1984).

[26] A. Tsumura, H. Koezuka, T. Ando, Macromolecular electronic device : Fieldeffect transistor with a polythiophene thin film, Appl. Phys. Lett. **49**, 1210 (2013).

[27] J.H. Burroughes, C.A. Jones, and R.H. Friend, New semiconductor device physics in polymer diodes and transistors, Nature **335**, 137 (1988).

[28] A. Assadi, C. Svensson, M. Willander, O. Inganäs, A. Assadi, C. Svensson, M. Wiilander, O. Inganas, Fieldeffect mobility of poly (3hexylthiophene), Appl. Phys. Lett. **53**, 195 (2013).

[29] C. Clarisse, M. T. Riou, M. Gauneau, M. Le Contellec, Field-effect transistor with diphthalocyanine thin film, M. Elect. Lett. **24**, 674 (1988).

[30] J. Paloheimo, E. Punkka, H. Stubb, P. Kuivalainen, in Lower Dimensional Systems and Molecular Devices, Proceedings of NATO ASI, Spetses, Greece, Plenum, New York 1989.

[31] G. Horowitz, D. Fichou, X. Peng, Z. Xu, F. Garnier, M. Molrculaires, H. Dunant, R. March, M. Balkanski, A Field-effect transistor based on conjugated alpha-sexithienyl, Solid State Commun. **72**, 381 (1989).

[32] G. Horowitz, X. Peng, D. Fichou, F. Garnier, Role of the semiconductor/insulator interface in the characteristics of π-conjugated-oligomer-based thin-film transistors, Synth. Met. **51**, 419 (1992).

[33] F. Garnier, A. Yassar, R. Hajlaoui, F. Deloffre, P. Alnott, Molecular Engineering of Organic Semiconductors: Design of Self-Assembly Properties in Conjugated Thiophene Oligomers, P. J. Am. Chem. Soc. **115**, 8716 (1993).

[34] H. Fuchigami, A. Tsumura, H. Koezuka, Polythienylenevinylene thinfilm transistor with high carrier mobility, Appl. Phys. Lett. **63**, 1372 (1993).

[35] F. Garnier, R. Hajlaoui, A. Yassar, P. Srivastava, All-Polymer Field-Effect Transistor Realized by Printing Techniques,P. Science **265,** 1684 (1994).

[36] A. Dodabalapur, L. Torsi, H.E. Katz, Organic Transistors : Two-Dimensional Transport and Improved Electrical Characteristics, Science **268**, 270 (1995).

[37] C.D. Dimitrakopoulos, A.R. Brown, A. Pomp, C.D. Dimitrakopoulos, A.R. Brown, A. Pomp, Molecular beam deposited thin films of pentacene for organic field effect transistor applications Molecular beam deposited thin films of pentacene for organic field effect transistor applications, J. Appl. Phys. **80**, 2501 (1996).

[38] Z. Bao, A.J. Lovinger, A. Dodabalapur, Z. Bao, A.J. Lovinger, A. Dodabalapur, Organic fieldeffect transistors with high mobility based on copper phthalocyanine Organic field-effect transistors with high mobility based on copper phthalocyanine, Appl. Phys. Lett. **69**, 3066 (1996).

[39] Z. Bao, A. Dodabalapur, A.J. Lovinger, transistor applications with high mobility Soluble and processable regioregular poly (3-hexylthiophene) for thin film field-effect transistor applications with high mobility, J. Appl. Phys. Lett. **69**, 4108 (1996).

[40] Y.Y. Lin, D.J. Gundlach, T.N. Jackson, In 54th Annual Device Research Conference Digest, IEEE: Santa Barbara, CA, USA, p.80, (1996).

[41] Y.Y. Lin, D.J. Gundlach, S. Nelson, T.N. Jackson, IEEE Electrin Device Lett. **18**, 606 (1997).

[42] H. Sirringhaus, R.H. Friend, X.C. Li, S.C. Moratti, A.B. Holmes, Bis (dithienothiophene) organic field-effect transistors with a high ON/ OFF ratio, Appl. Phys. Lett. **71**, 3871 (1997).

[43] C.D. Dimitrakopoulos, A. Afzali-ardakani, B. Furman, J. Kymissis, S. Purushothaman, Trans- trans- 2,5- Bis- [2- {5- (2,2'-bithienyl)} ethenyl] thiophene : synthesis, characterization , thin film deposition and fabrication of organic field-effect transistors, Synthetic Metals, **89** 193 (1997).

[44] H. Sirringhaus, N. Tessler, R.H. Friend, Integrated Optoelectronic Devices Based on Conjugated Polymers, Science **280**, 1741 (1998).

[45] H.E. Katz, A.J. Lovinger, J.G. Laquindanum, α,ω -Dihexylquaterthiophene: A Second Thin Film Single-Crystal Organic Semiconductor, Chem. Soc.**10**, 457 (1998).

[46] J.G. Laquindanum, H.E. Katz, A.J. Lovinger, M. Hill, R. V August, Synthesis , Morphology , and Field-Effect Mobility of Anthradithiophenes, J. Am. Chem. Soc. **120**, 664 (1998).

[47] H.E. Katz, A.J. Lovinger, J. Johnson, C. Kloc, T. Siegrist, W. Li, Y.Y. Lin, A. Dodabalapur, A soluble and air-stable organic semiconductor with high electron mobility, Nature **404**, 478 (2000).

[48] A. Afzali, C.D. Dimitrakopoulos, T.L. Breen, High-Performance , Solution-Processed Organic Thin Film Transistors from a Novel Pentacene Precursor, J. Am. Chem. Soc.**124**, 8812 (2002).

[49] P.R. L. Malenfant, C.D. Dimitrakopoulos, J.D.Gelorme, L.L.Kosbar, and T.O. Graham, N-type organic thin-film transistor with high field-effect mobility based on a N,N'-dialkyl-3,4,9,10-perylene tetracarboxylic diimide derivative, Appl. Phys. Letts. **80**, 2517

(2002).

[50] T.W. Kelley, L.D. Boardman, T.D. Dunbar, D. V Muyres, M.J. Pellerite, T.P. Smith, High-Performance OTFTs Using Surface-Modified Alumina Dielectrics, J. Phys. Chem. B. **107**, 5877 (2003).

[51] R.W.I. De Boer, M.E. Gershenson, A.F. Morpurgo, V. Podzorov, Organic single-crystal field-effect transistors, Phys. Status Solidi A. **201**, 1302 (2004).

[52] V.C. Sundar, J. Zaumseil, V. Podzorov, E. Menard, R.L. Willett, T. Someya, M.E. Gershenson, J.A. Rogers, Elastomeric Transistor Stamps : Reversible Probing of Charge Transport in Organic Crystals, Science **303**, 1644 (2004).

[53] N. Stingelin-stutzmann, E. Smits, H. Wondergem, C. Tanase, P. Blom, P. Smith, D.D.E. Leeuw, solution-processed rubrene hypereutectics, Nat Mater. **4**, 601 (2005).

[54] K.Takimiya, H. Ebata, K. Sakamoto, T. Izawa, T. Otsubo, Y. Kunugi, 2,7-Diphenyl[1]benzothieno[3,2-b]benzothiophene, A New Organic Semiconductor for Air- Stable Organic Field-Effect Transistors with Mobilities up to 2.0 $cm^2V^{-1}s^{-1}$, J. Am. Chem. Soc.**128**, 12604 (2006).

[55] S.K. Park, T.N. Jackson, J.E. Anthony, D. A. Mourey, High mobility solution processed 6,13-bis(triiopropyl-silylethynyl)pentacene organic thin film transistors, Appl. Phys. Lett. **91**, 063514 (2007).

[56] O.D. Jurchescu, M. Popinciuc, B.J. Van Wees, T.T.M. Palstra, Interface-Controlled , High-Mobility Organic Transistors, Adv. Mater. **19**, 688 (2007).

[57] M. Yamagishi, J. Takeya, Y. Tominari, Y. Nakazawa, T. Kuroda, S. Ikehata, M. Uno, T. Nishikawa, T. Kawase, High-mobility double-gate organic single-crystal transistors with organic crystal gate insulators, Appl. Phys. Lett. **90**, 182117 (2007).

[58] Y. Takahashi, T. Hasegawa, S. Horiuchi, R. Kumai, Y. Tokura, G. Saito, High mobility field-effect transistor based on hexamethylenetetrathiafulvalene with organic metal electrodes, Chem. Mater. **19**, 6382 (2007).

[59] B.L. Li, Q. Tang, H. Li, X. Yang, W. Hu, Y. Song, Z. Shuai, W. Xu, Y. Liu, D. Zhu, An Ultra Closely π -Stacked Organic Semiconductor for High Performance Field-Effect Transistors, Adv. Mater. **19**, 2613 (2007).

[60] S. Haas, Y. Takahashi, K. Takimiya, T. Hasegawa, High-performance dinaphtho-thiophene single crystal field-effect transistors. Appl. Phys. Lett. **95**, 022111 (2009).

[61] H. Minemawari, T. Yamada, H. Matsui, J. Tsutsumi, S. Haas, R. Chiba, R. Kumai, T. Hasegawa, Inkjet printing of single-crystal films, Nature. **475**, 364 (2011).

[62] G. Giri, E. Verploegen, S.C.B. Mannsfeld, S. Atahan-Evrenk, D.H. Kim, S.Y. Lee, H.A. Becerril, A. Asupuru-Guzik, M.G. Toney, Z. Bao, Tuning charge transport in solution-sheared organic semiconductors using lattice strain, Nature **480**, 504 (2011).

[63] M.J. Kang, I. Doi, H. Mori, E. Miyazaki, K. Takimiya, M. Ikeda, H. Kuwabaa, (C n -DNTTs): Organic Semiconductors for High- Performance Thin-Film Transistors, Adv. Mater, **23**, 1222 (2011).

[64] K. Nakayama, Y. Hirose, J. Soeda, M. Yoshizumi, T. Umemura, M. Uno, W. Li, M.J.Kang, M. Yamagishi, Y. Okada, E. Miyazaki, Y. Nakazawa, A. Nakao, K. Takimiya, J. Takeya, Patternable solution-crystallized organic transistors with high charge carrier mobility, Adv. Mater. **23**, 1626 (2011).

[65] A.N. Sokolov, S. Atahan-evrenk, R. Mondal, H.B. Akkerman, A.P. Zoombelt, Z. Bao, A. Aspuru-guzik, From computational discovery to expermental characterization of a high hole mobility organic crystal, Nature Communications **2**, 437 (2011).

[66] M. Watanabe, Y.J. Chang, S. W. Liu, T.H. Chao, K. Goto, M.M.Islam, C. H.Yuan, Y. T.Tao, T. Shinmyozu, T.J. Chow, The synthesis, crystal structure and charge-transport

properties of hexacene, Nat. Chem. **4**, 574 (2012).

[67] A.Y. Amin, A. Khassanov, K. Reuter, T. Meyer-friedrichsen, M. Halik, Low-voltage organic field effect transistors with a 2-Tridecyl[1] benzothieno[3,2-b][1] benzothiophene semiconductor layer, J. Am. Chem. Soc. 134, 16548 (2012).

[68] J. Li, Y. Zhao, H.S. Tan, Y. Guo, C.A. Di, G. Yu, Y. Liu, M. Lin, S.H. Lim, Y. Zhou, H. Su, B.S. Ong, A stable solution-processed polymer semiconductor with record high-mobility for printed transistor, Sci. Rep. **2**, 754 (2012).

[69] Y. Diao, B.C. Tee, G. Giri, J. Xu, D.H. Kim, H.A. Becerril, R.M. Stoltenberg, T.H. Lee, G. Xue, S.C.B. Mannsfeld, Z. Bao, Solution coating of large-area organic semiconductor thin films with aligned single-crystalline domains, Nat. Mater. **12**, 665 (2013).

[70] N. Kurihara, A. Yao, M. Sunagawa, Y. keda, K. Terai, H. Kondo, M. Saito, H. Ikeda, H. Nakamura, High-Mobility Organic Thin-Film Transistors Over 10 $cm^2 V^{-1} s^{-1}$ Fabricated Using Bis (benzothieno) naphthalene Polycrystalline Films, Japanese Journal of Applied Physics **52**, 05DC11-1 (2013).

[71] G. Kim, S. Kang, G.K. Dutta, Y. Han, T.J. Shin, Y. Noh, C. Yang, A thienoisoindigo-naphthalene polymer with ultrahigh mobility of 14.4 cm^2 /V s That Substantially Exceeds Benchmark Values for Amorphous Silicon Semiconductors, J. Am. Chem. Soc. **136**, 9477 (2014).

[72] S. Y. Yang, K. Shin, C.E. Park, The Effect of Gate-Dielectric Surface Energy on Pentacene Morphology and Organic Field-Effect Transistor Characteristics, Adv. Funct. Mater **15**, 1806 (2005).

[73] A. Swist, J. Soloducho, Organic semiconductors-materials of the future?, Chemik. **66**, 293 (2012).

[74] W. Brütting, Physics Organic Semiconductors, Wiley-VCH, (2005).

[75] G. Horowitz, Organic thin film transistors : From theory to real devices, J. Mater. Res.**19**, 1946 (2004).

[76] Y. Yuan, G. Giri, A.L. Ayzner, A.P. Zoombelt, S.C.B. Mannsfeld, J. Chen, D. Nordlund, M.F. Toney, J. Huang, Z. Bao, Ultra-high mobility transparent organic thin film transistors grown by an off-centre spin-coating method, Nat. Commun. **5**,1 (2014).

[77] A. Lv, Y. Li, W. Yue, L. Jiang, H. Dong, G. Zhao, Q. Meng, M. Jiang, Y.He, Z. Li, Z. Wang, and W.Hu, High performance n-type single crystalline transistors of naphthalene bis (dicarboximide) and their anisotropic transport in crystals, Chem. Commun. **48**, 5154 (2012).

[78] B. Song, C. Rolin, J.D. Zimmerman, S.R. Forrest, Effect of mixed layer crystallinity on the performance of mixed heterojunction organic photovoltaic cells, Adv. Mater. **26**, 2914 (2014).

[79] G. Malliaras, R. Friend, An Organic electronic primer, Phys. Today **58**, 53 (2005).

[80] D. Wohrle, D. Meissner, C. Liman, Organic Solar Cells, Adv. Mater. **3**, 129 (1991).

[81] M. Hiramoto, M. Suezaki, M. Yokoyama, Effect of thin gold interstitial layer on the photovoltaic properties of tandem organic solar cell, chemistry letter, 327 (1990).

[82] M. Hiramoto, H. Fujiwara, M. Yokoyama, Three-layered organic solar cell with a photoactive of codeposited pigments, Appl. Phys. Lett. **58**, 1062 (1991).

[83] J. Nunzi, Organic photovoltaic materials and devices, C. R. Physique **3**, 523 (2002).

[84] R.R. Lunt, N.C. Giebink, A.A. Belak, J.B. Benziger, S.R. Forrest, Exciton diffusion lengths of organic semiconductor thin films measured by spectrally resolved photoluminescence quenching, J. Appl. Phys **105**, 53711 (2011).

[85] A. Hinderhofer, F. Schreiber, Organic-Organic Heterostructures : Concepts and Applications, Chem Phys Chem **13**, 628 (2012).

[86] D. Voss, Cheap and cheerful circuits, Nature **407**, 442 (2000).

[87] Z. Zhu, J.T. Mason, R. Dieckmann, G.G. Malliaras, Humidity sensors based on pentacene thin-film transistors, Appl. Phys. Lett.**81**, 4643 (2005).

[88] H. Klauk, Organic thin-film transistors,Chem. Soc. Rev. **39**, 2643 (2010).

[89] B.G. Horowitz, Organic Field-Effect Transistors, Adv. Mater.**10**, 365 (1998).

[90] J. Yang, D. Yan, T.S. Jones, Molecular template growth and its applications in organic electronics and optoelectronics, Chem. Rev.**15**, 5570 (2014).

[91] A.A. Virkar, S. Mannsfeld, Z. Bao, N. Stingelin, Organic semiconductor growth and morphology considerations for organic thin-film transistors, Adv. Mater. **22**, 3857 (2010).

[92] K. Takimiya, I. Osaka, T. Mori, M. Nakano, Organic semiconductors based on [1]benzothieno[3,2- B][1]benzothiophene substructure, Acc. Chem. Res. **47**, 1493 (2014).

[93] N. Karl, Charge carrier transport in organic semiconductors, Synth. Met. **133-134**, 649 (2003).

[94] M. Sim, J. Shin, C. Shim, M. Kim, S.B. Jo, J. Kim, K. Cho, Dependence of Exciton Diff usion Length on Crystalline Order in Conjugated Polymers, J. Phys. Chem. C. **118**, 760 (2014).

[95] H. Dong, X. Fu, J. Liu, Z. Wang, W. Hu, 25th Anniversary Article : Key Points for High-Mobility Organic Field-Effect Transistors, Adv. Mater. **25**, 6158 (2013).

[96] J.L. Brédas, D. Beljonne, V. Coropceanu, J. Cornil, Charge-transfer and energy-transfer processes in π-conjugated oligomers and polymers: A molecular picture, Chem. Rev. **104** 4971 (2004).

[97] J.P. Calbert, D.A.S. Filho, J. Cornil, J.L. Bre, Organic semiconductors : A theoretical characterization of the basic parameters governing charge transport, Proceedings of the National Academy of Sciences **99**, 5804 (2002).

[98] B. Demøtrio, A. Silva, E. Kim, J. Brødas, Transport Properties in the Rubrene Crystal : Electronic Coupling and Vibrational Reorganization Energy, Adv. Mater. 17, 1072 (2005).

[99] S.T. Bromley, M. Mas-torrent, P. Hadley, Importance of Intermolecular Interactions in Assessing Hopping Mobilities in Organic Field Effect Transistors : Pentacene versus Dithiophene-tetrathiafulvalene, J. Am. Chem. Soc. **126**, 6544 (2004).

[100] B.J. Cornil, J. Brédas, J. Zaumseil, H. Sirringhaus, Ambipolar Transport in Organic Conjugated Materials, Adv. Mater.**19**, 1791 (2007).

[101] M. Gsänger, J.H. Oh, M. Könemann, H.W. Höffken, A. Krause, Z. Bao, F. Würthner, A Crystal-Engineered Hydrogen-Bonded Octachloroperylene Diimide with a Twisted Core : An n-Channel Organic Semiconductor, Angew. Chem. Int. Ed.**49**, 740 (2010).

[102] M. Mas-Torrent, C. Rovira, Role of molecular order and solid-state structure in organic field-effect transistors, Chem. Rev. **111**, 4833 (2011).

[103] Z.F. Yao, J.Y. Wang, J. Pei, Control of π-π Stacking via Crystal Engineering in Organic Conjugated Small Molecule Crystals, Cryst. Growth Des. **18**, 7 (2018).

[104] P.M. Beaujuge, J.M.J. Fr, Molecular Design and Ordering Effects in π -Functional Materials for Transistor and Solar Cell Applications, J. Am. Chem. Soc. **133**, 20009 (2011).

[105] H. Ebata, T. Izawa, E. Miyazaki, K. Takimiya, M. Ikeda, H. Kuwabara, T. Yui, Highly Soluble [1]Benzothieno[3,2-b]benzothiophene (BTBT) Derivatives for High-Performance, Solution-Processed Organic Field-Effect Transistors, J. Am. Chem. Soc. **129**, 15732 (2007).

[106] T. Uemura, Y. Hirose, M. Uno, K. Takimiya, J. Takeya, Very high mobility in solution-processed organic thin-film transistors of highly ordered [1]benzothieno[32-b]benzothiophene derivatives, Appl. Phys. Express. 2, 6 (2009).

[107] S. Wang, D. Niu, L. Lyu, Y. Huang, X. Wei, C. Wang, H. Xie, Y. Gao, Interface electronic structure and morphology of 2,7-dioctyl[1]benzothieno[3,2-b]benzothiophene (C8-BTBT) on Au film, Appl. Surf. Sci. **416**, 696 (2017).

[108] A.G. Ismail, I.G. Hill, Stability of n-channel organic thin-film transistors using oxide, SAM-modified oxide and polymeric gate dielectrics, Org. Electron. Physics, Mater. Appl. **12**, 1033 (2011).

[109] S. Duhm, G. Heimel, I. Salzmann, H. Glowatzki, R.L. Johnson, P. Rabe, N. Koch, Orientation-dependent ionization energies and interface dipoles in ordered molecular assemblies, Nature **7**, 327 (2008).

[110] J.A. Venables, G.D.T. Spiller, M. Hanbucken, Nucleation and growth of thin films, Reports Prog. Phys. **47**, 399 (1984).

[111] S. Kowarik, A. Gerlach, F. Schreiber, Organic molecular beam deposition : fundamentals , growth dynamics , and in situ studies, J. Phys. Condens. Matter. **20**, 184005 (2008).

[112] M. Izaki, J. Komori, K. Shimizu, T. Koyama, T. Shinagawa, Masanobu Izaki, Jun Komori , Kairi Shimizu , Takayuki Koyama , and Tsutomu Shinagawa, Phys. Status Solidi A **214**, 1600473 (2017).

[113] G. Hlawacek, P. Puschnig, P. Frank, A. Winkler, C. Ambrosch-Drax, C. Teichert, Characterization of step-edge barriers in organic thin-film growth, Science **321**, 108 (2008).

[114] F. Schreiber, Organic molecular beam deposition: Growth studies beyond the first monolayer, Phys. Status Solidi Appl. Res. **201**, 1037 (2004).

[115] T. Izawa, E. Miyazaki, K. Takimiya, Molecular ordering of high-performance soluble molecular semiconductors and re-evaluation of their field-effect transistor characteristics, Adv. Mater. **20**, 3388 (2008).

[116] T.N. Krauss, E. Barrena, X.N. Zhang, D.G. de Oteyza, J. Major, V. Dehm, F. Würthner, L.P. Cavalcanti, H. Dosch, Three-dimensional molecular packing of thin organic films of PTCDI-C8 determined by surface X-ray diffraction., Langmuir. **24,** 12742 (2008).

[117] A.L. Briseno, S.C.B. Mannsfeld, C. Reese, J.M. Hancock, Y. Xiong, S.A. Jenekhe, Z. Bao, Perylenediimide Nanowires and Their Use in Fabricating Field-Effect Transistors and Complementary Inverters, Nano Lett. **7**, 2847 (2007).

CHAPTER 2

Growth of C8-BTBT molecules on inorganic single crystal substrates with various orientations

2.1 Introduction

The electronics of organic thin-film transistors (OTFTs), organic photovoltaic devices (OPVs), and organic light-emitting diodes (OLEDs) have attracted increasing attention for industrial use.**[1-5]** Structural characteristics including the preferred orientation and grain structure strongly affect the performance of electronics**[6-8]** and have been controlled by adjusting

the conditions of growth e.g., a heteroepitaxial growth including the substrate material and orientation.**[9-11]**

The π-conjugated molecule of [1]benzothieno[3,2-b]benzothiophene (BTBT) derivatives, 2,7-dioctyl[1]benzothieno[3,2-b][1]benzothiophene (C8-BTBT), has recently attracted much attention owing to its high charge carrier mobility of ~1-170 $cm^2 V^{-1} s^{-1}$,**[12, 13]** and single-crystal- and thin-film-based electronics could be grown with a well-ordered structure.**[14-22]** In this chapter, the detailed study of the growth of the C8-BTBT layer on orientation-controlled single-crystal inorganic substrates supports the use of organic electronics.

The main purpose of this work is that characterization of structural relation between π-conjugated semiconductor C8-BTBT layers and single crystal inorganic substrates. We investigated the structure and preferred orientation of C8-BTBT layers formed by vacuum thermal evaporation on quartz glass, A-, C-, and R-single-crystal aluminum oxide (sapphire), and (100)-, and (111)-MgO substrates by X-ray diffraction analysis, atomic force microscopy (AFM) observation, and resistivity measurement by the van der Pauw method. And, organic layer structure-property relation is investigated.

2.2 Experimental procedures

100-nm-thick C8-BTBT (Sigma-Aldrich, 99% purity) layers were deposited at a substrate temperature of 343 K at a pressure of around 4×10^{-5} Pa on quartz glass, single-crystal substrates, namely, $(11\underline{2}0)$-Al_2O_3 (A-sapphire), (0001)-Al_2O_3 (C-sapphire), and $(1\underline{1}02)$-Al_2O_3 (R-sapphire), and (100)-MgO and (111)-MgO substrates using a vacuum thermal evaporation system (ULVAC VTS-350ERH/M) equipped with a turbomolecular pump and an oil-free scroll vacuum pump. Prior to the deposition, the substrates were annealed in air for 1 h at 1200℃ for sapphire substrates and 1100℃ for MgO substrates. The thickness and deposition rate were controlled using a quartz crystal deposition control system (ULVAC CRTM- 6000G).

X-ray diffraction (XRD) measurements were carried out using a conventional θ/2θ scanning technique with monochromatic Cu Kα radiation (Rigaku RINT 2500) and a two- dimensional (2D) imaging plate detector with monochromatic Cu Kα radiation (Rigaku RINT-Rapid II). XRD patterns were recorded at 2θ angles ranging from 5 to 35°. The morphology was observed in air by atomic force microscopy (AFM; Shimadzu SPM-9700-Kai). The electrical resistivity was estimated with a Hall effect measurement system (Toyo Technica Resitest 8310) by the van der Pauw method at room temperature.

2.3 Results and discussion

2.3.1 Effects of the substrate materials on the preferred orientation of the C8-BTBT layers

In order to understand the effect of substrate material on the growth of C8-BTBT molecules, firstly, deposited layers were characterized by XRD analysis. **Figure 2.1** shows out-of-plane XRD patterns of 100-nm-thick C8-BTBT layers on quartz glass, A-, C-, and R-sapphire, and (100)- and (111)-MgO substrates, and of C8-BTBT powder. Periodic weak peaks could be observed from 6.1° (each at approximately 3°) and were assigned as (00n) (n = 2, 3, 4, ….) of the C8-BTBT layers with the characteristic monoclinic lattice, in addition to the broadened peak

of quartz glass and strong sharp peaks of sapphire and MgO substrates. The (001) diffracted X-ray peak at approximately 3° could not be detected in this measurement because of the instrumental limitation. The sharp and intense peaks originating from (002) and (003) were observed for all the C8-BTBT layers, indicating the development of the (001) out-of-plane orientation, irrespective of the substrate material and orientation. Since the diffracted (002) peak could be observed at 6.17° for quartz glass, 6.10° for MgO(100) and MgO(111), and 6.11, 6.12, and 6.13° for A-, R-, and C-sapphire substrates, respectively, the d-spaces of the (002) plane were almost the same for all the substrates. In accordance with the (001) out-of-plane orientation, the herringbone arrangement of the C8-BTBT molecules with the standing-up position in the direction nearly normal to the substrate surface was predominant on all the substrates. The d-space was calculated from well-defined diffraction peaks using Bragg's equation,

$$n\lambda=2d_{hkl}\sin\theta, \tag{2.1}$$

where λ is the wavelength of the X-ray beam (0.154059 nm), the d-space is the interlayer separation, and θ is the Bragg angle of the lattice planes with respect to the incident X-ray beam. The C8-BTBT layer possesses a monoclinic lattice with a = 0.5927 nm, b = 0.788 nm, c = 2.918 nm, and β = 92.443°. The d-space of the (002) plane was calculated to be 1.45-1.43 nm from the experimental values of 6.10-6.17° and was close to that calculated from the standard values.**[23]** The lattice relationship between the C8-BTBT layer and the substrates was expressed as (001) $_{C8\text{-}BTBT}$//(11$\underline{2}$0)$_{Al2O3}$, (001) $_{C8\text{-}BTBT}$// (0001) $_{Al2O3}$, (001) $_{C8\text{-}BTBT}$// (1$\underline{1}$02)$_{Al2O3}$, (001) $_{C8\text{-}BTBT}$// (100) $_{MgO}$, and (001) $_{C8\text{-}BTBT}$// (111) $_{MgO}$.

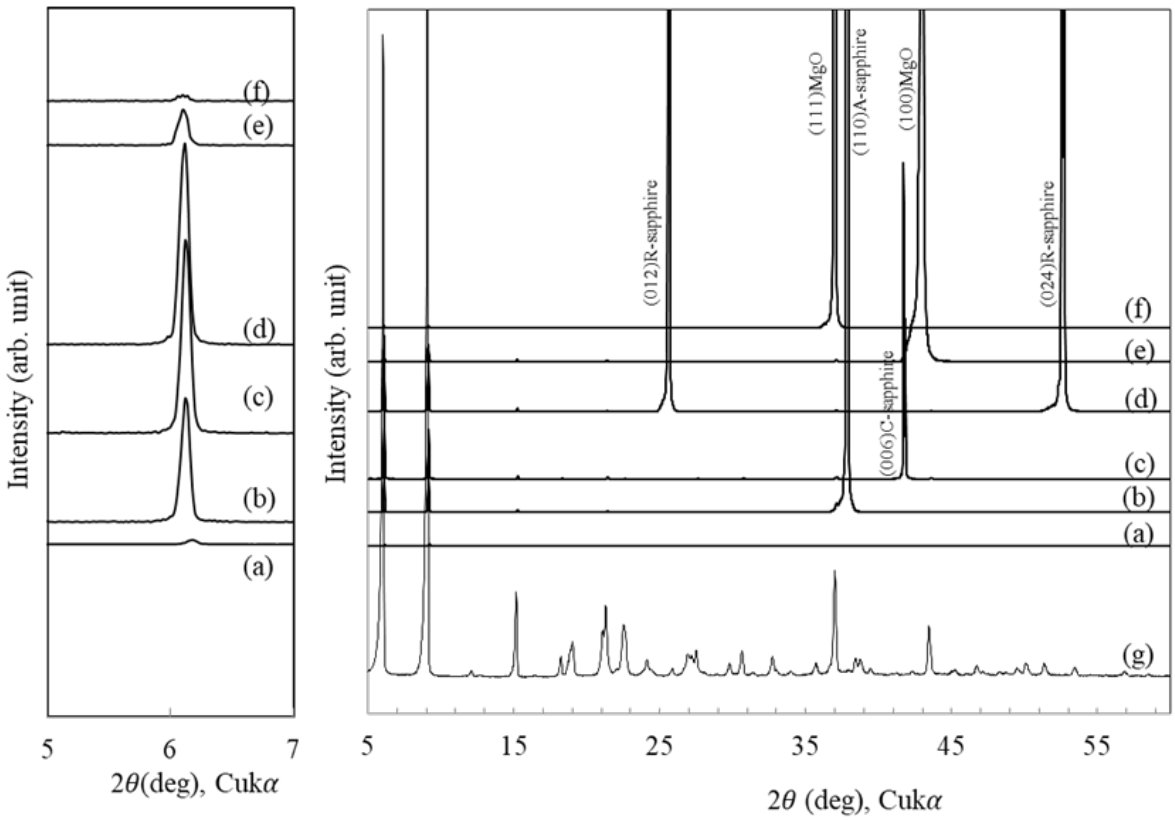

Figure 2.1 X-ray diffraction patterns of C8-BTBT layers prepared on (a) quartz glass, (b) C-Sapphire, (c) A-Sapphire, (d) R-Sapphire, and (e) (100)-MgO, (f) (111)-MgO substrates and (g) of C8-BTBT powder.

The intensity of the (002) plane differed depending on the substrate material, in spite of the constant thickness of 100 nm. A strong (002) peak was observed for the sapphire substrates irrespective of the orientation; such a peak was stronger than those for quartz glass and MgO substrates. The full width at half maximum (FWHM) was determined to be 0.081° for sapphire substrates and 0.11° for quartz glass and MgO substrates.

Figure 2.2 shows the XRD patterns of C8-BTBT layers prepared on quartz glass, C- and A-sapphire, and (100)-MgO substrates. The two dashed lines in **Figure 2.2(a)** show the 2θ angle corresponding to the horizontal axis in **Figure 2.1** and β-rotation. The C8-BTBT layer

prepared on the quartz glass substrate showed a broadened ring originating from the amorphous glass structure and two spots presented by arrow ① at 2θ angles of approximately 6° and 9°, which corresponded to the (002) and (003) C8-BTBT planes shown in **Figure 2.1**, respectively, in addition to six weak peaks presented by arrow ②. Similar spot patterns shown by arrows ① and ② could be observed for all C8-BTBT layers, irrespective of the substrate material and orientation, although the intensity of spots ② increased. The X-ray diffraction patterns indicated that (001) out-of-plane orientations with similar in-plane orientations formed for all the C8-BTBT layers, irrespective of the substrate material and orientation.

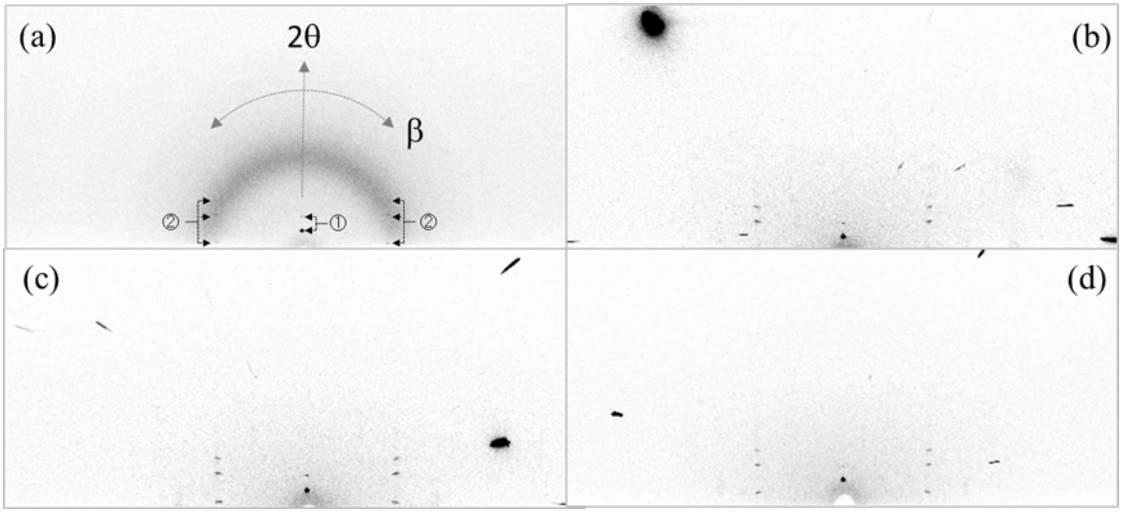

Figure 2.2 Imaging plate-XRD patterns of C8-BTBT layers prepared on (a) quartz glass, (b) C-Sapphire, (c) A-Sapphire, and (d) (100)-MgO substrates.

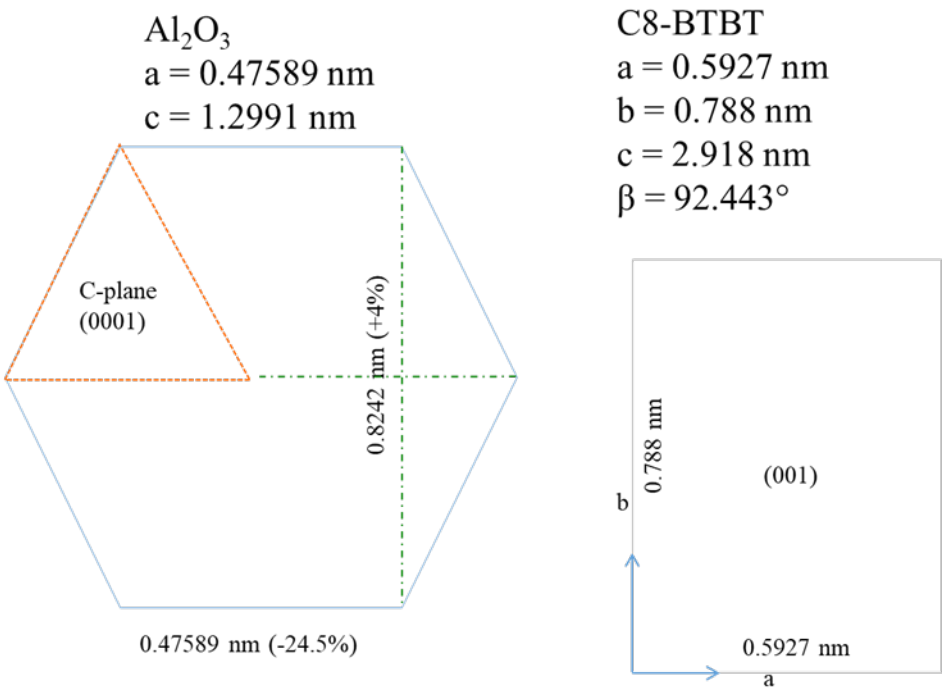

Figure 2.3 Schematic illustration of lattice relationship between (0001) plane of Al_2O_3 and (001)-plane of C8-BTBT.

Figure 2.3 shows the schematic illustration of the lattice relationship between the C8-BTBT(001) and Al_2O_3(0001) planes. Al_2O_3 has a hexagonal lattice with unit-cell parameters of 0.47589 nm in the a-axis and 1.2991 nm in the c-axis,**[24]** and MgO has a cubic lattice with a unit-cell parameter of 0.4213 nm.**[25]** The lattice mismatch was estimated to be approximately -24 and 4% on the a- and b-axes of C8-BTBT for the lattice relationship $(001)_{C8\text{-}BTBT}$ // $(0001)_{Al2O3}$, approximately -24 and -21% on the a- and b-axes of C8-BTBT for the lattice relationship $(001)_{C8\text{-}BTBT}$ // $(11\underline{2}0)_{Al2O3}$, and approximately -40 and 6.5% on the a-and b-axes of C8-BTBT for the lattice relationship $(001)_{C8\text{-}BTBT}$ // $(100)_{MgO}$, respectively. The lattice mismatch varied in a wide range depending on the substrate material and orientation, but it did not affect

the molecular arrangement of the C8-BTBT layer as demonstrated by the obtained similar preferred orientation that did not depend on the substrate material and orientation. Many diffracted X-ray peaks could be observed for the XRD pattern of the C8-BTBT powder shown in **Figure 2.1 (g)**, and all the peaks were assigned as (00n) (n=1,2,3, ….) planes of C8-BTBT, indicating molecular ordering in the b-axis induced by the formation of the C8-BTBT aggregate by π-π-stacking even in the powder form. The molecular ordering by π-π-stacking resulted in the formation of the (001) out-of-plane orientation for all the C8-BTBT layers.

2.3.2 Grain structure of the C8-BTBT layers prepared on the single crystal substrate

The grain structure and morphology of single crystal substrates and vacuum-evaporated-C8-BTBT layers were observed by AFM. **Figure 2.4** shows AFM images of the surfaces of bare quartz glass, C-sapphire, and (100)-MgO substrates. Microscratch-like irregularity and undulation were observed on the surface of the quartz glass substrate, and the surface roughness (R_a) was estimated to be 0.70 nm from the AFM image. Periodic steps around 0.45 nm in height were observed for the C-sapphire substrate, and R_a was estimated to be 0.099 nm. A small granular irregularity was observed over the surface of the (100)-MgO substrate, and R_a was estimated to be 0.884 nm.

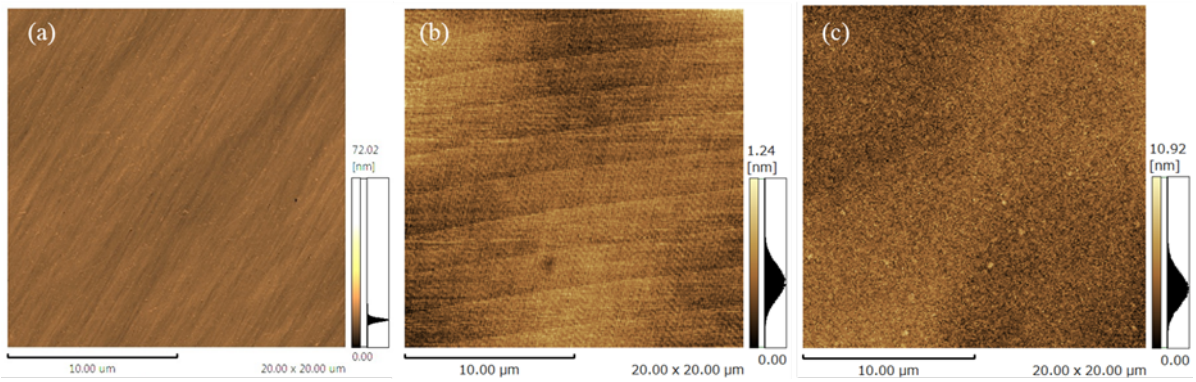

Figure 2.4 AFM images of the surface of (a) quartz glass, (b) C-sapphire, and (c) (100)-MgO substrates.

Figure 2.5 shows AFM images of the surfaces of C8-BTBT layers prepared on quartz glass, C-sapphire, and (100)-MgO substrates. The C8-BTBT layers were composed of aggregates of granular grains, irrespective of the substrate material. The grain size was estimated to be 0.83, 1.25, and 0.55 μm for quartz glass, C-Sapphire, and (100)-MgO substrates, and R_a was estimated to be 4.4, 10.6, and 13.4 nm for quartz glass, C-sapphire, and (100)-MgO substrates, respectively. All the C8-BTBT layers exhibited the (001) out-of-plane orientation with a similar in-plane orientation, but the intensity of the (002) peak and the FWHM differed depending on the substrate material, irrespective of the orientation. Although it was speculated that the (001) out-of-plane orientation was governed by the π-π-stacking of C8-BTBT molecules, the degree of such orientation was reflected slightly by the grain structure.

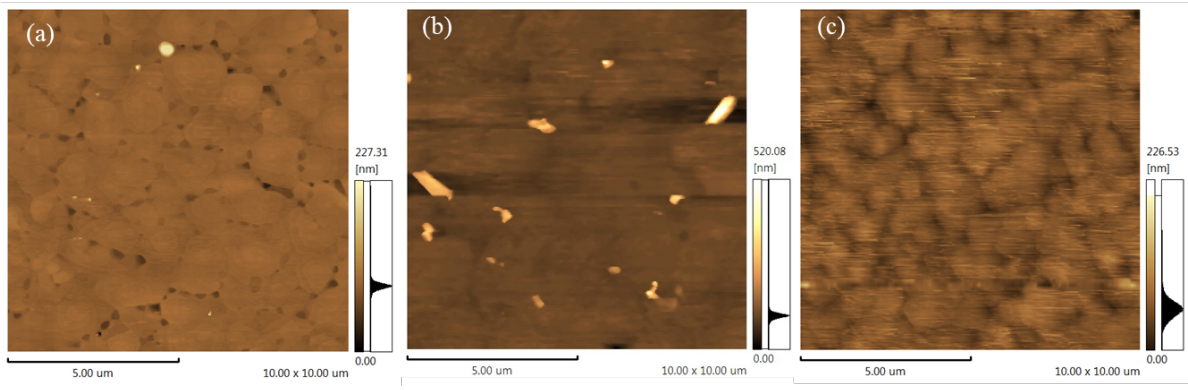

Figure 2.5 AFM images of the surface of C8-BTBT layers deposited on (a) quartz glass, (b) C-sapphire, and (c) (100)-MgO substrates.

The resistivity of 100-nm-thick C8-BTBT layers was estimated to be 2.7×10^5, 4.13×10^5, and 5×10^5 Ω cm for quartz glass and A- and C-sapphire substrates, respectively. The resistivities could be considered as almost the same for C8-BTBT layers regardless of the substrate type, because of almost the same preferred orientation and grain structure. The carrier

concentration and mobility could not be estimated by the technique used in this study; this problem has already been reported.**[26, 27]**

2.3.3 Tentative growth model of the C8-BTBT layer on single crystal substrates

The C8-BTBT molecules were preferably to grow the standing up configuration on the sapphire and MgO substrates irrespective of the orientation of the substrate materials. According to XRD results, the C8-BTBT layers showed good crystallinity on the single crystal substrates than those on the amorphous substrate, quartz glass. **Figure 2.6** shows the schematic illustration of C8-BTBT layer growth on the substrates. The tentative growth model of C8-BTBT on single crystal substrates was proposed based on our experimental results.

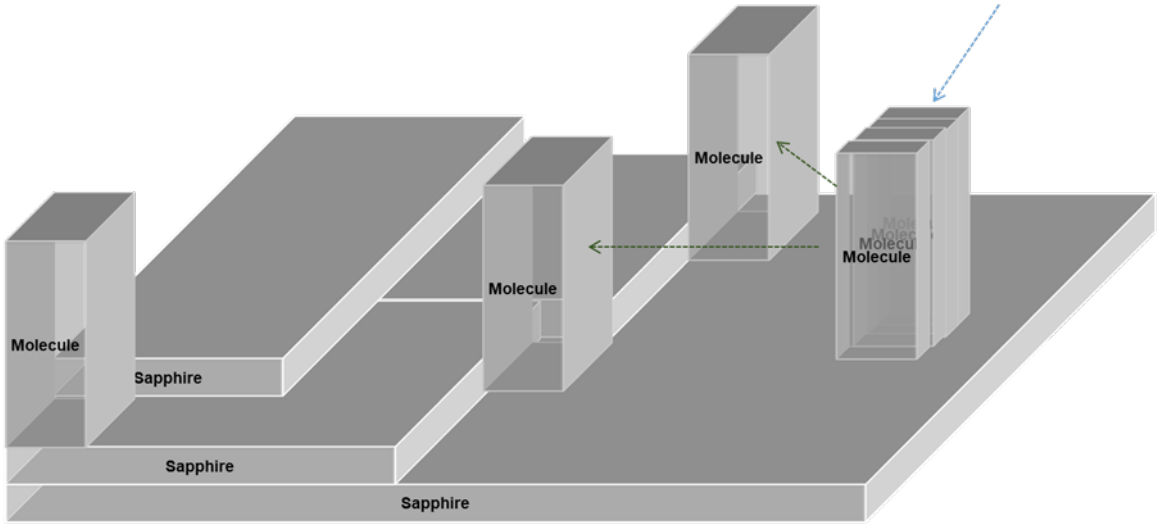

Figure 2.6 Schematic illustration of formation of C8-BTBT layer on inorganic single crystal substrates.

It was reported for inorganic semiconductors such as oxides that the lattice relationship including the lattice mismatch strongly affected the growth of the oxide layer, as demonstrated

for the <0001>-ZnO layer growth on <111>-Au **[28, 29]** and <0001>-Ga:ZnO layers**[30]**.**[31]** However, the atomic arrangement and lattice mismatch did not affect the growth of the C8-BTBT layer, and (001) preferred orientation was obtained regardless of the material and orientation. The C8-BTBT layer formed a continuous layer with the growth of the C8-BTBT island in the direction parallel to the substrate surface and then transferred to layer-by-layer growth in the direction normal to the substrate surface in the case of the C-sapphire substrate.**[32]** The C8-BTBT aggregate bounded by π-π-stacking reached the substrate in the evaporation process and then diffused on the surface. There are steps periodically formed on the surface of the C-sapphire substrate, and the diffused C8-BTBT molecules were stopped by the steps resulting in the formation of C8-BTBT islands with (001) out-of-plane orientations.

2.4 Conclusions

The organic molecule 2,7-dioctyl[1]benzothieno[3,2-b][1]benzothiophene (C8-BTBT) was deposited on quartz glass, (11$\underline{2}$0) A-, (0001) C-, and (1$\underline{1}$02)R-single-crystal Al_2O_3 (sapphire), and (100)- and (111)-single crystal MgO substrates by vacuum thermal evaporation. The (001) out-of-plane orientation with a similar in-plane orientation was obtained irrespective of the substrate material and orientation, and its formation was governed by π-π-stacking-induced molecular ordering. The degree of orientation was reflected by the grain structure related to the substrate material. The growth model of the oriented C8-BTBT layer was speculated on the basis of experimental results. The results demonstrated here show the importance of molecular ordering in controlling the preferred orientation of C8-BTBT molecules, although further investigation of the growth is required.

REFERENCES

[1] C. D. Dimitrakopoulos and D. J. Mascaro, Organic thin- film transistors: A review of recent advances, IBM J. Res. Dev. **45**, 11 (2001).

[2] K. Kudo, Organic light emitting transistors, Curr. Appl. Phys. **5**, 337 (2005).

[3] A. Facchetti, Semiconductors for organic transistors, Mater. Today **10**, 28 (2007).

[4] C. W. Tang and S. A. VanSlyke, Organic electrolumescent diodes,Appl. Phys. Lett. **51**, 913 (1987).

[5] X. Guo, M. Baumgarten, and K. Müllen, Designing π-conjugated polymers for organic electronics, Prog. Polym. Sci. **38**, 1832 (2013).

[6] H. N. Tsao, D. Cho, J. W. Andreasen, A. Rouhanipour, D. W. Breiby, W. Pisula, and K. Mullen, The influence of morphology on high-performance polymer field-effect transistors, Adv. Mater. **21**, 209 (2009).

[7] F. Dinelli, M. Murgia, P. Levy, M. Cavallini, and F. Biscarini, Spatially correlated charge transport in organic thin film transistors, Phys. Rev. Lett. **13**, 90 (2004).

[8] C. Wang, H. Dong, W. Hu, Y. Liu, and D. Zhu, Semiconducting π-Conjugated Systems in Field-Effect Transistors: A Material Odyssey of Organic Electronics, Chem. Rev. **112**, 2208 (2012).

[9] A. O. F. Jones, B. Chattopadhyay, Y. H. Geerts, and R. Resel, Substrate-induced and thin-film phases: polyrphism of organic materials on surfaces, Adv. Funct. Mater. **26**, 2233 (2016).

[10] H. Huang, Y. Huang, S. Wang, M. Zhu, H. Xie, L. Zhang, X. Zheng, Q. Xie, D. Niu and Y. Gao, Van Der Waals heterostructures between small organic moleucles and layered substrates, Crystals **6**, 113 (2016).

[11] B. Y. Noh, J. Kim, and Y. Yoshida, Effect of molecular orientation of epitaxially grown Platimum(Ⅱ) Octaethyl Porphyrin films on the performance of field-effect transistors, Adv. Mater. **15**, 699 (2003).

[12] Y. Tsutsui, G. Schweicher, B. Chattopadhyay, T. Sakurai, J. B. Arlin, C. Ruzie, A. Aliev, A. Ciesielski, S. Colella, A. R. Kennedy, V. Lemaur, Y. Olivier, R. Hadji, L. Sanguinet, F. Castet, S. Osella, D. Dudenko, D. Belijonne, J. Cornil, P. Samori, S. Seki, and Y. H. Geerts, Unraveling unprecedented charge carrire mobility through structure property relationship of four isomers of Didodecyl[1]benzothieno[3,2-b][1]benzothiophene, Adv. Mater. **28***,* 7106 (2016).

[13] H. Ebata, T. Izawa, E. Miyazaki, K. Takimiya, M. Ikeda, H. Kuwabara, and T. Yui, Highly soluble [1]benzothieno[3,2-b]benzothiophene (BTBT) derivatives for high-performance, solution-processed organic field-effect transistors, J. Am. Chem. Soc. **129**, 15732 (2007).

[14] C. Liu, T. Minari, X. Lu, A. Kumatani, K. Takimiya, and K. Tsukagoshi*,* Solution-processable organic single crystals with bandlike transport in filed-effect transistors, Adv. Mater. **23**, 523 (2011).

[15] T. Uemura, Y. Hirose, M. Uno, K. Takimiya, and J. Takeya, Very high mobility in solution-processed organic thin-film transistors of highly ordered [1] Benzothieno [3,2-b] benzothiophene derivatives, Appl. Phys. Express **2**, 111501 (2009).

[16] A. Kumatani, C. Liu, Y. Liu, P. Darmawan, K. Takimiya, T. Minari, and K. Tsukagoshi*,*Solution-processed, self-organized organic single crystal arrays with controlled crystal orientation*,* Sci. Rep. **2**, 393 (2012).

[17] H. Minemawari, T. Yamada, H. Matsui, J. Tsutsumi, S. Haas, R. Chiba, R. Kumai, and T. Hasegawa*,* Injet printing of single-crystal films, Nature **475**, 364 (2011).

[18] L. Lyu, D. Niu, H. Xie, N. Cao, H. Zhang, P. Liu and Y. Gao, Orientation-dependent energy level alignment and film growth of 2,7-dioctyl[1]benzothieno[3,2-b]benzothiophene (C8-BTBT) on HOPG, J. Chem. Phys. **144**, 034701 (2016).

[19] Y. Yuan, G. Giri, A. L. Ayzner, A. P. Zoombelt, S. C. B. Mannsfeld, J. Chen, D. Nordlund, M. F. Toney, J. Huang, and Z. Bao, Ultra-high mobility transparent organic thin film transistors grown by an off-centre spin-coating method, Nat. Commun. **5**, 3005-1 (2014).

[20] M. Dohr, O. Werzer, Q. Shen, I. Salzmann, C. Teichert, C. Ruzie, G. Schweicher, Y. H. Geerts, M. Sferrazza, and R. Resel, Dynamics of monolayer-island transistions in 2,7-dioctyl benzothienobenzothiophene thin films, ChemPhysChem **14**, 2554 (2013).

[21] M. Dohr, H. M. A. Ehmann, A. O. F. Jones, I. Salzmann, Q. Shen, C. Teichert, C. Ruzie, G. Schweicher, Y. H. Geerts, R. Resel, M. Sferrazza, and O. Werzer, Reversibility of temperature driven discrete layer-by-layer formation of dioctyl-benzothieno-benzothiophene films, Soft Matter **13**, 2322 (2017).

[22] G. Gbabode, M. Dohr, C. Niebel, J. Blandier, C. Ruzie, P. Negrier, D. Mondieig, Y. H. Geerts, R. Resel and M. Sferrazza , X- ray structural investigation of nonsymmetrically and symmetrically alkylated [1]benzothieno[3,2- b]benzothiophene derivatives in bulk and thin films, ACS Appl. Mater. Interfaces **6**, 13413 (2014).

[23] T. Izawa, E. Miyazaki, and K. Takimiya, Molecular ordering of high-performance soluble molecular semiconductors and re-evaluation of their field-effect transistor characteristics, Adv. Mater. **20**, 3388 (2008).

[24] Joint Committee on Powder Diffraction Standards, Powder Diffraction File (International Data for Diffraction Data No. 00-042-1468).

[25] Joint Committee on Powder Diffraction Standards, Powder Diffraction File (International Data for Diffraction Data No. 00-004-0829).

[26] C. Ohashi, S. Izawa,Y. Shinmura, M. Kikuchi, S. Watase, M. Izaki, H. Naito, and M. Hiramoto, Hall effect in bulk-doped organic singel crystals, Adv. Mater. **29**, 1605619 (2017).

[27] M. Kikuchi, K. Takagi, H. Naito, and M. Hiramoto, Single crystal organic photovoltaic cells using lateral electron trasport, Org. Electron. **41**, 118 (2017).

[28] M. Izaki, S. Watase, and H. Takahashi, Low-temperature electrodeposition of room temperature ultraviolet light emitting zinc oxide, Adv. Mater. **15**, 2000 (2003).

[29] M. Izaki, S. Watase, and H. Takahashi, Room-temperature ultraviolet light-emitting zinc oxide micropatterns prepared by low-temperature electrodeposition and photoresist, Appl. Phys. Lett. **83**, 4930 (2003).

[30] M. Izaki, M. Kobayashi, T. Shinagawa, T. Koyama, K. Uesugi, and A. Takeuchi, Electrochemically grown ZnO vertical nanowire scintillator with light guiding effect, Phys. Status Solidi A **214**, 1700285 (2017).

[31] M. Izaki, J. Komori, K. Shimizu, T. Koyama, and T. Shinagawa, Room temperature ultraviolet light-emitting ZnO vertical nanowires prepared by electrochemical growth, Phys. Status Solidi A **214**, 1600473 (2017).

[32] A. M. Moh, P. L. Khoo, K. Sasaki, S. Watase, T. Shinagawa, and M. Izaki, Growth and characteristics of C8-BTBT layer on C-sapphire substrate by thermal evaporation, Phys. Status Solidi A **215**, 1700862 (2018).

CHAPTER 3

Growth and characteristics of C8-BTBT layers on C-sapphire substrate by thermal evaporation

3.1 Introduction

The π-conjugated organic semiconductors have been technologically great impact in fields of organic electronics; organic thin layer transistors (OTFT), organic field effect transistors (OFETs), organic light-emitting diodes (OLEDs), and organic photovoltaics (OPVs).**[1–4]** The electrical characteristics including the charge transportation property**[5,6]** strongly affects

the performance of electronic devices and relates to the structure, molecular orientation, morphology**[7]**, grain size, and defect density of organic semiconductor layers.**[8,9]** The surface defects such as steps and vacancies of the underlying substrate could influence the structure of the molecular ordering and subsequent growth of the organic layers.

Molecular semiconductor of π-conjugated core with two octyl chains, 2,7-dioctyl[1]benzothieno[3,2-b][1]benzothiophenes (C8-BTBT) is one of the promising semiconducting materials for fabricating the organic electronic devices because of their high mobility value of 31.3 and 43 $cm^2V^{-1}s^{-1}$.**[10,11]** The C8-BTBT layer has been prepared by several techniques of organic molecular beam evaporation, inkjet printing, and spin-coating method, and the mobility value changed depending on the preparation techniques.**[9,11-12]** Furthermore, the orientation of C8-BTBT molecules changed depending on the substrate materials of graphene, boron nitride, and SiO_2/Si.**[11,13-14]** However, the growth of C8-BTBT molecules on single crystal sapphire substrate appropriate to consider the structural relation between the organic layers and single crystal substrate have not been reported yet. The C8-BTBT layer growth still remains rich subject to be better understanding of the linkage between the structural properties and electrical properties of C8-BTBT active layer.

In this chapter, we prepared (001)-orientated C8-BTBT layers on a single crystal Al_2O_3 (C-sapphire) substrate by a vacuum thermal evaporation. The structural, optical and electrical properties were investigated with X-ray diffraction (XRD), atomic force microscopy (AFM), optical absorption spectra measurement, and van-der-Pauw method to make the growth process clear. The main purpose of this study is that examining the effects of the layer thickness and preparation temperature on the structural, morphological, optical and electrical properties.

3.2 Experimental procedures

Organic semiconductor layers of 2,7-dioctyl[1]benzothieno[3,2-b][1]benzothiophene (C8-BTBT) were prepared on a (0001) [11$\underline{2}$0] Al_2O_3 single crystal (C-sapphire) substrates at thickness ranging from 5 to 100 nm and preparation temperatures of 300 K, 343 K and 373 K by a vacuum thermal evaporation. The C8-BTBT powder (99% purity, Sigma-Aldrich) was used as a source material in the vacuum evaporation system (ULVAC, VTS-350ERH/M) connected with turbo molecular pump and oil-free scroll vacuum pump. The one side polished C-sapphire substrates were annealed in air at 1200℃ for 1 hr. The preparation was carried out in the pressure around 4×10^{-5} Pa, and C8-BTBT layers were deposited in the thickness ranging from 5 to 100 nm at a constant deposition rate 0.1 nm/s and preparation temperatures 300 K, 343 K, and 373 K. The deposition rate was monitored by a quartz crystal oscillator sensor in a vacuum evaporation system (ULVAC, CRTM- 6000G). The thickness of the C8-BTBT layers were determined by using a surface profiler measurement system (ULVAC, DekTak150).

Conventional out-of-plane X-ray diffraction were performed by a θ/2θ scanning technique using Rigaku RINT 2500 X-ray diffractometer at monochromatic CuKα radiation operated at 20 kV, 10 mA with a wavelength (λ = 0.154059 nm). X-ray diffraction spot patterns were recorded by using 2D imaging plate detector with monochromatic CuKα radiation using Rigaku RINT- Rapid II. Surface morphologies were observed by an atomic force microscopy (AFM, Shimadzu, SPM-9700 Kai) in non-contact mode in air. Absorption spectra measurements were performed using a UV-VIS-NIR spectrophotometer (HITACHI, U4100) with a reference of (0001) C-sapphire bare substrate. Electrical properties were measured by using van-der-Pauw method at room temperature (Toyo Technica, Resitest 8310) with and without AM1.5G (air mass global condition) light irradiation (Asahi Spectra, HALC100).

3.3 Results and discussion

3.3.1 Orientation of the C8-BTBT layers prepared on the C-Sapphire substrate

Figure 3.1 shows out-of-plane X-ray diffraction patterns (A) for 5, 10, 15, 50 and 100-nm-thick C8-BTBT layers prepared on C-sapphire substrate at 300 K, (B) for 100 nm-thick layers prepared at 300, 343, and 373 K, and (C) the dependence of the FWHM values on the thickness. Two peaks were observed at around 6.1 and 9.1 degrees on X-ray diffraction patterns irrespective of the layer thickness and preparation temperature. These two peaks could be identified as (002) and (003) planes of the C8-BTBT layer with the characteristic monoclinic lattice. The (001) out-of-plane orientation was developed irrespective of the preparation temperature. The peak intensity increased with increase in layer thickness keeping almost constant intensity ratio. The peak angle of (002) peak showed almost constant value of 6.1 degree regardless of the layer thickness and preparation temperature. The FWHM value drastically decreased from 0.3 ~ 0.6 degree to 0.1 degree with increase in layer thickness from 5 nm to 50 nm and then showed almost constant value. The FWHM value relates to the grain size and heterogeneous strain, and the decrease in FWHM value gives increase in the grain size and/or decrease in the heterogeneous strain.

Figure 3.2 shows the X-ray diffraction patterns recorded by the imaging plate for annealed bare C-sapphire substrate with the radial and circumferential directions represent by the 2θ and β angles and 100-nm-thick C8-BTBT layers deposited at 300 and 343 K. Many diffraction spots could be observed on the XRD image for 100 nm-C8-BTBT layers in addition to the spots observed for bare C-sapphire substrate. Similar spot pattern represented by arrow① and ② could be observed irrespective of the layer thickness and preparation temperature, and two diffraction spots represented by arrow① were identified as (002) and (003) planes of C8-BTBT layer. Debye ring could not be observed on the XRD image irrespective of the layer thickness

and preparation temperature. The out-of-plane XRD represented in **Figure 3.1** showed the formation of the (001) out-of-plane preferred orientation, and the similar spot patterns suggested that the preferred orientation including the in-plane orientation was almost the same, although it was difficult to estimate quantitatively.

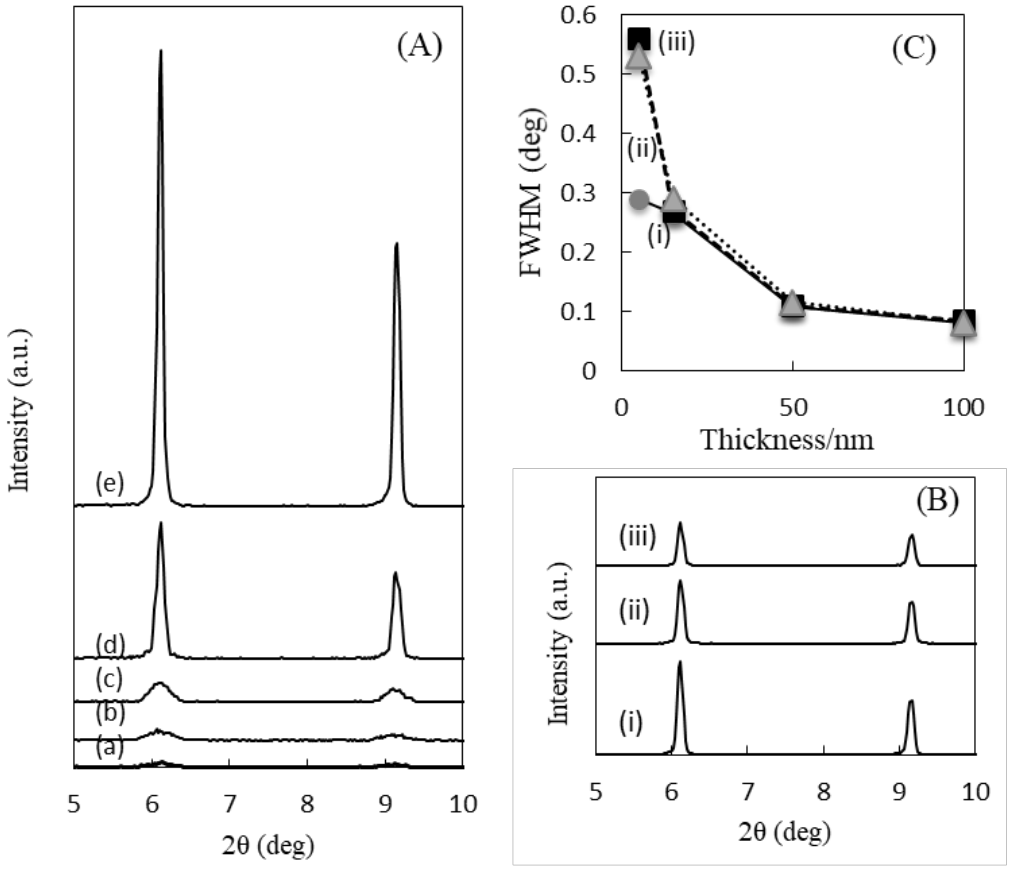

Figure 3.1 X-ray diffraction patterns (A) 5 (a), 10 (b), 15 (c), 50 (d), 100-nm-thick-C8-BTBT layers (e) prepared on C-sapphire substrate at 300K and (B) 100-nm-thick layers prepared at (i)300, (ii) 343 and (iii) 373K, and (C) the dependence of the FWHM values on the thickness.

The C8-BTBT possessed the monoclinic lattice with lattice constants of 0.5927 nm in a-axis, 0.788 nm in b-axis, 2.918 nm in c-axis, and 92.443 degree in β-angle, **[15]** and Al_2O_3

possessed the characteristic hexagonal lattice with lattice constants of 0.47589 nm in a-axis, and 1.2991 nm in c-axis. **[16]** The lattice mismatch was estimated to be -24.5 % along a-axis, and +4% along b-axis for the lattice relationship of (001)[100]C8-BTBT//(0001)[11$\underline{2}$0]Al_2O_3. The (001)-out-of-plane orientation was developed for the C8-BTBT layer on C-sapphire substrate inspite of the large lattice mismatch.

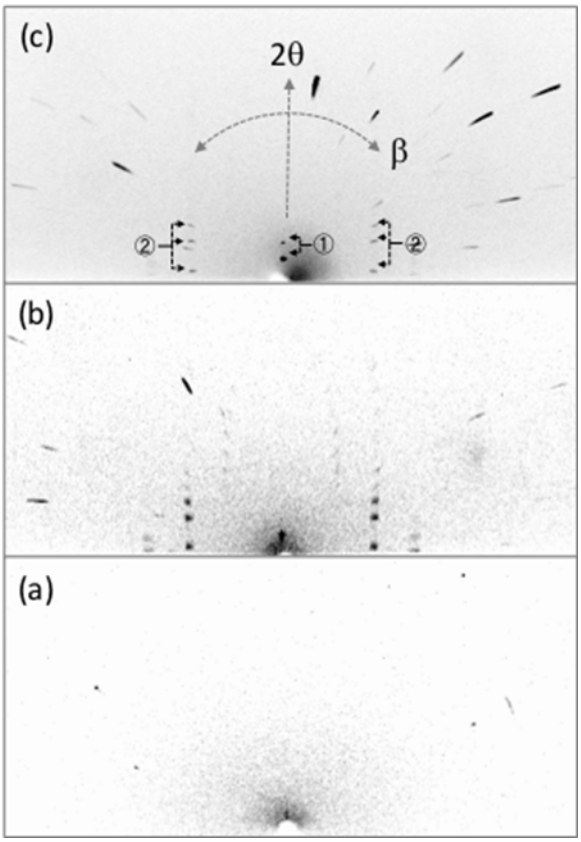

Figure 3.2 X-ray diffraction patterns recorded for (a) bare C-sapphire substrate, and 100-nm-thick C8-BTBT layers deposited on C-sapphire substrate (b) at 300 K, and (c) at 343 K with imaging plate.

The spot pattern suggested that the C8-BTBT layers possessed an in-plane orientation in addition to the (001)-out-of-plane orientation and a lattice relationship to the C-sapphire substrate, in spite of the large lattice mismatch. It was difficult to decide the in-plane lattice relationship with X-ray diffraction techniques used in this study due to the characteristic monoclinic lattice of the C8-BTBT and difficulty in the precise analysis, resulting in not being able to identify whether the C8-BTBT layer was a single crystal or polycrystalline with the (001)-out-of-plane orientation and not identified in-plane orientation.

3.3.2 Growth of the C8-BTBT layers on the C-Sapphire substrate

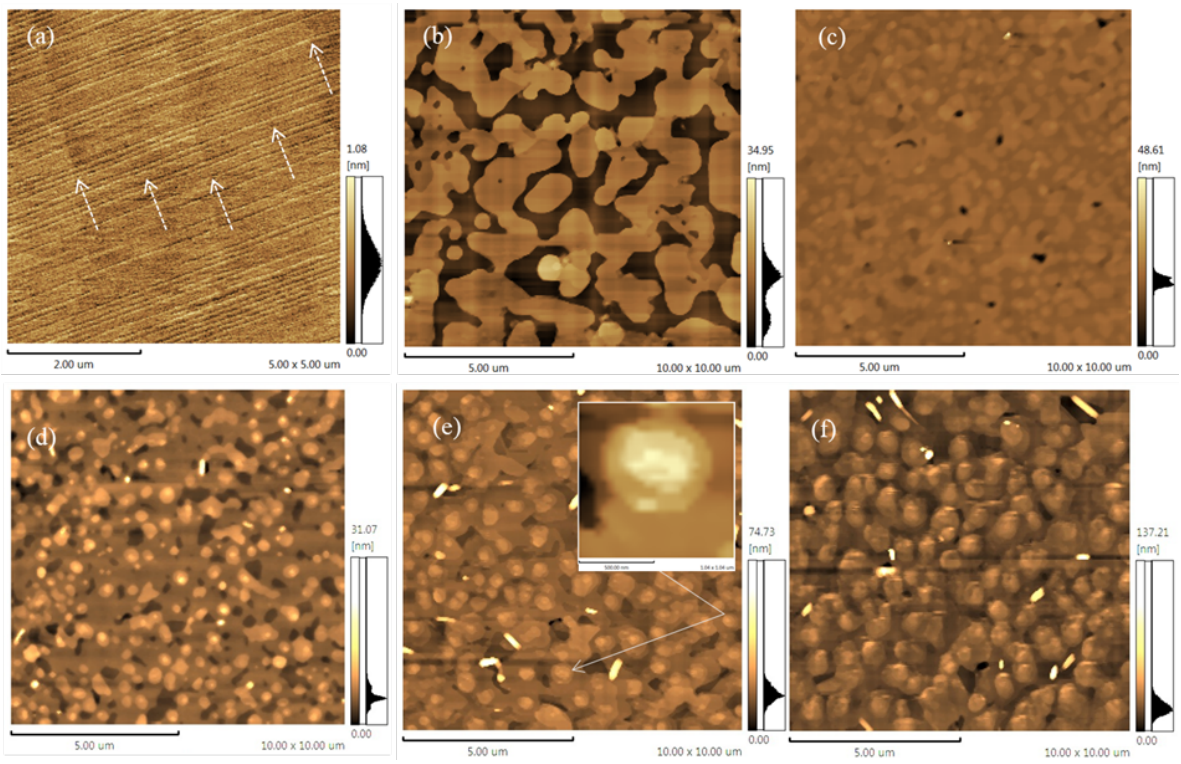

Figure 3.3 AFM images for (a) bare C-sapphire substrate and C8-BTBT layers prepared at 300K with the thickness of (b) 5, (c) 10, (d) 15, (e) 50, and (f) 100 nm.

Figure 3.3 shows AFM images for the bare C-sapphire substrate and C8-BTBT layers prepared at 300 K with the thickness of 5, 10, 15, 50, and 100 nm. Several atomic steps, approximately 1 μm in interval could be observed on the AFM image, although the image was

with noise. Isolated C8-BTBT islands were formed on the C- sapphire substrate, and the height of 11.5 ~ 11.8 nm corresponded to be approximately fourth the c-axis values of C8-BTBT molecule. The islands were growing up in direction parallel to the substrates surface, keeping the almost constant height with the smooth top surface, resulting in the formation of continuous layer, although some pores could be located between the grains. The surface roughness Ra was estimated to be 1.26 nm at 10-nm-thick C8-BTBT layer. According to the AFM observation of 15-nm-thick C8-BTBT layer, the small grains with the size of 0.2 ~ 0.68 μm stacked on the continuous layer, although the Ra was estimated to be 1.23 nm almost same as that at 10-nm-thick layer. The small grains were growing up to 0.3 ~ 1 μm with keeping smooth top surface and terraces as represented in inset could be observed clearly, indicating that the small grains grew by layer-by-layer growth. The surface roughness increased from 1.23 nm at 15-nm-thickness to 5.2 nm at 100-nm-thickness via 3.1 nm at 50-nm-thickness, suggesting that the small grains grew up in direction normal to the substrate surface. The C8-BTBT layer grew up on the C-sapphire substrates by following process. The (001)-orientated C8-BTBT islands were growing up in direction parallel to the substrate surface until forming the continuous layer by the coalescence, and then small grains grew on the continuous layers by layer-by-layer growth.

The growth of the C8-BTBT layer at 343 K and 373 K proceeded by the similar process as that at 300 K. AFM images for C8-BTBT layers prepared at 343 K with the thickness of 5, 10, 15, 50 and 100 nm which were shown in **Figure 3.4**. The height of the C8-BTBT islands before the coalescence changed depending on the preparation temperature, and the height at 343 K was estimated to be 2.4 ~ 2.9 nm nearly corresponding to the c-axis values of C8-BTBT lattice. The size of grain grown on the continuous layer after the coalescence increased from 0.45 ~ 0.76 μm to 1.8 ~ 2.7 μm with increase in thickness from 15 to 100 nm.

The C8-BTBT islands prepared at 373K showed approximately 0.69 μm in size at average thickness of 5 nm and increased to approximately 4.0 μm at the 100-nm-thickness after

the coalescence of islands. The change in the surface roughness was similar tendency to that at 343 K, and the Ra value was estimated to be 9.2 nm at 100-nm-thickness.

Figure 3.5 shows the dependence of the surface roughness on the C8-BTBT layer thickness at 300 K and 343 K and the effects of the preparation temperature on the C8-BTBT grain size at the thickness of 5 and 100 nm. The surface roughness, Ra showed almost constant value up to 15 nm irrespective of the preparation temperature, because C8-BTBT islands with smooth top surface grew in direction parallel to the substrate surface. And, then the Ra value increased with increase in the layer thickness, since the growth of the C8-BTBT transferred to layer-by-layer growth after forming continuous layer.

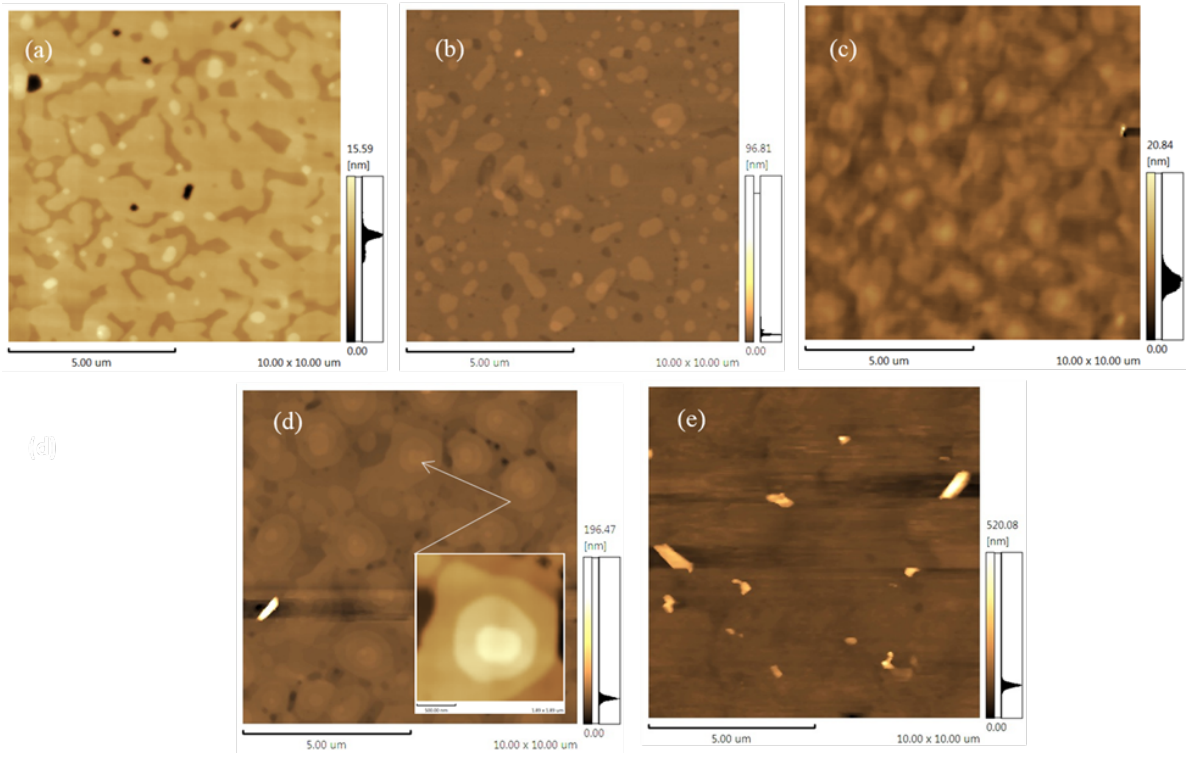

Figure 3.4 AFM images for C8-BTBT layers prepared at 343K with the thickness of (a) 5, (b) 10, (c) 15, (d) 50 and (e) 100 nm.

The grain size of C8-BTBT islands at the 5-nm-thickness showed almost constant value of 0.69 ~ 0.74 μm irrespective of the preparation temperature, indicating that the preparation temperature did not affect the size of C8-BTBT islands directly deposited on C-sapphire substrate. The clear effect of the preparation temperature on the grain size of C8-BTBT layer was observed at the layer thickness of 100 nm. These results suggested that the growth of C8-BTBT islands before the coalescence of the C8-BTBT layer was dominated by the substrate material and the growth after forming the continuous layer was affected by the preparation temperature.

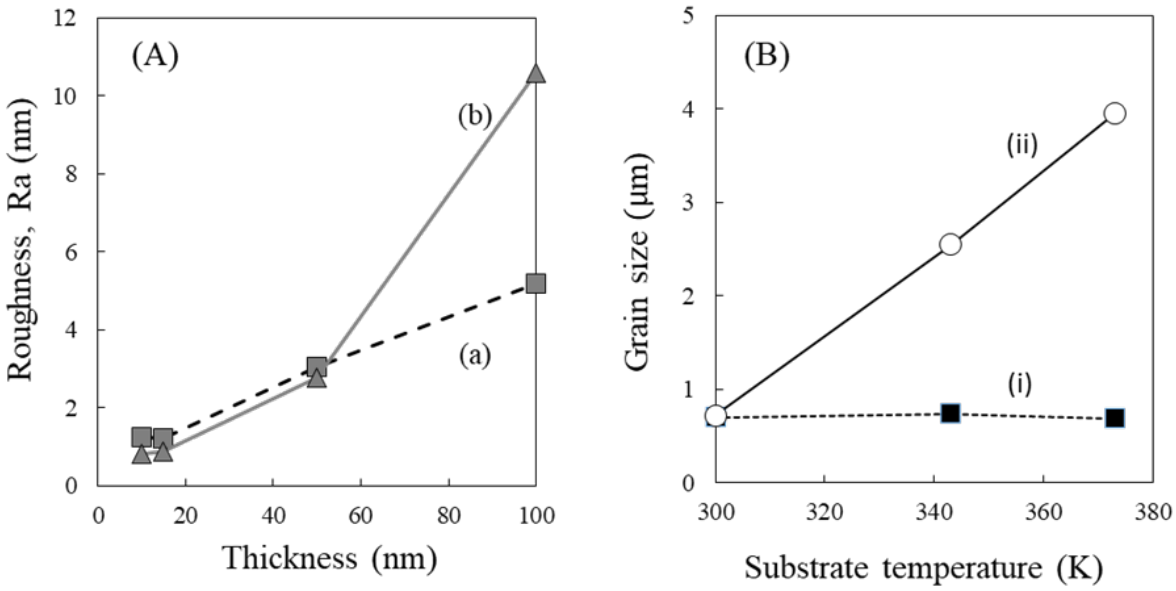

Figure 3.5 Dependence(A) of the surface roughness (Ra) on the C8-BTBT thickness (a) at 300K and (b) 343K, and the Effect (B) of the substrate temperature on the C8-BTBT grain size at the average thickness of (i) 5 and (ii) 100 nm.

3.3.3 Optical and electrical characteristics of the C8-BTBT layers

Figure 3.6 shows absorption spectra for 5, 10, 15, 50 nm- and 100 nm-thick-C8-BTBT layers deposited on C- sapphire substrate at preparation temperature at 300 K. The absorption spectra were almost the same in profile and peak wavelength irrespective of the thickness and the absorbance increased with increase in layer thickness. A weak shoulder was observed at the wavelength of approximately 340 nm, and maximum absorption peaks were seen at the wavelength of 358 nm for all C_8-BTBT layers. The spectra were almost the same in profile and peak wavelength as that already reported for C8-BTBT layer prepared on quartz substrate.**[17]** The optical band gap energy was evaluated from the absorption edge wavelength by using following equation,

$$Eb = h\nu = hc/\lambda_{ae} \quad (3.1)$$

Where, Eb, λ_{ae}, h, c, and ν are band gap energy, absorption edge wavelength**,** Planck constant, velocity of light, and frequency.[18] The bandgap energy was estimated by extrapolating the linear part to $\alpha=0$ on the relationship between the photon energy and absorption coefficient was calculated from the absorbance and thickness. The optical band gap energy of C8-BTBT layers was estimated to be 3.32-3.35 eV regardless of the layer thickness and preparation temperature. The absorption coefficient at 358 nm wavelength was calculated for the absorbance and thickness and ranged from 3.2×10^4 cm^{-1} to 6.8×10^4 cm^{-1}.

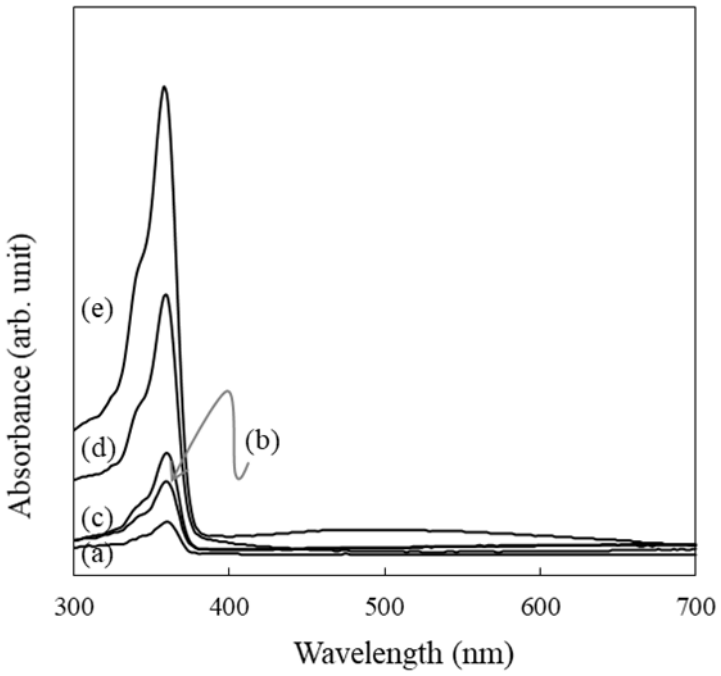

Figure 3.6 Optical absorption spectra of 5 (a), 10 (b), 15 (c), 50 (d), 100-nm-thick-C8-BTBT layers (e) prepared on C-sapphire substrate at 300K.

Figure 3.7 shows the resistivity of C8-BTBT layers prepared at 300, 343, and 373 K without light irradiation and with AM1.5G light irradiation. The resistivity was estimated by van-der-Pauw technique with Hall-effect measuring system with and without light irradiation, but the carrier concentration and mobility could not be estimated in this technique. The resistivity in dark drastically decreased from 2.1×10^6 Ω cm to 1.2×10^2 Ω cm with increase in preparation temperature from 300 to 373 K. The (002) peak angle and preferred orientation were almost the same for all C8-BTBT layers. The grain size, however, changed depending on the preparation temperature. The grain boundary act as scattering defects for transporting carrier as reported in inorganic semiconductors, **[19,20]** although the carrier transporting phenomena

is deflect among organic and inorganic semiconductor. The result revealed that the grain size was an important factor affecting to the resistivity of C8-BTBT layers in dark.

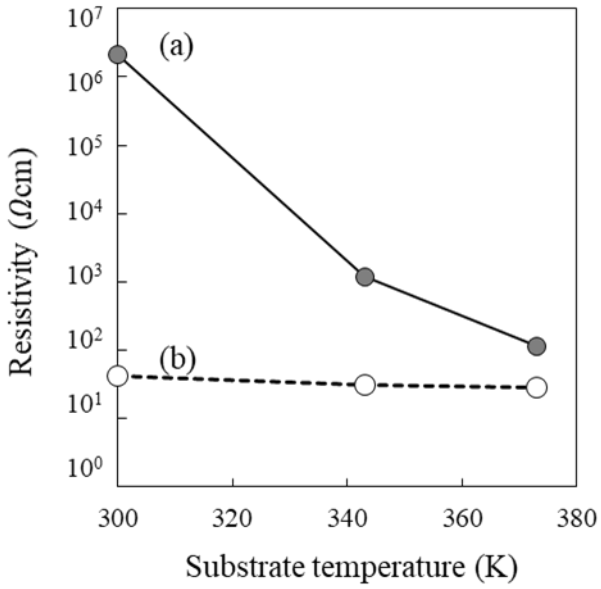

Figure 3.7 Resistivity of 100-nm-thick-C8-BTBT layers prepared at 300-373K (a) without light irradiation, and (b) with AM 1.5G light irradiation.

The resistivity drastically decreased to 42 ~ 28 Ω cm by irradiating the light. Since the AM1.5G light irradiated to C8-BTBT layers contained a light at the photon energy higher than the bandgap energy, the excitation of electron was occurred inside the C8-BTBT molecules. Although further investigation is needed on the electrical characteristics, the light irradiation affects the carrier transporting phenomenon inside the grains.

3.4 Conclusions

C8-BTBT layers were prepared on a single crystal (0001) Al_2O_3 (C-sapphire) substrate by a vacuum evaporation technique, and the (001) out-of-plane orientation were developed irrespective of the preparation condition of the thickness and preparation temperature. The C8-BTBT layer was formed by the growth of (001)-C8-BTBT islands in direction parallel to the substrate surface and then the growth in direction normal to the substrate surface after the formation of the continuous layer. The growth model proposed in chapter two was continued by investigating the growth of C8-BTBT layer on C-sapphire substrate. The optical band gap energy was estimated to be 3.32-3.35 eV. The resistivity of 100 nm thick C8-BTBT layers in dark decreased from 2.1×10^{6} Ω cm to 1.2×10^{2} Ω cm with increasing the preparation temperature 300 K to 373 K, and the resistivity value also decrease to 42 ~ 28 Ω cm by a light irradiation.

REFERENCES

[1] X. Guo, M. Baumgarten, K. Müllen, Designing π-conjugated polymers for organic electronics, Prog. Polym. Sci. **38**, 1832 (2013).

[2] A. Facchetti, Semiconductors for organic transistors, Mater. Today. **10,** 28 (2007).

[3] L. Bian, E. Zhu, J. Tang, W. Tang, F. Zhang, Recent progress in the design of narrow bandgap conjugated polymers for high-efficiency organic solar cells, Prog. Polym. Sci. **37**, 1292 (2012).

[4] Y. Guo, G. Yu, Y. Liu, Functional Organic Field-Effect Transistors, Adv. Mater. **22**, 4427 (2010).

[5] F. Dinelli, M. Murgia, P. Levy, M. Cavallini, F. Biscarini, Spatially Correlated Charge Transport in Organic Thin Film Transistors, Phys. Rev. Lett. **92**, 116802 (2004).

[6] N. Karl, Charge carrier transport in organic semiconductors, Synth. Met. **134**, 649 (2003).

[7] S. Wang, D. Niu, L. Lyu, Y. Huang, X. Wei, C. Wang, H. Xie, Y. Gao, Interface electronic structure and morphology of 2,7-dioctyl[1]benzothieno[3,2-b]benzothiophene (C8-BTBT) on Au film, Appl. Surf. Sci. **416**, 696 (2017).

[8] G. Gbabode, M. Dohr, C. Niebel, J.Y. Balandier, C. Ruzié, P. Négrier, D. Mondieig, Y.H. Geerts, R. Resel, M. Sferrazza, X- ray structural investigation of nonsymmetrically and symmetrically alkylated [1]benzothieno[3,2- b]benzothiophene derivatives in bulk and thin films, ACS Appl. Mater. Interfaces. **6**, 13413 (2014).

[9] Y. Yuan, G. Giri, A. L. Ayzner, A. P. Zoombelt, S.C.B. Mannsfeld, J. Chen, D. Nordlund, M. F. Toney, J. Huang, Z. Bao, Ultra-high mobility transparent organic thin film transistors grown by an off-centre spin-coating method, Nat. Commun. **5**, 1 (2014).

[10] T. Uemura, Y. Hirose, M. Uno, K. Takimiya, J. Takeya, Very high mobility in solution-processed organic thin-film transistors of highly ordered [1]benzothieno[32-b]benzothiophene derivatives, Appl. Phys. Express. **2,** 111501 (2009).

[11] H. Minemawari, T. Yamada, H. Matsui, J. Tsutsumi, S. Haas, R. Chiba, R. Kumai, T. Hasegawa, Injet printing of single-crystal films, Nature. **475** 364 (2011).

[12] C. Liu, T. Minari, X. Lu, A. Kumatani, K. Takimiya, K. Tsukagoshi, Solution-processable organic single crystals with bandlike transport in filed-effect transistors, Adv. Mater. **23**, 523 (2011).

[13] L. Lyu, D. Niu, H. Xie, N. Cao, H. Zhang, Y. Zhang, P. Liu, Y. Gao, Orientation-dependent energy level alignment and film growth of 2,7-dioctyl[1]benzothieno[3,2-b]benzothiophene (C8-BTBT) on HOPG, J. Chem. Phys. **144,** 034701 (2016).

[14] D. He, Y. Zhang, Q. Wu, R. Xu, H. Nan, J. Liu, J. Yao, Z. Wang, S. Yuan, Y. Li, Y. Shi, J. Wang, Z. Ni, L. He, F. Miao, F. Song, H. Xu, K. Watanabe, T. Taniguchi, J.-B. Xu, X. Wang, Two-dimensional quasi-freestanding molecular crystals for high-performance organic field-effect transistors, Nat. Commun. **5,** 5162 (2014).

[15] T. Izawa, E. Miyazaki, K. Takimiya, Molecular ordering of high-performance soluble molecular semiconductors and re-evaluation of their field-effect transistor characteristics, Adv. Mater. **20**, 3388 (2008).

[16] Joint Committee on Powder Diffraction Standards, Powder Diffraction File (International Data for Diffraction Data) pp 042-1468.

[17] R. Miscioscia, F. Loffredo, G. Nenna, F. Villani, C. Minarini, M. Petrosino, A. Rubino, M. Denti, A. Facchetti, Analysis of the persistent photoresponse of C8BTBT transistors in the near-bandgap spectral region, Physics. Mater. Appl. **30**, 83 (2016).

[18] J.C.S. Costa, R.J.S. Taveira, C.F.R.A.C. Lima, A. Mendes, L.M.N.B.F. Santos, Optical band gaps of organic semiconductor materials, Opt. Mater. (Amst). **58,** 51 (2016).

[19] T. Shinagawa, M. Onoda, B.M. Fariza, J. Sasano, M. Izaki, Annealing effects and phtoelectric properties of single-oriented Cu_2O films electrodeposited on Au(111)/Si(100) substrates, J. Mater. Chem. *A*. **1**, 9182 (2013).

[20] T. Shinagawa, M. Chigane, K.Murase, and M. Izaki, Drastatic change in electrical properties of electrodeposited ZnO: systematic study by Hall effect measurements, J. Phys.Chem.C, **116**, 15925 (2012).

CHAPTER 4

Growth and characteristics of PTCDI-C8 layers on single crystal substrates with various orientations

4.1 Introduction

The organic semiconductors have been successfully employed in electronic and optoelectronic devices such as field effect transistors (FETs), light emitting diodes (LEDs), and photovoltaic cells (PVs).**[1–6]** In addition, it is possible to be applied in new application such as thyristor, and magnetoresistance devices.**[7,8]** The device performance mainly relies on the

crystal structure including the orientation and grain structure of the organic semiconductor layers.**[9,10]** The structure has been controlled by optimizing the substrate material including the orientation,**[11,12]** and the growth containing the preparation process and conditions such as substrate temperature and layer thickness.**[13,14]**

Perylene derivatives of N,N'-dioctyl-3,4,9,10-perylenedicarboximide (PTCDI-C8) have attracted much attention to fabricate molecular based devices due to their high mobility up to 0.6 $cm^2V^{-1}s^{-1}$.**[15]** The 1D-PTCDI-C8 nanoribbons were prepared by a rapid transfer method, and the optical properties made it possible to be utilized in optoelectronic circuitry and laser resonator.**[16,17]** The unit cell of the PTCDI-C8 was reported to be a triclinic lattice but the lattice constant was different for the bulk and films.**[18,19]**

We have reported that the (001)-2,7-dioctyl[1]benzothieno[3,2-b][1]benzothiophene (C8-BTBT) layer was grown on Al_2O_3 and MgO single crystal substrates with various orientations and orientation of layers by the strong π-π stacking, and the electrical resistivity related the grain structure.**[20]** The π-π stacking plays an important role in developing the out-of-plane and in-plane orientation for the organic semiconductor, and the tentative growth model has been proposed.**[21]**

In this chapter, we investigated the effect of substrate materials and the orientation on the growth and orientation of vacuum evaporated PTCDI-C8 layers, and also investigated the effect of layer thickness and substrate temperature on C-Sapphire substrate with X-ray diffraction (XRD), atomic force microscopy (AFM), and optical absorption spectra measurement. The (001)-PTCDI-C8 layers were grown on the single crystal Al_2O_3 and MgO substrates regardless of the substrate material and orientation. The aim of this work is that characterization of structural relation between π-conjugated semiconductor PTCDI-C8 layers and single crystal inorganic substrates and examining the effects of the layer thickness and preparation temperature on the structural, morphological and optical properties.

4.2 Experimental procedures

The 100-nm-thick PTCDI-C8 layers were deposited at substrate temperature of 343 K at a pressure around 4×10^{-5} Pa on single crystal substrates with various orientations, (11$\underline{2}$0)-Al_2O_3 (A-sapphire), (0001)- Al_2O_3 (C-sapphire), (1$\underline{1}$02)-Al_2O_3 (R-sapphire), (100)-MgO, (111)-MgO, and quartz glass substrates by a vacuum thermal evaporation system (ULVAC, VTS-350 ERH/M) connected with turbo molecular pump and oil-free scroll vacuum pump. The annealing was carried out in air for 1 hr at 1200 °C for sapphire substrates and 1100 °C for MgO substrates. The deposition rate 0.1 nm/s was controlled by a quartz crystal deposition control system (ULVAC, CRTM-6000G).

To characterize the effect of layer thickness and substrate temperature in PTCDI-C8 layers, vacuum evaporated 15 to 100 nm-thick-PTCDI-C8 layers were prepared only on C-Sapphire substrate at substrate temperature 300 K, 343 K and 373 K. The thickness of the organic layers was determined by a surface profiler system (ULVAC, Dek Tak 150). X-ray diffraction spot patterns were recorded by using 2D imaging plate detector with monochromatic CuKα radiation using Rigaku RINT- Rapid Ⅱ. The out-of-plane X-ray diffraction were performed at 2θ value from 5 degrees to 30 degrees by a θ/2θ scanning technique using Rigaku RINT 2500 X-ray diffractometer at monochromatic CuKα radiation operated at 40 kV, 100 mA with a wavelength ($\lambda = 0.154059$ nm). Surface morphologies were observed by an atomic force microscopy (AFM, Shimadzu, SPM-9700 Kai) in dynamic mode in air. Absorption spectra measurements were performed using a UV-VIS-NIR spectrophotometer (HITACHI, U4100) with a reference of (0001) C-Sapphire bare substrate.

4.3 Results and Discussion

4.3.1 Effects of the substrate material and orientation of the PTCDI-C8 layers

X-ray diffraction methods were performed to analyse the structure and orientation of the PTCDI-C8 layers prepared on quartz glass substrate, single crystal sapphire substrates of (11$\underline{2}$0) A-sapphire, (0001) C-sapphire, (1$\underline{1}$02) R-sapphire, and single crystal (100) and (111) MgO substrates. X-ray diffraction patterns recorded by the imaging plate for 100 nm-thick-PTCDI-C8 layers deposited on quartz, (0001) C-sapphire, (11$\underline{2}$0) A-sapphire, and (100) MgO substrates at substrate temperature 343 K were shown in **Figure 4.1** The two dashed lines in **Figure. 4.1(a)** represent the radial direction of 2θ and circumferential direction of β angles. There was only one spot represented by arrow ① corresponding to the (001)-plane of the PTCDI-C8 and broadened diffraction ring originating from the quartz glass substrate. The (001) diffraction spot could be observed for all diffraction patterns of PTCDI-C8 layers. Similar spot patterns inside the dash-line square could be observed for all the PTCDI-C8 layers prepared on the single crystal substrates, regardless of the substrate materials and orientation. Two diffraction spots were observed at 2θ angle of 8.2 and 12.3 degrees represented by arrow ② and ③ in addition to those originated from the substrate. Two diffracted spots were assigned as (002) and (003) planes of the PTCDI-C8, indicating the development of the (001)-out-of-plane orientation, irrespective of the substrate materials and orientation. Almost the same spot patterns suggested the development of the (001)-out-of-plane orientation, in addition to the similar in-plane orientation for the 100-nm-thick PTCDI-C8 layers, but it was difficult to identify accurately. The lattice relationship between PTCDI-C8 layers and substrate materials could be identified as; $(001)_{PTCDI\text{-}C8}$ // $(11\underline{2}0)_{Al2O3}$, $(001)_{PTCDI\text{-}C8}$ // $(0001)_{Al2O3}$, $(001)_{PTCDI\text{-}C8}$ // $(1\underline{1}02)_{Al2O3}$, $(001)_{PTCDI\text{-}C8}$ // $(100)_{MgO}$, $(001)_{PTCDI\text{-}C8}$ // $(111)_{MgO}$.

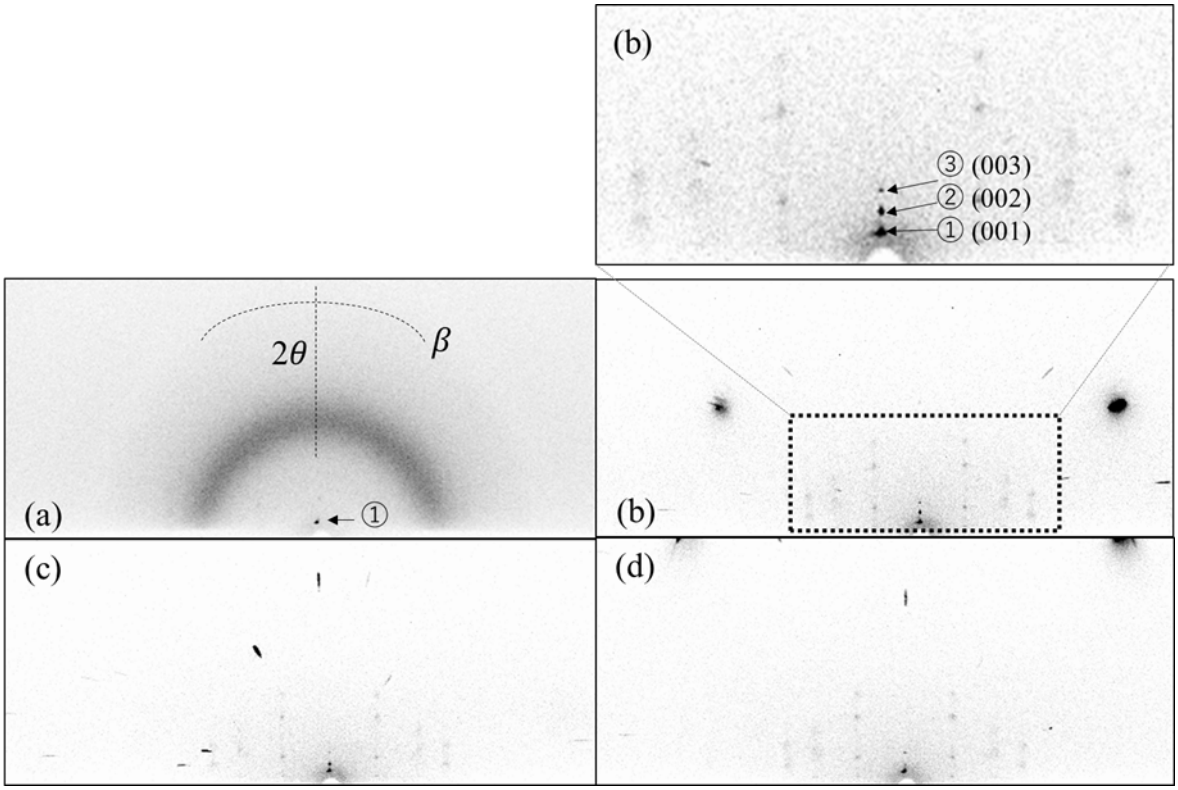

Figure 4.1 Imaging plate-X-ray diffraction patterns of 100-nm-thick PTCDI-C8 layers on (a) quartz glass, (b) C-sapphire, and (c) A-sapphire and (d) (100) MgO.

Figure 4.2 shows the schematic illustrations of the lattice configurations of the (001) PTCDI-C8, (0001)-Al_2O_3, (11$\underline{2}$0)-Al_2O_3 and (100)-MgO planes. The PTCDI-C8 possesses a triclinic lattice with a = 0.900 nm, b = 0.489 nm, c = 2.165 nm, α =95.0 degree, β = 100.7 degree, and γ= 112.8 degree, and the lattice parameters changed depending on the type of the PTCDI-C8 such as powder and layer.**[18,19][22]** The Al_2O_3 possesses a hexagonal lattice with a = 0.47589 nm, and c = 1.2991 nm, and MgO possesses a cubic lattice with a = 0.4213 nm.[23][24] The lattice mismatch was estimated to be approximately 0.58% and 2.68% on a- and b-axis of PTCDI-C8 for the lattice relationship of $(001)_{PTCDI\text{-}C8}//(0001)_{Al2O3}$, approximately -56.7% and -15.7% on a- and b-axis of PTCDI-C8 for the lattice relationship of $(001)_{PTCDI\text{-}C8}//(11\underline{2}0)_{Al2O3}$, approximately -1.64 % and 13.8 % on a- and b-axis of PTCDI-C8 for the lattice relationship of

$(001)_{PTCDI-C8}//(1x2)(100)_{MgO}$. The lattice mismatch varied in wide range depending on the substrate materials and orientation, but the lattice mismatch did not affect the out-of-plane orientation of the PTCDI-C8 layers as demonstrated by the X-ray diffraction patterns. The C8-BTBT layers showed the (001) out-of-plane orientation on single crystal Al_2O_3 and MgO substrates with different orientation like that for the PTCDI-C8 layers reported here, and the growth mechanism governed by the strong π–π stacking between the molecules has been proposed in addition to the surface steps formed on the substrate surface.**[20]** Since the preferred orientation of the PTCDI-C8 was similar irrespective of the substrate material and orientation, the growth was investigated only on the C-sapphire substrate.

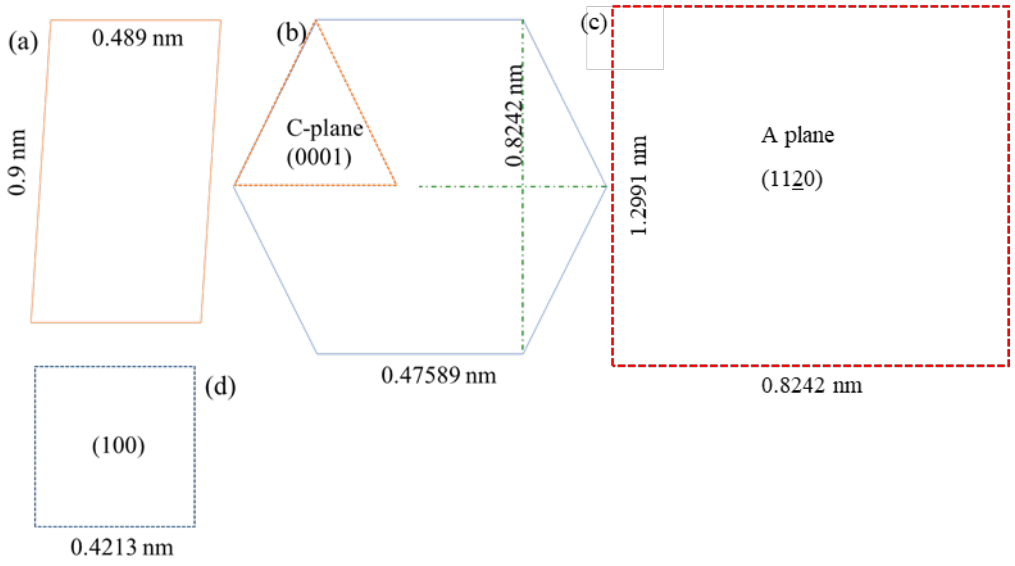

Figure 4.2 Schematic illustrations of (a) (001) plane of PTCDI-C8, (b) (0001) plane, and (c) (11$\underline{2}$0) plane of Al_2O_3, and (d) (100) plane of MgO.

4.3.2 Orientation of the PTCDI-C8 layers on C-Sapphire substrate

Figure 4.3 shows out-of-plane X-ray diffraction patterns for 100-nm-thick PTCDI-C8 layers prepared at 300, 343, and 373 K. The diffracted X-ray peaks could be observed from 8.4 degrees and each approximately 4 degrees, and these peaks were assigned as (002), (003), (004), and (005) planes, respectively. One sharp and intense peak at around 21 degrees which was originated from the single crystal C-sapphire substrate. The spacing d of the (002) plane of 100 nm-thick-PTCDI-C8 layers could be estimated to be 1.03 nm, which was close to 0.98 nm calculated from the lattice parameters mentioned above. It was confirmed from the out-of-plane X-ray diffraction patterns that PTCDI-C8 layers possessed the (001)-out-of-plane orientation, in which PTCDI-C8 molecules with almost upright standing position were preferably to grow on C-sapphire substrate regardless of the preparation temperature.

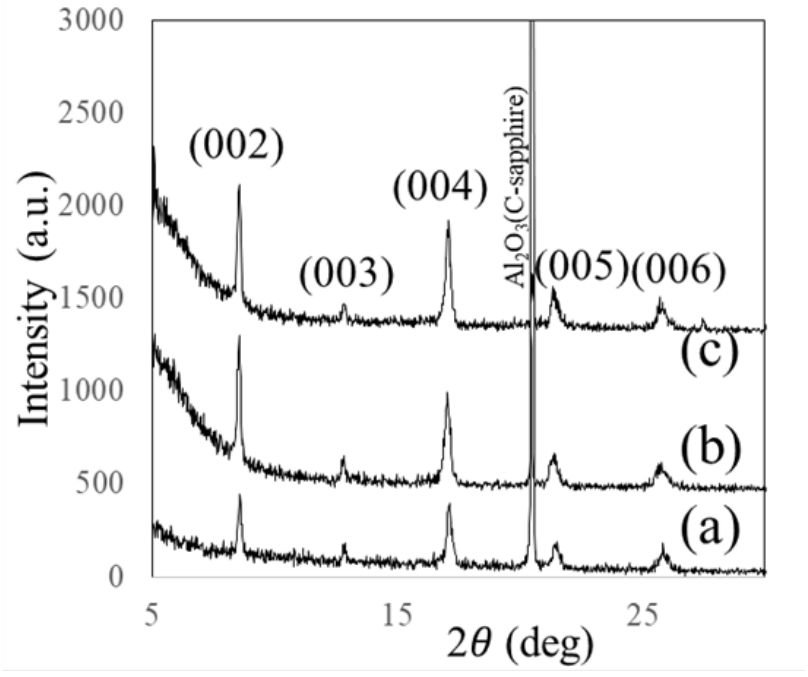

Figure 4.3 X-ray diffraction patterns of 100-nm-thick PTCDI-C8 layers at (a) 300 K, (b) 343 K, and (c) 373 K.

4.3.3 Grain structure and growth of the PTCDI-C8 layers

The surface morphology of 15 nm, 50 nm, and 100 nm-thick PTCDI-C8 layers prepared at 300 K, 343 K, and 373 K was observed by AFM. AFM images for bare C-sapphire substrate, 15, 50, and 100-nm-thick-PTCDI-C8 layers prepared at 373 K were shown in **Figure 4.4**. Periodic atomic steps with approximately 1 μm in interval could be observed on the AFM image of the bare C-sapphire substrate. And, the surface roughness (Ra) was estimated to be 0.097 nm. The changes in grain morphology were similar irrespective of the preparation temperature from 300 K to 373 K. The elongated needle-like grains were formed regardless of the layer thickness, and the grains deposited over the entire substrate surface at the thickness of 15 nm. The width and length of needle-like grains increased from 40 nm in width and 136 nm in length to 74 nm and 242 nm with increase in the thickness from 15 to 100 nm. The surface roughness Ra was estimated to be 0.71 nm at 15-nm-thickness and 1.27, 1.65 nm for increasing the layer thickness to 50 nm and 100 nm. The PTCDI-C8 grains grew up with increase in the thickness keeping the needle-like shape.

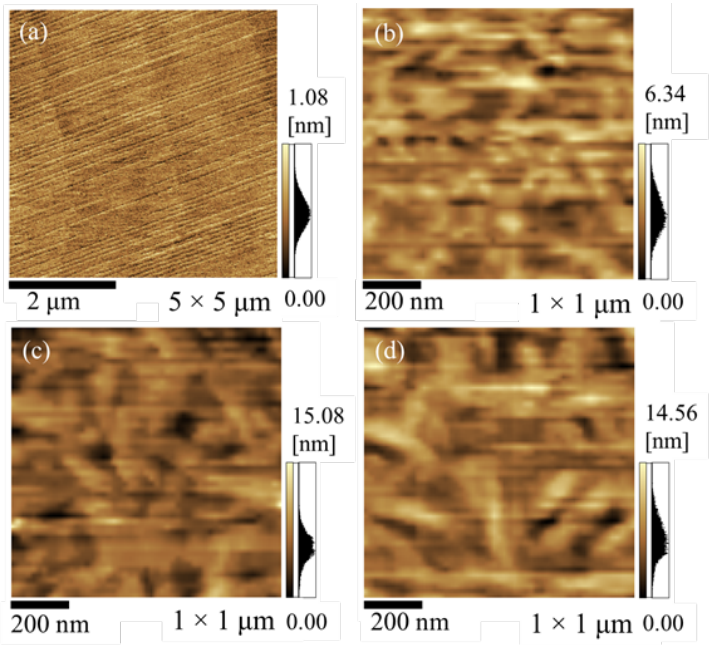

Figure 4.4 AFM images for (a) bare C-sapphire substrate, (b) PTCDI-C8 layers prepared at 373 K with the thickness of 15 nm, (c) 50 nm, and (d) 100 nm.

Figure 4.5 shows AFM images for 100-nm-thick-PTCDI-C8 layers prepared at substrate temperature of 300 K, 343 K and 373 K. Similar needle-like grains were formed over the C-sapphire substrate surface, and the grain length was estimated to be 124 nm at 300 K and became larger to 242 nm at 373 K. The surface roughness (Ra) decreased from 2.03 nm to 1.65 nm with increase in preparation temperature from 300 K to 373 K.

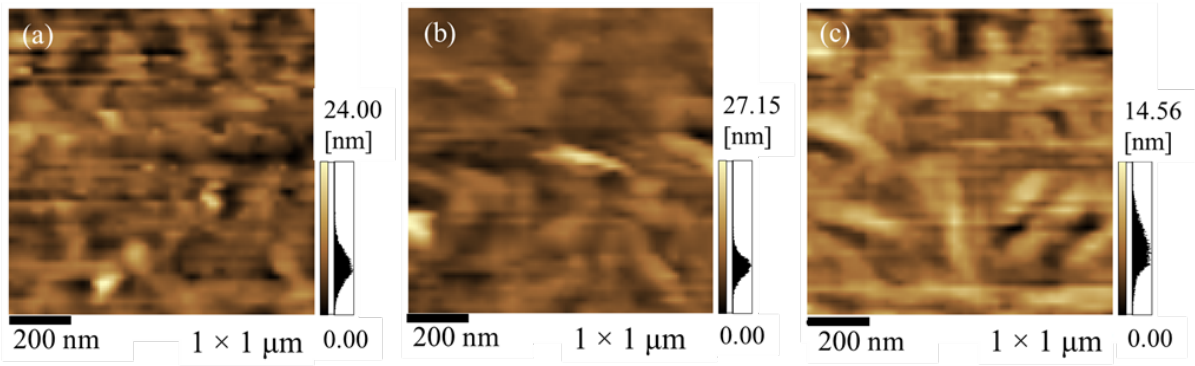

Figure 4.5 AFM images for 100-nm-thick-PTCDI-C8 layers prepared at (a) 300 K, (b) 343 K, and (c) 373 K.

The effects of the thickness and preparation temperature on the grain length and surface roughness (Ra) were summarized in **Figure 4.6**. The PTCDI-C8 grain length increased from 74 nm to 120 nm at 300 K, 80 nm to 210 nm at 343 K, and 120 nm to 240 nm at 373 K, with increase in thickness from 15 nm to 100 nm. The grain length at same thickness was larger at higher preparation temperature. The PTCDI-C8 layers possessed a relatively smooth surface with the surface roughness (Ra) ranging from 0.59 nm to 2.03 nm, and the Ra value increased with increase in thickness irrespective of the preparation temperature. The grain morphology and surface roughness were similar tendency to that previously reported for the PTCDI-C8 on silicon substrate at room temperature.**[25]** Although there was no information on the growth of the PTCDI-C8 at the thickness below 15 nm, the needle-like islands with the (001)-out-of-plane orientation were formed on the single crystal substrate by governing the π–π stacking,

according to the results shown here and growth model already proposed on the C8-BTBT layer.**[20]** The needle-like islands formed a continuous layer at the thickness of 15 nm or below, and the needle-like grains grew up with the thickness keeping the smooth surface.

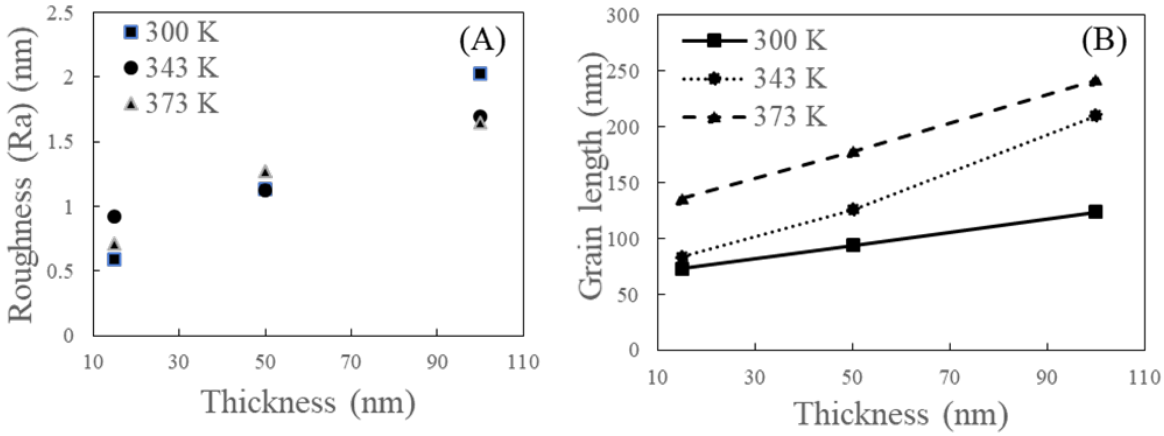

Figure 4.6 The effects of the thickness and preparation temperature on (A) the surface roughness (Ra) and (B) grain length.

Figure 4.7 shows the optical absorption spectra for 100-nm-thick-PTCDI-C8 layers at 300 K, 343 K, and 373 K and at the thickness of 15, 50, 100 nm at 300 K. The PTCDI-C8 layers possessed three absorption peaks at the wavelength of 565 nm, 480 nm, and 228 nm and a weak shoulder at 525 nm regardless of the thickness and preparation temperature. The spectra were almost the same in profile as that already reported for the PTCDI-C8 layer.**[26]** Since the C-sapphire substrate showed no absorption at wavelength from 200 to 700 nm, the absorption peaks at the wavelength of 228 nm also was originated from the PTCDI-C8 layers. The intensity of absorption peaks increased with increase in the thickness, and the preparation temperature showed slight effect on the intensity. The PTCDI-C8 layers showed an absorption edge at wavelength of 610 nm corresponding to the photon energy of 2.03 eV. The absorption edge wavelength was determined by extrapolating the linear line. The absorption coefficient was

calculated from the absorbance at the wavelength of 228 nm and thickness, and values ranging from 7.34×10^4 cm^{-1} to 8.9×10^4 cm^{-1} for 100-nm-thick-PTCDI-C8 layers.

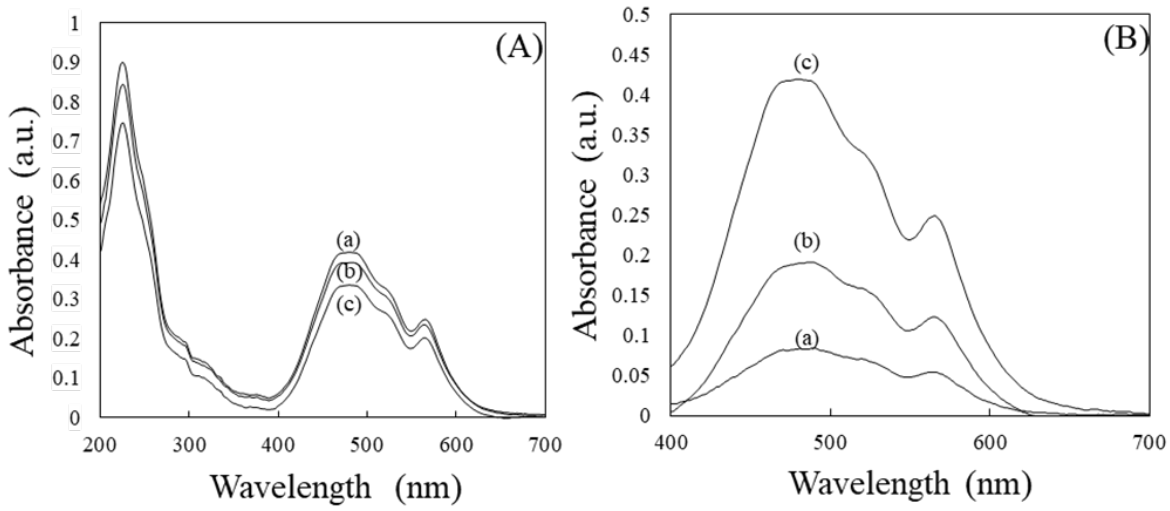

Figure 4.7 (A) Optical absorption spectra of 100-nm-thick-PTCDI-C8 layers at (a) 300 K, (b) 343 K, and (c) 373 K, and (B) of (a) 15 nm, (b) 50 nm, and (c) 100 nm -thick PTCDI-C8 layers at 300 K.

We have reported the growth of the (001)-C8-BTBT layer on single crystal Al_2O_3 and MgO substrates, irrespective of the lattice mismatch. And, the tentative growth model governed by the surface steps of the substrate and π-π-stacking of the C8-BTBT molecule has been proposed. The growth of the PTCDI-C8 layers showed the similar tendency to that of C8-BTBT. It was accepted for inorganic semiconductors such as oxides that the lattice relationship including the lattice mismatch strongly affected the growth of the oxide layer, as demonstrated for the <0001>-ZnO layer growth on <111>-Au and <0001>-Ga:ZnO layers.**[27–29]** However, there was no effect of the atomic arrangement and lattice mismatch on the growth of the PTCDI-C8 layers, and the similar preferred orientation was obtained regardless of the substrate material and the orientation. We can propose the growth of PTCDI-C8 layer on single crystal substrates

as follow: the PTCDI-C8 aggregates bounded by the π-π-stacking reached on the substrate in the evaporation process and then diffused on the surface. There were steps periodically formed on the surface of the C-sapphire substrate and other single crystal sapphire substrates, and the diffused PTCDI-C8 molecules were stopped by the steps, resulting in the formation of the PTCDI-C8 layer with (001)-out-of-plane orientation.

4.4 Conclusions

PTCDI-C8 layers were deposited on quartz and single crystal Al_2O_3 and MgO substrates with a various orientation by a vacuum evaporation technique. The (001)-out-of-plane orientation was developed irrespective of the substrate materials and orientation in spite of the difference in the lattice mismatch. The needle-like PTCDI-C8 grains grew up on C-Sapphire substrate and the grain size and surface roughness increased with increase in thickness. The optical band gap energy of 2.03 eV was estimated from the absorption spectra. The results demonstrated here support the growth model of organic semiconductors by the surface steps of single crystal substrate and strong π-π stacking between the organic molecules.

REFERENCES

[1] C.D. Dimitrakopoulos, D.J. Mascaro, Organic thin-film transistors: A review of recent advances, IBM J. Reasearch Dev. **45**, 11 (2001).

[2] C.D. Dimitrakopoulos, P. Malenfant, Organic thin film transistors for large area electronics, Adv. Mater. **14**, 99 (2002).

[3] A. Facchetti, Semiconductors for organic transistors, Mater. Today. **10**, 28 (2007).

[4] C.W. Tang, S.A. Vanslyke, Organic electroluminescent diodes, Appl. Phys. Lett. **51**, 913 (1989).

[5] H. Hoppe, N.S. Sariciftci, Organic solar cells: An overview, J. Mater. Res. **19**, 1924 (2004).

[6] T. Uemura, Y. Hirose, M. Uno, K. Takimiya, J. Takeya, Very high mobility in solution-processed organic thin-film transistors of highly ordered [1] benzothieno [3,2-b] benzothiophene derivatives, Appl. Phys. Express. **2**, 6 (2009).

[7] F. Sawano, I. Terasaki, H. Mori, T. Mori, M. Watanabe, N. Ikeda, Y. Nogami, Y. Noda, An organic thyristor, Nature. **437**, 522 (2005).

[8] S. Sakai, K. Yakushiji, S. Mitani, K. Takanashi, H. Naramoto, P. V Avramov, K. Narumi, V. Lavrentiev, Y. Maeda, Tunnel magnetoresistance in Co nanoparticle/Co–C60 compound hybrid system, Appl. Phys. Lett. **89**, 113118 (2006).

[9] H.N. Tsao, D. Cho, J.W. Andreasen, A. Rouhanipour, D.W. Breiby, W. Pisula, K. Müllen, The influence of morphology on high-performance polymer field-effect transistors, Adv. Mater. **21**, 209 (2009).

[10] F. Dinelli, M. Murgia, P. Levy, M. Cavallini, F. Biscarini, D.M. De Leeuw, Spatially Correlated Charge Transport in Organic Thin Film Transistors, Phys. Rev. Lett. **92**, 7 (2004).

[11] H. Huang, Y. Huang, S. Wang, M. Zhu, H. Xie, L. Zhang, X. Zheng, Q. Xie, D. Niu, Y.

Gao, Van Der Waals Heterostructures between Small Organic Molecules and Layered Substrates, Crystals. 6, 113 (2016).

[12] E.J. Kintzel, D.M. Smilgies, J.G. Skofronick, S.A. Safron, D.H. Van Winkle, Ultrathin film growth of p-phenylene oligomers on alkali halide substrates, J. Cryst. Growth. **289**, 345 (2006).

[13] L. Zhang, Y. Yang, H. Huang, L. Lyu, H. Zhang, N. Cao, H. Xie, X. Gao, D. Niu, Y. Gao, Thickness-dependent air-exposure-induced phase transition of CuPc ultrathin films to well-ordered one-dimensional nanocrystals on layered substrates, J. Phys. Chem. C. **119**, 4217 (2015).

[14] A. Andreev, R. Resel, D.M. Smilgies, H. Hoppe, G. Matt, H. Sitter, N.S. Sariciftci, D. Meissner, H. Plank, O. Zrzavecka, Oriented organic semiconductor thin films, Synth. Met. **138**, 59 (2003).

[15] P.R.L. Malenfant, C.D. Dimitrakopoulos, J.D. Gelorme, L.L. Kosbar, T.O. Graham, A. Curioni, W. Andreoni, N-type organic thin-film transistor with high field-effect mobility based on a N,N′-dialkyl-3,4,9,10-perylene tetracarboxylic diimide derivative, Appl. Phys. Lett. **80**, 2517 (2002).

[16] C.O.N. Spectus, One-Dimensional Self-Assembley of Planar π-Conjugated Molecules : Adaptable Building Blocks for Organic Nanodevices, Acc. Chem. Res. **41**, 1596 (2008).

[17] T. Abhijith, M.Y. Ameen, V.S. Reddy, Synthesis of PTCDI-C8 one dimensional nanostructures for photovoltaic applications, IOP Conf. Ser. Mater. Sci. Eng. **73**, 6 (2015).

[18] A.L. Briseno, S.C.B. Mannsfeld, C. Reese, J.M. Hancock, Y. Xiong, S.A. Jenekhe, Z. Bao, Perylenediimide Nanowires and Their Use in Fabricating Field-Effect Transistors and Complementary Inverters, Nano Lett. **7**, 2847 (2007).

[19] T.N. Krauss, E. Barrena, X.N. Zhang, D.G. de Oteyza, J. Major, V. Dehm, F. Würthner,

L.P. Cavalcanti, H. Dosch, Three-dimensional molecular packing of thin organic films of PTCDI-C8 determined by surface X-ray diffraction., Langmuir. **24**, 12742 (2008).

[20] A.M. Moh, K. Sasaki, T. Shinagawa, S. Watase, M. Izaki, Preferred orientation of 2,7-dioctyl[1]benzothieno[3,2-b][1]benzothiophene molecules on inorganic single crystal substrates with various orientations. Jpn. J. Appl. Phys. PV17001 (2018) "to be published".

[21] Z.F. Yao, J.Y. Wang, J. Pei, Control of π-π Stacking via Crystal Engineering in Organic Conjugated Small Molecule Crystals, Cryst. Growth Des. **18**, 7 (2018).

[22] T.N. Krauss, E. Barrena, D.G. De Oteyza, X.N. Zhang, V. Dehm, F. Wu, H. Dosch, X-ray /Atomic Force Microscopy Study of the Temperature-Dependent Multilayer Structure of PTCDI-C8 Films on SiO_2, J. Phys. Chem. C. **113**, 4502 (2009).

[23] Joint Committee on Powder Diffraction Standards, Powder Diffraction File (International Data for Diffraction Data), No.00-042-1468.

[24] Joint Committee on Powder Diffraction Standards, Powder Diffraction File (International Data for Diffraction Data), No. 00-004-0829.

[25] R. Rahimi, V. Narang, D. Korakakis, Optical and morphological studies of thermally evaporated PTCDI-C8 thin films for organic solar cell applications, Int. J. Photoenergy. **2013**, 1 (2013).

[26] B. Mukherjee, Large photoresponse from a small molecule: Application in photodetector and pseudo-transistor, Optik (Stuttg). **126**, 1258 (2015).

[27] M. Izaki, S. Watase, H. Takahashi, Low-temperature electrodeposition of room-temperature ultraviolet-light-emitting zinc oxide, Adv. Mater. **15**, 2000 (2003).

[28] M. Izaki, S. Watase, H. Takahashi, Room-temperature ultraviolet light-emitting zinc oxide micropatterns prepared by low-temperature electrodeposition and photoresist, Appl. Phys. Lett. **83**, 4930 (2003).

[29] M. Izaki, M. Kobayashi, T. Shinagawa, T. Koyama, K. Uesugi, A. Takeuchi, Electrochemically Grown ZnO Vertical Nanowire Scintillator with Light-Guiding Effect, Phys. Status Solidi. A **214**, 1700285 (2017).

CHAPTER 5

Fabrication and structure of PTCDI-C8/C8-BTBT bi-layer

5.1 Introduction

Organic-organic heterostructure of small molecules to polymers constituents have been applied in electronic devices such as organic photovoltaics (OPVs).**[1-5]** The devices have been fabricated by stacking p- and n-type molecular semiconductor layers, and the performance

closely relates to the preferred orientation and interface morphology of the resultant hetero-structure due to the introduction of structural defects and electrostatic disorder, resulting in being the importance of the growth on organic semiconductor.**[6-9]**

Perylene derivatives (n-PTCDI-C8) and BTBT derivatives (p-C8-BTBT) are promising materials to be used in active layers of OFETs and OPVs.**[10-18]** The growth of the single C8-BTBT and PTCDI-C8 layers were reported on the some types of substrates such as HOPG, and Au.**[19-21]** And, we reported the growth of (001)-oriented-C8-BTBT layer on (0001)Al_2O_3 (C-sapphire) substrate by coalescence the (001)-oriented islands.**[22]**

In this chapter, we prepare bi-layers of C8-BTBT and PTCDI-C8 with a different stacking sequence and report the effect on the surface morphology and potential homogeneity on the resultant bi-layers. The (001) C8-BTBT/(001)PTCDI-C8 bi-layer showed an excellent performance in the surface morphology and potential homogeneity compared with the (001) PTCDI-C8/(001) C8-BTBT bi-layer.

5.2 Experimental procedures

The single layers and bi-layers of C8-BTBT and PTCDI-C8 were prepared on single crystal (0001)-Al_2O_3 (C-Sapphire) substrate with surface roughness(Ra) 0.1 nm by a vacuum thermal evaporation system (ULVAC, VTS-350 ERH/M) connected with a turbo molecular pump and oil-free scroll vacuum pump and at pressure around 4×10^{-4} Pa. The powder of 99 % purity C8-BTBT and PTCDI-C8 were purchased from Sigma Aldrich and used as source materials. Prior to deposition of organic materials, (0001)Al_2O_3 C-sapphire substrates were annealed in air at 1200 ℃ for 1 h and then cleaned with acetone and deionized water, after that dried at room temperature.

The 100-nm thick single layer of C8-BTBT and PTCDI-C8 were prepared at substrate temperature 343 K with the deposition rate 0.1 nm/s which were monitored by using quartz crystal sensor with deposition control system (ULVAC, CRTM- 6000G). After the deposition of organic single layers of C8-BTBT and PTCDI-C8, the subsequence layers were prepared at similar manners for bi-layer films.

Single layers and bi-layers were characterized by X-ray diffraction technique using 2D imaging plate detector with monochromatic CuKα radiation using Rigaku RINT-Rapid II and out-of-plane X-ray diffraction by a θ/2θ scanning technique using Rigaku RINT 2500 X-ray diffractometer. Topography and surface potential images were observed by contact mode Kelvin force microscopy (KFM) in air with Pt-Ir-coated Si cantilever with scanning probe microscopy (SPM, Shimadzu SPM-9700-Kai).

5.3 Results and discussion

5.3.1 Effects of the stacking sequence on preferred orientation of PTCDI-C8/C8-BTBT bi-layers

Figure 5.1 shows X-ray diffraction patterns of C8-BTBT and PTCDI-C8 single layers, and the bi-layers with the different stacking sequence. The PTCDI-C8 single layer showed peaks at approximately 8.5 and 12.8 degrees in 2θ angle, and the peaks were identified as (002) and (003) planes of PTCDI-C8 with the characteristic triclinic lattice. And, some peaks with the approximately 4 degree interval could be observed on the X-ray diffraction pattern recorded ranging from 5 to 35 degrees, and all the peaks were assigned as (00n) (n = 2, 3, ···), indicating the formation of (001)-out-of-plane orientation. The C8-BTBT layer showed three peaks at 6.1, 9.1, and 12.3 degrees, and the peaks were assigned as (002), (003), and (004) planes of the C8-BTBT layer with the characteristic monoclinic lattice, indicating the formation of (001)-out-of-plane orientation, as already reported.**[22]** The C8-BTBT/PTCDI-C8 bi-layers showed 5 peaks composed of the 2 peaks and 3peaks originated from the PTCDI-C8 and C8-BTBT layers irrespective of the stacking sequence, and the peak angles agreed with those of both single layers, indicating the formation of (001)-out-of-plane orientation even for the bi-layers. The lattice relationship of (001)-C8-BTBT // (001)-PTCDI-C8 // (0001)-Al_2O_3 was kept for the bi-layer structures, in spite of the large lattice mismatch of -23.47 % PTCDI-C8 along b-axis // C8-BTBT along a-axis, -12.21% C8-BTBT along b-axis // PTCDI-C8 along a-axis, respectively.

Figure 5.2 shows X-ray diffraction patterns of C8-BTBT and PTCDI-C8 single layers and the bi-layers recorded by the imaging plate. The diffraction spots could be observed at 2θ angle around 3.3, 6, 9 degrees identified as (001), (002), and (003) planes for single C8-BTBT layer and around 4.1 and 8 degrees identified as (001) and (002) plane for single PTCDI-C8 layer. Both the C8-BTBT/PTCDI-C8/C-sapphire bi-layers showed XRD spot patterns with the

combination of the C8-BTBT and PTCDI-C8 characteristic spots with the (001) out-of-plane orientation. Any differences could not be observed among the patterns of PTCDI-C8/C8-BTBT/C-sapphire and C8-BTBT/PTCDI-C8/C-sapphire bi-layers, indicating that formation of a similar in-plane orientation relationship.

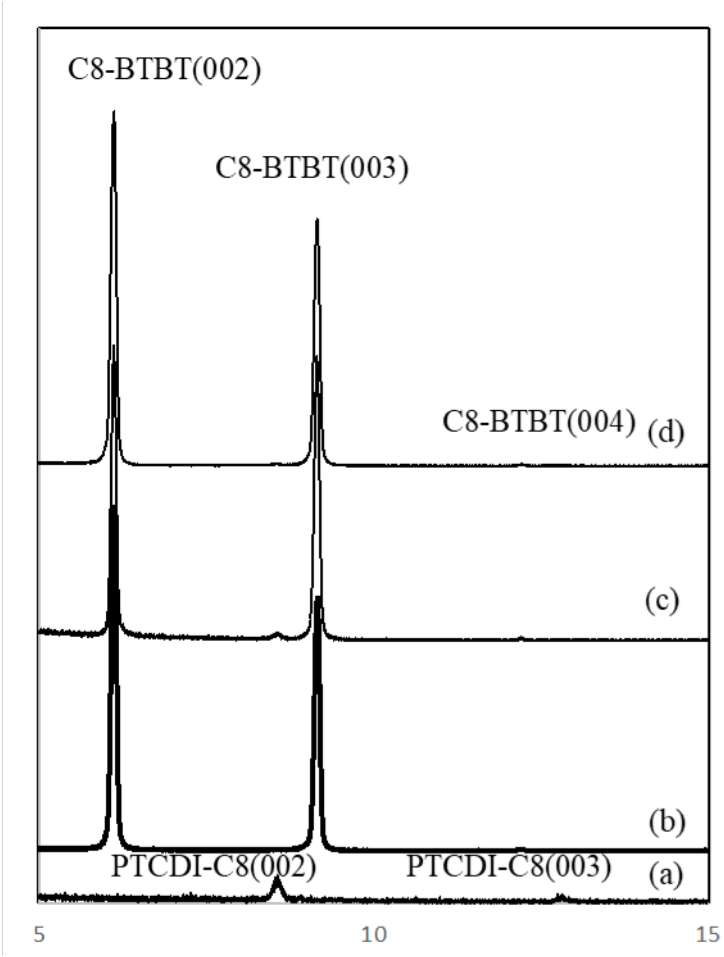

Figure 5.1 X-ray diffraction patterns of (a) PTCDI-C8 single layer, (b) C8-BTBT single layer, (c) PTCDI-C8/C8-BTBT/C-sapphire, and (d) C8-BTBT/PTCDI-C8/C-sapphire.

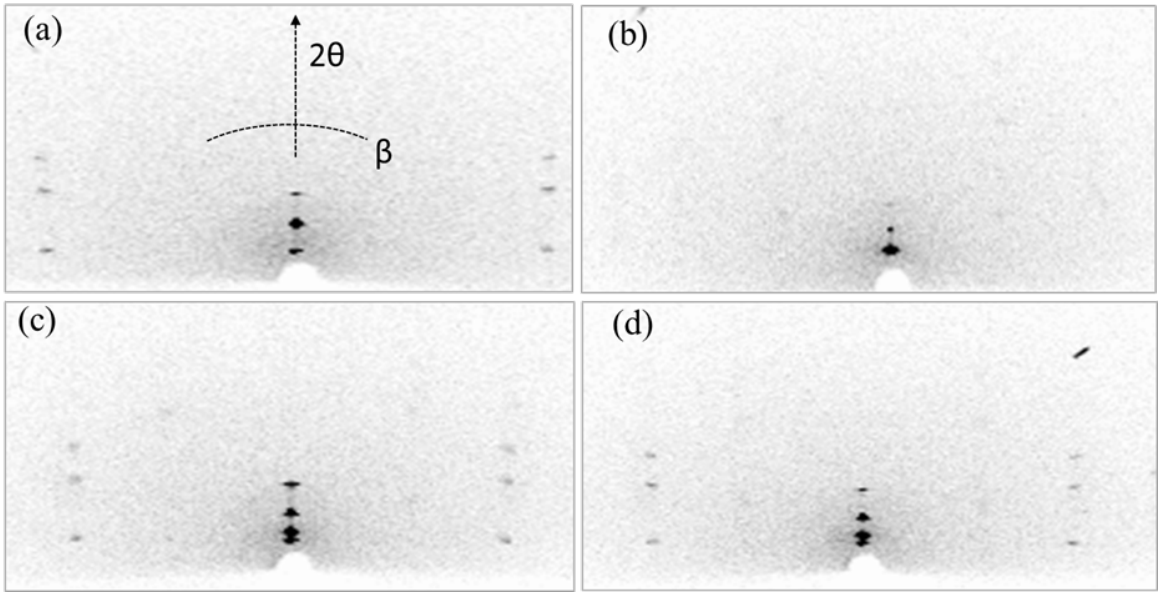

Figure 5.2 X-ray diffraction patterns for (a) C8-BTBT, (b) PTCDI-C8, (c) PTCDI-C8/C8-BTBT/C-sapphire, and (d) C8-BTBT/PTCDI-C8/C-sapphire.

5.3.2 Surface homogeneity of the PTCDI-C8/C8-BTBT bi-layer

Figure 5.3 shows the topography and surface potential images of the PTCDI-C8 and C8-BTBT single layers and bi-layers with different stacking sequences. The C8-BTBT layer was formed by the lateral growth after the formation of continuous layer by the coalescence of the islands, as already reported,**[22]** and the 100-nm-thick-layer was composed of 2 ~ 2.7 μm-size-granular grains with the surface roughness (Ra) with 16.8 nm. The surface potential was almost constant over the entire the surface. The PTCDI-C8 layer with the smooth surface of 1.9 nm in Ra was composed of rod-like grains with 0.13 μm in width and 0.63 μm in length, and the surface potential was almost constant due to the homogenous surface state.

The surface morphology and homogeneity of the surface potential was so different among the bi-layers by the stacking sequences, in spite of almost the same in preferred orientation. The granular grains of the upper C8-BTBT layer was observed for the C8-BTBT/PTCDI-

C8 bi-layer like the C8-BTBT single layer, and the surface roughness (Ra) was estimated to be 2.8 nm.

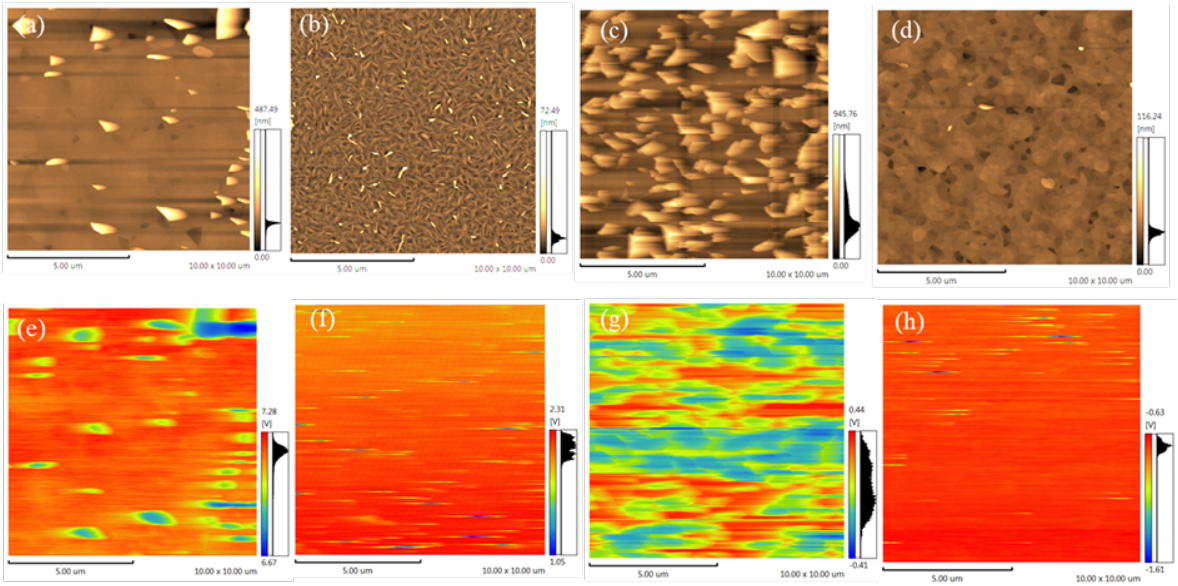

Figure 5.3 Topography and surface potential images of (a,e) C8-BTBT layer, (b,f) PTCDI-C8 layer, (c,g) PTCDI-C8/C8-BTBT/C-sapphire, and (d,h) C8-BTBT/PTCDIC8/C-sapphire.

5.3.3 Growth model of the PTCDI-C8/C8-BTBT bi-layer

The growth of the upper C8-BTBT layer was almost same as that for the single layer. The surface potential was almost constant on the potential image indicating that the C8-BTBTlayer stacked entirely on the bottom PTCDI-C8 layer. The PTCDI-C8/C8-BTBT bi-layer showed a roughed surface of the increased Ra of 95.6 nm, and edged island-type irregularities could be observed on the lower continuous layer. The large surface irregularity reflected to the surface potential image, where the two potentials were distributed on the image, suggesting the growth of isolated PTCDI-C8 edged island on the C8-BTBT layer. There is a possibility of the growth of the PTCDI-C8 with a process different to that of the single layer, although there was a different in the surface roughness of the lower layers. Further investigation on the growth is

needed to clarify the reason for the difference in the growth, the stacking sequence strongly affects the surface state of the resultant bi-layer. And, the estimation of the surface potential with KFM is a powerful tool to estimate the homogeneity of the surface energy state of the semiconductor device.

5.4 Conclusions

The preferred orientation and surface homogeneity of the C8-BTBT/PTCDI-C8 bi-layers were estimated by X-ray diffraction, and KFM. The C8-BTBT and PTCDI-C8 single layers showed the surface roughness (Ra) of 16.8 nm and 1.9 nm, respectively, and the surface potential was homogenous over the surface for both the single layer. The stacking sequence strongly affected to the morphology and surface potential of the bi-layer, and C8-BTBT/PTCDI-C8 bi-layer showed a surface roughness of 2.8 nm and homogenous surface potential, compared with those of PTCDI-C8/C8-BTBT bi-layer. The results demonstrated here indicates the importance of the stacking sequence for the bi-layers and availability of the KFM measurement on the estimation of the surface state.

REFERENCES

[1] P. Peumans, A. Yakimov, and S.R. Forrest, Small moleucular weight organic thin-film photodetectors and solar cells, J. Appl. Phys. **93**, 3693 (2003).

[2] P. Peumans, S. Uchida, and S.R. Forrest, Effiecient bulk heterojunction photovoltaic cells using small-molecular-weight organic thin films, Nature.**425**, 158 (2003).

[3] D. Gebeyehu, B. Maennig, J. Drechsel, K. Leo, and M. Pfeiffer, Bulk-heterojunction photovoltaic devices based on donor-acceptor organic small molecule blends, Sol. Energy Mater. Sol. Cells **79**, 81 (2003).

[4] S. Uchida, J. Xue, B.P. Rand, and S.R. Forrest, Organic small molecule solar cells with a homogeneously mixed copper phthalocyanine: C60 active layer, Appl. Phys. Lett. **84**, 4218 (2004).

[5] B. Song, C. Rolin, J.D. Zimmerman, and S.R. Forrest, Effect of mixed layer crystallinity on the performance of mixed heterojunction organic photovoltaic cells, Adv. Mater. **26**, 2914 (2014).

[6] B. Kang, M. Jang, Y. Chung, H. Kim, S.K. Kwak, J.H. Oh, and K. Cho, Enhancing 2D growth of organic semiconductor thin films with macroporous structures via a small-molecule heterointerface, Nat. Commun. **5**, 4752 (2014).

[7] R. Rahimi, A. Roberts, V. Narang, and D. Korakakis, Investigate the role of the active layers' structures and morphology in the performance of the organic solar cell device, Appl. Phys. Lett. **102**, 73105-1 (2013).

[8] M. Aghamohammadi, Ph.D thesis, Universidad Autonoma de Barcelona, (2016).

[9] J. Yang, D. Yan, and T.S. Jones, Molecular template growth and its applications in organic electronics and optoelectronics, Chem. Rev. **115**, 5570 (2015).

[10] H. Minemawari, T. Yamada, H. Matsui, J. Tsutsumi, S. Haas, R. Chiba, R. Kumai, and T. Hasegawa, Injet printing of single-crystal films, Nature **475**, 364 (2011).

[11] R. Miscioscia, F. Loffredo, G. Nenna, F. Villani, C. Minarini, M. Petrosino, A. Rubino, M. Denti, and A. Facchetti, Analysis of the persistent photoresponse of C8-BTBT transistors in the near bandgap spectral region, Org. Electron. Physics, Mater. Appl. **30**, 83 (2016).

[12] D. He, Y. Zhang, Q. Wu, R. Xu, H. Nan, J. Liu, J. Yao, Z. Wang, S. Yuan, Y. Li, Y. Shi, J.Wang, Z. Ni, L. He, F. Miao, F. Song, H. Xu, K. Watanabe, T. Taniguchi, J.-B. Xu, and X.Wang, Two-dimensional quasi-freestanding molecular crystals for high performance organic field-effect transistors, Nat. Commun. **5**, 5162 (2014).

[13] S. Karak, V.S. Reddy, S.K. Ray, and a. Dhar, Organic photovoltaic devices based on pentacene/N,N'-dioctyl-3,4,9,10-perylenedicarboximide heterojunctions, Org. Electron. **10**, 1006 (2009).

[14] N. Hiroshiba, R. Hayakawa, M. Petit, T. Chikyow, K. Matsuishi, and Y. Wakayama, Structural anlysis and transistor properties of heteromolecular bilayers, Thin Solid Films **518**, 441 (2009).

[15] S.H. Han, K.J. Lee, S.H. Lee, and J. Jang, N-type organic thin-film transistor using N, N' -dioctyl-3,4,9,10-perylene tetracarboxylic diimides grwon by organic vapor deposition, J. Non. Cryst. Solids **354**, 2870 (2008).

[16] H. Fan, W. Shi, X. Yu, and J. Yu, High performance nitrogen dioxide sensor based on organic field-effect transistor utilizing ultrathin CuPc/PTCDI-C8 hetrojunction, Synth. Met. **211**, 161 (2016).

[17] R. Rahimi, V. Narang, and D. Korakakis, Optical and morphological studies of thermally evaporated PTCDI-C8 thin films for organic solar cell applications, Int. J. Photoenergy **2013**, (2013).

[18] L. K. Mao, J.C. Hwang, and Y. L. Chueh, Materials and interfaces issues in pentacene/PTCDI-C8 ambipolar organic field-effect transistors with solution based

gelation dielectric, Org. Electron. Physics, Mater. Appl. **15**, 2400, (2014).

[19] L. Lyu, D. Niu, H. Xie, N. Cao, H. Zhang, Y. Zhang, P. Liu, and Y. Gao, Orientation-dependent energy level alignment and film growth of 2,7-dioctyl[1]benzothieno[3,2-b]benzothiophene (C8-BTBT) on HOPG, J. Chem. Phys. **144**, 034701-1 (2016).

[20] S. Wang, D. Niu, L. Lyu, Y. Huang, X. Wei, C. Wang, H. Xie, and Y. Gao, Interface electronic structure and morphology of 2,7-dioctyl[1]benzothieno[3,2-b] benzothiophene (C8-BTBT) on Au film, Appl. Surf. Sci. **416**, 696 (2017).

[21] N. Hiroshiba, R. Hayakawa, T. Chikyow, K. Matsuishi, and Y. Wakayama, Ambipolar carrier transport in hetero-layered organic transistors consisting of quaterrylene and N,N'-dioctyl-3,4,9,10-perylenedicarboximide, Org. Electron. Physics, Mater. Appl. **12**, 1336 (2011).

[22] A. M. Moh, P. L. Khoo, K. Sasaki, S.Watase, T. Shinagawa, M. Izaki, Growth and characteristics of C8-BTBT layer on C-sapphire substrate by thermal evaporation, Phys. Status Solidi A **215**, 1700862 (2018).

CHAPTER 6

Summary

6.1 Research summary

In this thesis, the preparation of vacuum-evaporated π-conjugated organic n-type and p-type semiconductor layers and characterization of deposited layers by x-ray diffraction (XRD), atomic force microscopy (AFM), Kelvin force microscopy (KFM), optical absorption measurment, Hall effect measurement by van dar Paul method were in the focus of this study.

The growth, structure including preferred orientation, and morphology of p-type (C8-BTBT) and n-type (PTCDI-C8) organic semiconductor layers on single-crystal substrates with various orientations have mainly analyzed by XRD and AFM. The effect of layer thickness and substrate temperature on structural and optical properties of vacuum-evaporated C8-BTBT, and PTCDI-C8 layers only on single-crystal (0001)-Al_2O_3 (C-sapphire) were investigated. And, the effect of stacking sequences of C8-BTBT and PTCDI-C8 layers on the surface states of the deposited layers, including suface homogenity and surface potential variations were observed by the use of XRD techniques and Scanning probe microscopy (SPM).

In chapter two, vacuum-evaporated 100-nm-thick 2,7-dioctyl[1]benzothieno[3,2-b][1]benzothiophene (C8-BTBT) layers were prepared on quartz glass, (11$\underline{2}$0) A-, (0001) C-, and (1$\underline{1}$02) R-single-crystal Al_2O_3 (sapphire), and (100)-, and (111)-single-crystal MgO substrates. Structural characterizations were carried out by X-ray diffraction analysis and atomic force microscopy (AFM) observation. XRD analysis revealed that the (001) out-of-plane orientation with a similar in-plane orientation was developed irrespective of the substrate material and orientation. The molecule-molecule interaction is stronger than molecule-substrate interaction because long axis of C8-BTBT molecules are arranged almost normal to the single crystal substrates and formation of the layer was governed by π-π-stacking-induced molecular ordering. The grain structure influenced the resistivities of the C8-BTBT layers on various single crystal substrates.

In chapter three, the effects of the layer thickness and preparation temperature on structural, morphological, optical, and electrical characteristics of vacuum-evaporated C8-BTBT layers on a single crystal (0001) Al_2O_3 (C-sapphire) have been investigated with XRD, AFM, optical absorption measurement, and resistivity measurement with and without light irradiation. Concerning the results obtained from the XRD, it is observed that the C8-BTBT layers possessed the (001) out-of-plane orientation irrespective of the layer thickness and preparation

temperature. According to AFM observation, the C8-BTBT grains were growing up in direction parallel to the substrate surface keeping almost constant height, and the continuous layer was formed by the coalescence of the C8-BTBT grains. The grain size of the continuous C8-BTBT layer increased with raise in preparation temperature. The optical band gap energy could be estimated to be 3.32-3.35 eV regardless of the layer thickness and preparation temperature. The electrical resistivity decreased from 2.1×10^6 Ωcm to 1.2×10^2 Ωcm with increase in the preparation temperature due to the increase in the grain size, and the light irradiation induced drastically decrease to 42 to 28 Ωcm.

In chapter four, the growth of N,N'-dioctyl-3,4,9,10-perylenedicarboximide (PTCDI-C8) layers on single crystal Al_2O_3 and MgO substrates with various orientations were characterized by XRD analysis. The (001) out-of-plane orientation was developed on all the single crystal substrates, irrespective of the substrate materials and orientation. Since the structure of PTCDI-C8 on single crystal substrates showed similar manners, the growth of PTCDI-C8 layers only on (0001) Al_2O_3 C-sapphire substrate were prepared by investing the effect of layer thickness and substrate temperature. AFM observation revealed that needle-like grains formations irrespective of the preparation parameters. The grain size and surface roughness increased with increase in layer thickness from 15 nm to 100nm and preparation temperature 300 K – 373 K. The optical band gap energy of 2.03 eV which value is consistent and band gap energy of PTCDI- C8 layer did not depend on preparation parameters. The growth of PTCDI-C8 on single crystal substrates was governed by the π-π stacking structure.

In chapter five, the single layers and bi-layers with different sequences of 2,7-dioctyl[1]benzothieno[3,2-b][1]benzothiophene (C8-BTBT) and N,N'-dioctyl-3,4,9,10-perylenedicarboximide (PTCDI-C8) on single crystal Al_2O_3 (C-sapphire) substrate were investigated by XRD and SPM observation. The topography images observed from KFM showed the surface potential distribution is homogenous for both single layers of C8-BTBT and PTCDI-C8 with

the surface roughness (Ra) of 16.8 nm and 1.9 nm, respectively. The stacking sequences strongly affected to the morphology and surface potential of the bi-layers, and C8-BTBT/PTCDI-C8 bi-layer showed a surface roughness of 2.8 nm and homogenous surface potential as compared to those of PTCDI-C8/C8-BTBT bi-layer.

In this work, the structural, morphological characteristics, optical and electrical properties of vacuum evaporated organic semiconductor layers on single crystal substrates were studied. This study supports the understanding of the growth of π-conjugated molecules on single crystal substrates and the optimize condition of growth for organic semiconductors to obtain high ordered structure with high performance organic-based electronics and optoelectronic devices.

6.2 Acknowledgement

This thesis is the outcome of my research from Oct 2015 until Sep 2018 at Thin Film Laboratory, Department of Mechanical Engineering, Toyohashi University of Technology, Japan, under supervision of Prof. Dr. Masanobu Izaki. This research work could not be accomplished without the help of several individuals who in direct or indirect way contributed and extended their valuable assistance in the preparation and completion of this study.

First and foremost, I am grateful to my supervisor, Prof. Dr. Masanobu Izaki for being an excellent adviser. He is not only a scientist, he is also a kind and caring person. Not only did I learn about material science and semiconductor devices, but he trained me how to conduct my research work and writing papers. He supported me my research work with his ideas, discussions, and comments.

I would like to give special thanks to examiners, Prof. Dr. Yoshikazu Todaka, Assoc. Prof. Dr. Toshiaki Yasui, and Assoc. Prof. Dr. Masakazu Kobayashi for their advice, suggestions and comments which support the improvement this thesis.

Next, I would like to thanks to Assc. Prof. Dr. Seiji Yokoyama and Dr. Junji Sasano for their kind comments and ideas during the discussion in laboratory's seminars. Then, I also want to give my gratefulness to Dr. Seiji Watase and Prof. Dr. Tsutomu Shinagawa for their help in some of my measurement, ideas and discussions.

I was fortunate to attend doctorate course with Mr. Khoo. He is my great tutor and a friend who help me throughout my student life in Japan. I am grateful for his patience and supporting. In

my daily work, I have been blessed with a friendly and cheerful group of lab members. They are very helpful and always assisted me to complete my works, especially to the thin film lab group members, Mr. Koumori , Mr. Niki, Mr. Shimizu for teaching me how to operate vacuum evaporation system, and atomic force microscopy measurement and XRD measurement.

I would like to express many thanks to AUN-SEED.net (JICA) for their financial supports.

I want to thank to my family, and my teachers in Myanmar. Especially, my Dad, U Kyi Htun is the person who gave me the freedom to pursue my interests and ideas in my studying field. And my Mom who raised me with her kindness, caring and love. Thanks to you all, for all your love and support.

Toyohashi, Japan

Aye Myint Moh

6.3 Research achievements

6.3.1 List of publications

[1] Growth and Characteristics of C8-BTBT Layer on C-Sapphire Substrate by Thermal Evaporation, Aye Myint Moh, Pei Loon Khoo, Kimihiro Sasaki, Seiji Watase, Tsutomu Shinagawa and Masanobu Izaki, Phys. Status Solidi A 215, 1700862, (2018).

[2] Preferred orientation of 2,7-dioctyl[1]benzothieno[3,2-b][1]benzothiophene molecules on inorganic single crystal substrates with various orientations, Aye Myint Moh, Kimihiro Sasaki, Seiji Watase, Tsutomu Shinagawa and Masanobu Izaki, Japanese Journal of Applied Physics, Jpn. J. Appl. Phys. 57, 08RE04, (2018).

[3] Surface State of Thermally Evaporated PTCDI-C8/C8-BTBT Bi-Layer, Aye Myint Moh, Seiji Watase, Masanobu Izaki, Journal of the Surface Finishing Society of Japan, J. Surf. Finish. Soc. Jpn. 69, 249, (2018).

6.3.2 List of conferences

[1] Preferred Orientation and Morphology of C8-BTBT layer Prepared on C-Sapphire Substrate by Thermal Evaporation, Aye Myint Moh, Pei Loon Khoo, Kimihiro Sasaki, Seiji Watase, Tsutomu Shinagawa and Masanobu Izaki, European Materials Research Society International Conference, Strasbourg, France, 2017.

[2] Preferred Orientation of C8-BTBT Molecules on Inorganic Single Crystal Substrates with Various Orientation, Aye Myint Moh, Kimihiro Sasaki, Seiji Watase, Tsutomu Shinagawa and Masanobu Izaki, PVSEC-27 International Conference, Shiga, Japan, 2017.

[3] Effect of Stacking Sequence on the Structure of PTCDI-C8/C8-BTBT Bi-layer", Aye Myint Moh, Seiji Watase, and Masanobu Izaki, The 8^{th}, International Conference on Advanced Materials Research (ICAMR), Fukuoka, Japan, 2018.